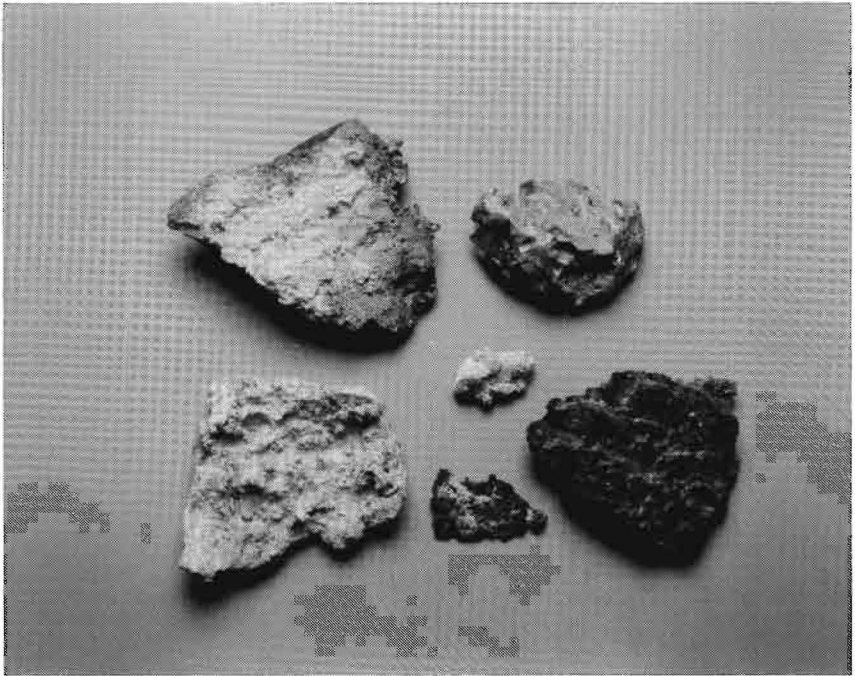


# Deposits and Condensation from Flue Gases in Glass Furnaces



R.G.C. Beerkens

## **Deposits and Condensation from Flue Gases in Glass Furnaces**

# DEPOSITS AND CONDENSATION FROM FLUE GASES IN GLASS FURNACES

PROEFSCHRIFT

ter verkrijging van de graad van doctor aan  
de Technische Universiteit Eindhoven, op gezag  
van de rector magnificus, prof. dr. F.N. Hooge,  
voor een commissie aangewezen door het college  
van dekanen in het openbaar te verdedigen op  
dinsdag 16 december 1986 om 16.00 uur

door

RUDOLF GERARDUS CATHERINA BEERKENS

geboren te Venlo

Aan mijn ouders.

## CONTENTS

INTRODUCTION	1
1. COMBUSTION AND GLASS MELTING IN INDUSTRIAL FURNACES	4
1.1 The industrial glass melting process	4
1.1.1 The combustion of fossil fuels in the melting furnace	7
1.1.1.1 The combustion of the fuels in glass furnaces	9
1.1.1.2 Heat transfer from the flames	11
1.1.1.3 The gas flow in the combustion chamber	12
1.1.1.4 NO <sub>x</sub> -formation in the combustion chamber	13
1.1.1.5 Other aspects of mineral fuel combustion	15
1.1.2 Volatilization from the glass melt	18
1.1.2.1 Volatilization and particulate entrainment in furnace atmosphere	21
1.1.2.2 Volatilization mechanisms	22
1.1.2.3 Conclusions	28
1.1.3 Heat exchanging devices in the glass industry	29
1.1.3.1 Regenerative systems	29
1.1.3.2 Recuperative systems	33
1.1.3.3 Waste heat boilers	34
1.2 Exhaust gas emissions from the glass industry	35
1.2.1 Introduction	35
1.2.2 Gaseous emissions from glass melting furnaces	35
1.2.3 Dust formation and emission from the stack of glass melting furnaces	37
1.2.4 Filter installations	39
Literature references	40
Nomenclature	44
2. LITERATURE SURVEY OF THE THERMODYNAMIC PARAMETERS AND MASS TRANSPORT PROCESSES IN EXHAUST GASES OF GLASS FURNACES	46
2.1 Introduction	46
2.2 Evaluation of reactions in the glass melter atmosphere and the exhaust gases	47
2.2.1 Flue gases with sulphur, chlorides and sodium compounds	47
2.2.2 Flue gases with sulphur, chlorides, potassium and sodium	49
2.2.3 Flue gases with sodium, calcium, sulphur and chlorides	50
2.2.4 Flue gases with sodium and boron	51

2.2.5	Flue gases with potassium, sulphur, boron and fluorides	52
2.2.6	Flue gases only doped with volatilized lead	53
2.2.7	Flue gases with lead and sulphur	54
2.3	Thermodynamic properties of flue gas components: Equilibrium Constants and Vapor Pressures	55
2.4	Condensation and deposition from exhaust gases doped with inorganic components	59
2.5	Analytical procedures for measurements of gaseous components in the exhaust of glass melting furnaces	63
2.5.1	Deposition on water cooled paddles in hot exhaust gases	63
2.5.2	Mass spectrometric in situ analysis of exhaust gas compositions	65
	Literature references	67
	Nomenclature	72
3.	CONDENSATION PRODUCTS AND GASEOUS COMPONENTS IN COOLING	
	EXHAUST GASES	73
3.1	Introduction	73
3.2	Thermodynamic approach to evaluate changing compositions during the cooling of exhaust gases from glass furnaces	74
3.2.1	The thermodynamic equilibrium model	74
3.2.2	Chemical compositions of exhaust gases from different glass furnaces	75
3.2.2.1	The calculation of flue gas compositions in soda-lime glass furnaces	75
3.2.2.2	Calculations of flue gas compositions in borosilicate glass furnaces	86
3.2.2.3	Calculated flue gas compositions in lead glass furnaces	92
3.2.3	Restrictions of the thermodynamic equilibrium model	96
3.2.3.1	Reaction kinetic limitations	96
3.2.3.2	Condensation kinetic limitations	98
3.2.3.3	Inaccuracies in the thermodynamic data	98
3.3	Experiments on the condensation of salt or metal oxide components from simulated flue gas compositions	99
3.3.1	The experimental procedure	99
3.3.2	Comparison of the results of the thermodynamic equilibrium model with the experimental investigations	103

3.4	Conclusions	111
	Literature references	114
	Nomenclature	115
4.	BOUNDARY LAYER MASS TRANSPORT IN DEPOSITION PROCESSES	116
4.1	Introduction	116
4.2	Theories describing mass transfer and deposition at cold surfaces	117
4.2.1	Derivation of mass transport parameters	120
4.3	CFBL-predictions for deposition from exhaust gas on a relatively cool surface	122
4.3.1	Experimental procedures	123
4.3.2	Comparison of experimental results with CFBL- predictions for the deposition on cylindrical surfaces in cross flow configuration	124
4.4	Application of the CFBL model to describe deposition in glass furnace regenerators and recuperators	139
4.4.1	Influence of chemical conversion in the boundary layer on transport rates	139
4.4.2	Homogeneous nucleation in boundary layers	141
4.4.3	Heterogeneous nucleation	143
4.4.4	Reaction kinetic limitations at the deposition surface	143
4.4.5	Transport of condensed material from the exhaust gas to the deposition surface	144
4.4.6	Conclusions	144
4.5	Deposition processes in cylindrical tubes: A laboratory study	145
4.5.1	Equipment to study deposition processes at the inner wall of cylindrical exhaust gas channels	145
4.5.2	Application of the the deposition model for exhaust gas channels	147
4.5.3	Deposition rates of sodium sulphate for various flue gas compositions	150
4.5.4	Deposition rates of sodium metaborate for various flue gas compositions	154
4.5.5	Deposition rates of potassium sulphate	156
4.5.6	Deposition rates of lead oxide	158
4.6	Summary and conclusions	160
	Literature references	164
	Nomenclature	166

5. APPLICATION OF THEORETICAL SIMULATION MODEL TO INVESTIGATE DEPOSITION FROM AND CONDENSATION IN EXHAUST GASES FROM INDUSTRIAL GLASS FURNACES	168
5.1 Introduction	168
5.2 Deposition processes in checkers of glass furnace regenerators	169
5.2.1 Heat and mass transfer in different regenerator construction	169
5.2.2 Temperature distribution in regenerators	172
5.2.3 Deposition of salt components in regenerators of soda-lime glass furnaces	172
5.2.3.1 Influence of changing flue gas compositions on deposition behaviour in regenerators of soda-lime glass furnaces	174
5.2.3.2 Effect of operating conditions and construction of regenerator on deposition of sodium sulphate	177
5.2.4 Deposition of salt components in regenerators of borosilicate glass furnaces	179
5.2.5 Deposition of salt components in regenerators of lead glass furnaces	184
5.3 Deposition processes in recuperators of glass furnaces	186
5.3.1 Flow conditions in radiative recuperators	186
5.3.2 Temperature distribution in the recuperator	187
5.3.3 Deposition of salt components in recuperators of soda-lime glass furnaces	189
5.3.4 Deposition of salt components in recuperators of sodium-borosilicate glass furnaces	192
5.4 Deposition of particulates in secondary heat exchangers and in the colder parts of regenerators	195
5.4.1 Mechanisms for particulate deposition from dust laden flue gases	195
5.4.2 Deposition by inertia effects	195
5.5 Emission of particulates and gaseous components from glass furnaces according to equilibrium calculations	198
5.5.1 Composition of dust and gaseous pollutants from soda-lime glass furnaces	198
5.5.2 Composition of dust and gaseous pollutants from sodium-borosilicate glass furnaces	199

5.5.3	Composition of dust and gaseous pollutants from lead glass furnaces	200
5.6	Summary and conclusions	201
	Literature references	203
	Nomenclature	204
	APPENDIX A	205
	APPENDIX B	206
	APPENDIX C	207

## INTRODUCTION

Up to now the chemical and physical processes occurring in exhaust gases doped with volatilized matter from the glass melt are only understood in general terms. During transport from the furnace to the stack, the exhaust gases are cooled down from 1800 K to approximately 500 K. During this transportation the exhaust gas flow passes surfaces with lower temperatures. Heat transport from the exhaust gas to these relatively cold surfaces is accompanied by mass transport of gaseous species towards the surface resulting in deposition of exhaust gas components.

Recuperation of part of the heat content of the exhaust gases is a procedure generally applied in the glass industry. Heat is transferred from the flue gases to the combustion air by means of regenerators or recuperators.

Deposition of several condensing exhaust gas components at the relatively cool surfaces in regenerators may cause blockage of the channels, a decreasing heat transfer and corrosion.

Inorganic salts like sodium sulphate, lead sulphate or sodium borates are the main constituents of the deposits in regenerators or recuperators.

Alkali, sulphur and occasionally lead, boron, chloride and fluoride components are introduced in the exhaust gas by fuel impurities or, have volatilized from the glass melt. The chemical composition of the exhaust gas is strongly dependent on the temperature. Variations in temperature, result in changing thermodynamic conditions causing chemical conversions in the exhaust gases. Generally, the chemical composition of the bulk exhaust gas is different from the composition of the gaseous phase near a colder surface. This causes diffusion mainly of salt forming elements like sodium, sulphur, lead or boron towards the wall. In this study the deposition behaviour has been investigated for several exhaust gas compositions under different conditions. Physical models have been developed in this field and applied to calculate the deposition rates and the nature of the deposited product for practical cases.

To obtain a better understanding of the processes that cause the entrainment of certain chemical elements in the flue gases of the furnace, a detailed description of the glass melting process is given in chapter 1.

In this chapter a survey is given of the volatilization processes in the furnace resulting in exhaust gases loaded with components originating from the glass melt, the raw material batch or the fuel. The impurities in the exhaust gases cause fouling of heat exchanging systems and emission of hazardous dust or gaseous components.

The behaviour of the exhaust gases depends on:

- the chemical gas composition;
- the flow characteristics of the exhaust gases;
- the temperature profile in the main gas stream;
- the presence of relatively cold surfaces or objects.

Thermodynamic approaches can be applied to calculate the 'thermodynamically stable' exhaust gas compositions as a function of temperature and dopant concentrations. The most important chemical equilibrium reactions in exhaust gases of glass furnaces are given in chapter 2. The relevant thermodynamic parameters like the equilibrium constants and saturation pressures as derived from extensive literature studies are also presented in that chapter. Mass transport processes and deposition processes that take place in the exhaust gas flows are also mentioned according to theories and observations described in the literature. Chapter 3 deals with calculations to estimate the chemical behaviour of flue gases during cooling. This chapter also presents the outcome of our laboratory investigations to characterize the condensation products. These results are compared with the thermodynamically expected condensates.

Mass transport processes determining the deposition behaviour in exhaust channels are presented in chapter 4. Theoretical models are applied to investigate the nature and the rates of deposition of simulated exhaust gases. Calculations based on these model are executed to obtain deposition rates for the most common flue gas compositions in the glass industry. The application of this method in actual industrial situations is discussed in the last chapter. From this chapter the validity of the theoretical approaches and the laboratory studies for the evaluation of the industrial situation will be shown.

In the scheme on page 3 a presentation is given of the physical and chemical processes in the exhaust gases from regenerative glass furnaces.

Schematic presentation of processes taking place during the transport of exhaust gases to the atmosphere.

### Glass Furnace

- Production of exhaust gases from the combustion of mineral fuels, temperatures varying from 1800 to 2000 K.
- Entrainment of batch volatiles, dust particles and volatile components from 0 to 1000 volume ppm.
- Chemical reactions producing sulphur oxides and nitrogen oxides in the hot gases or flames.

### Regenerators

- Exhaust gas flow through channels made by a checker work of refractory material, the gas velocities vary from 2 to 4 m/s.
- Formation of boundary layers adjacent to the surfaces of the submerged bricks; the average thickness of these velocity boundary layers is in the order of a few centimetres.
- Simultaneous mass and heat transfer to the surfaces of the checker work, Nusselt numbers vary from 10 to 30 and Sherwood numbers also vary from 10 to 30.
- Deposition of condensed salt components caused by the mass transport of the salt constituting elements through the boundary layer, deposition rates vary from 0 to 5 mg/m<sup>2</sup>.s., depending on the location and the composition.
- Cooling of the exhaust gases caused by the heat transfer to the checker work, the temperature drops from 1700 K to 750 K in the regenerator.
- Dust formation in regenerators is caused by condensation of supersaturated components in the exhaust gases.

### Stack

- Further cooling of exhaust gases till temperatures of approximately 500 K.
- Formation of sticky dust by reaction of water or sulphur oxides with the particles in the exhaust gases.
- Emission of hazardous gaseous components, like hydrogen fluoride, hydrogen chlorides, boric acid or sulfuric acid.
- Emission of dust, the constituting particles have diameters between 0.05 µm and 20 µm.

## **1. COMBUSTION AND GLASS MELTING IN INDUSTRIAL FURNACES**

### **1.1 The industrial glass melting process - introduction**

The industrial production of glass from raw material batch is generally a continuous process. The main glass products are (see also table 1.1 for the chemical compositions):

- container glass;
- flat glass;
- re-reinforcement fibres;
- insulation fibres;
- borosilicate glass for laboratory ware;
- crystal glass;
- optical glass;

The glass output of continuous glass melting furnaces varies from 5 tons/day to 800 tons/day. In most countries fossil fuels are the chief energy-suppliers.

Furnace temperatures vary from 1700 K to 1900 K, dependent on glass composition and glass quality. A well-mixed batch of raw materials is continuously charged to the furnace. For the common soda-lime glasses (container and flat glasses) these raw materials are:

silica sand, feldspar, soda ash, limestone, dolomite and salt cake (sodium sulphate). The batch floats on the glass melt and is heated by the radiation of the flames in the combustion chamber and the transfer of heat from the hot glass melt. Several chemical and physical changes occur during the heating of the raw materials. Solid state reactions between particles of the raw materials result in the formation of eutectic melts. The batch particles dissolve in this melt, often accompanied by dissociation reactions resulting in formation of gaseous components like carbon dioxide and water vapor.

The dissolution of all solid particles, the homogenisation and the removal of gaseous products has been the glass producer's main concern. The quality of the glass product is strongly dependent on the glass melter temperature, the residence time distribution, the mean residence time and the batch composition.

Table 1.1: Typical compositions of commercial glass products.

Perc. in weight-%	container glass	flat glass	borosilicate glass	E-glass for reinforcement fibres	lead crystal glass	special lead glass	A-glass insulation glass fibres
SiO <sub>2</sub>	70.0 - 74.0	70.0 - 73.0	80.0 - 81.0	54.0	± 60.0	45.0	72.0
Al <sub>2</sub> O <sub>3</sub>	1.0 - 2.0	0.1 - 1.7	2 - 2.6	14.5	< 0.1	2.7	2.5
Fe <sub>2</sub> O <sub>3</sub>	0 - 1.0	0.05 - 0.2	< 0.1	0.3	0.02	0.03	0.5
CaO	8.5 - 11.0	7.0 - 10.0	< 0.2	17.0 - 23.0	-	2.0	9.0
MgO	0 - 3.0	3.0 - 4.0	-	4.3	-	-	1.0
BaO	-	-	-	-	-	-	-
Na <sub>2</sub> O	12.0 - 15.0	12.5 - 15.0	3.5 - 5.0	0.3	1.0 - 1.5	1.7	12.5
K <sub>2</sub> O	0.5 - 1.0	0 - 0.8	± 0.5	0.2	13.0 - 15.0	11.1	1.5
SO <sub>3</sub>	0 - 0.2	0.15 - 0.3	-	0 - 0.1	-	-	-
F <sub>2</sub>	-	-	-	-	-	-	-
B <sub>2</sub> O <sub>3</sub>	-	-	12.0 - 13.0	7.0 - 9.0	< 1.5	-	0.5
Cr <sub>2</sub> O <sub>3</sub>	0 - 0.2	-	-	-	-	-	-
PbO	-	-	-	-	24.0 - 25.0	37.0	-

The mean residence time in industrial glass furnaces varies from 25 to 60 hours. In general three processes are distinguished in the melting tank:

- the melting process
- the refining process
- the homogenisation process.

These three essential glass melting processes may partly overlap each other inside the furnace.

The furnace design mainly depends on the glass products to be formed.

For instance the glass melt of a container glass furnace is transported through a so-called throat towards the working-end or refiner.

The glass leaves the working-end, flowing to the forehearth and feeders respectively. The lay-out of a typical industrial container glass furnace is given in figure 1.1.

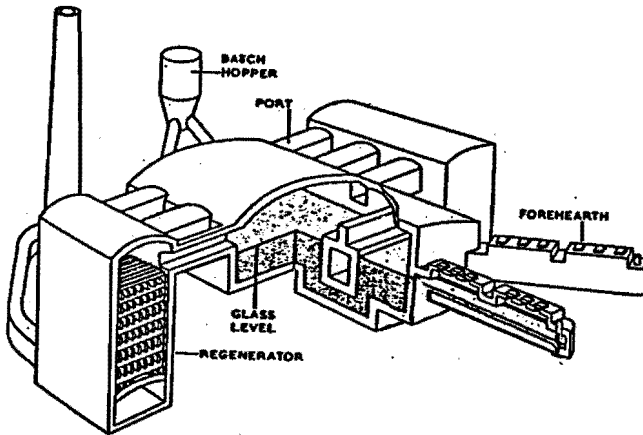


Figure 1.1: Regenerative side-port fired container glass melting furnace.

### 1.1.1 The combustion of fossil fuels in the melting furnace

Worldwide the most frequently used energy sources in the glass industry are:

- natural gas;
- mineral oils;
- electricity.

The oxidant supplier is mainly ambient air, sometimes enriched with pure oxygen. The furnaces with fossil fuel combustion are usually equipped with two burner systems to have the possibility to use natural gas as well as oil. In Western Europe (1981) 45% of glass furnaces' energy consumption is on account of natural gas combustion, in the USA the consumption of natural gas in glass furnaces is even more important, 84% in 1982.

The energy consumption depends on glass quality, glass composition and the capacity of the glass melting furnace. The combustion air is directly heated by exhaust gases in recuperators or indirectly by the exhaust gases in regenerator systems.

The most common furnaces are:

- side-port fired regenerative furnaces;
- side-port fired recuperative furnaces;
- end-port fired regenerative furnaces.

An illustration of the last two types is given in figure 1.2.

In case of a regenerative furnace with side-port firing, preheated air and fuel are combusted by several burners along one side of the furnace. The exhaust gases leave the combustion chamber at the opposite furnace side. The direction of the flames is reversed after periods of twenty minutes.

Recuperative furnaces are mostly side-port fired but the combustion takes place from both sides of the furnace, this is a continuous process. The exhaust gases flow from the combustion chamber to one or two recuperators at the front of the furnace.

In an end-port fired furnace the burners and exhaust ports are positioned at the same end of the furnace. During a firing period the flame from the burner is reversed by the shadow wall and the exhaust gases leave the furnace through the regenerator adjacent to the burner port. This process is reversed after approximately 20 minutes. After the reversal the burner port functions as exhaust port and vice versa.

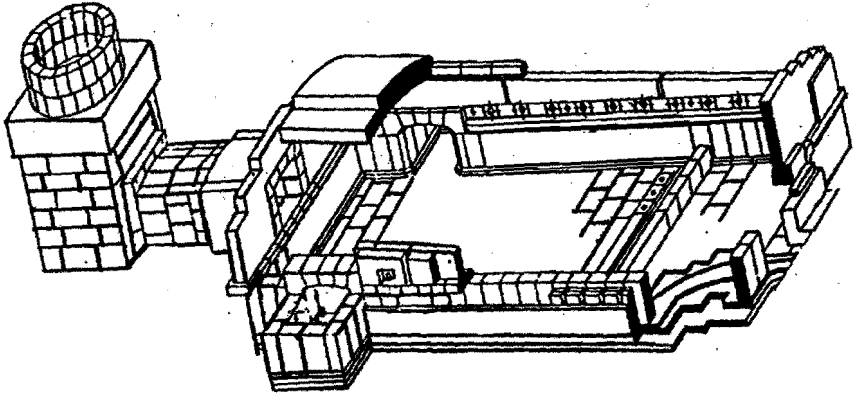


Figure 1.2a: Recuperative side-port furnace.

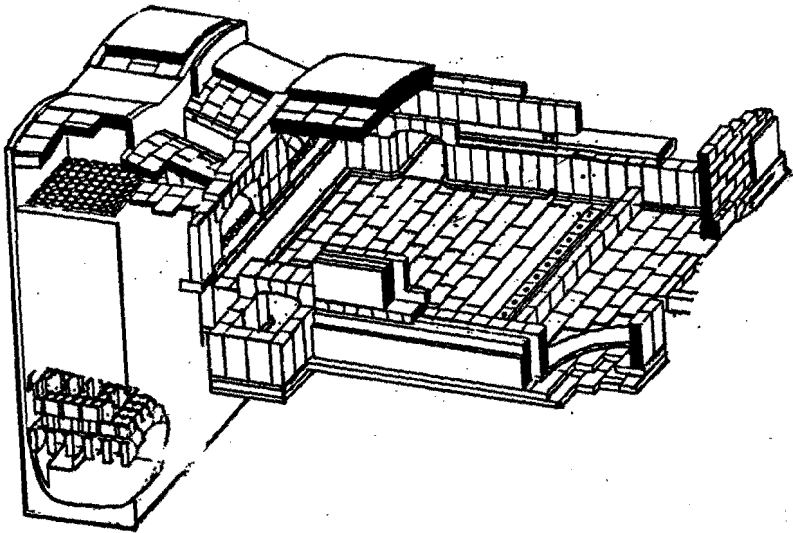


Figure 1.2b: Regenerative end-port furnace.

### 1.1.1.1 The combustion of the fuels in glass furnaces

The fuel is generally injected into the combustion air by means of a nozzle. The flame-length is approximately proportional to the nozzle diameter. Trier [1] has given a relation (1.1) for the estimation of the length of a turbulent diffusion flame, without back-mixing of the furnace gases.

$$L_F = 5.3 \frac{C_o}{C_e} \cdot d_o \sqrt{\frac{\rho_o}{\rho_c}} \quad (1.1)$$

where:

$C_o$  = concentration of fuel at the injection point;

$C_e$  = concentration of fuel at the stoichiometric mixing point;

$d_o$  = nozzle diameter;

$\rho_o$  = fuel density at the injection point;

$\rho_c$  = density combustion air;

$L_F$  = total flame-length.

Back mixing of the exhaust gases normally will increase the flame-length by 10% to 20%, and enhances the homogeneity and stability of the flame.

The flame-length is increased by:

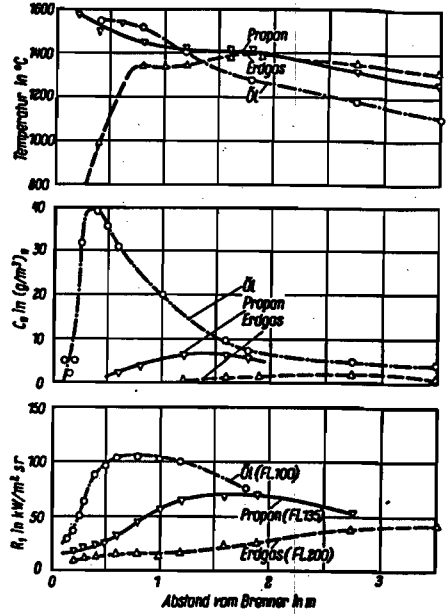
- back-mixing of furnace gases;
- influences of adjacent furnace or port walls;
- parallel flow of fuel and combustion air.

In case of natural gas firing, short flames may be obtained if the angle between the flow directions of the fuel and the air is approximately  $45^\circ$ . The decreasing length of the flames in this case is caused by an increased mixing rate. The average temperature of a flame increases with decreasing flame-length. Temperature profiles for three different flames are given in figure 1.3.

The first 10% of the flame-length has a relatively high temperature in case of oil-combustion. This part of the flame hardly contributes to the heat transfer to the glass melt. The temperature of a natural gas-fired flame reaches its maximum in the end of the flame.

**Figure 1.3:**

Temperature (T) soot concentration ( $C_O$ ) and radiative emissivity (R) for different flames in the glass furnace from literature reference [1].



The heat transfer from natural gas flames is rather small, because of the relatively low emissivity. This results in only a slight decrease of the flame temperature at the end of the flame. The heat transfer from oil flames is enhanced by soot formation, resulting in high values for the emission coefficient. Soot formation is favoured by fuel with high carbon/hydrogen ratios, the emissivity of these flames can reach a value of nearly 1.

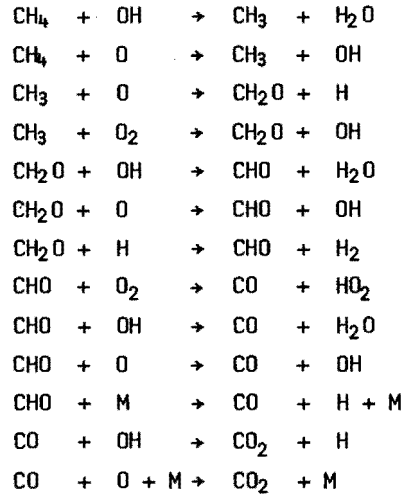
The temperature of a natural gas flame in a regenerative end port furnace may reach a temperature of 2000 K. These high flame temperatures partly compensate for the decreasing heat exchange caused by low emissivities.

The reactions of methane oxidation are given in figure 1.4.

The local oxygen availability, flame temperature and stage of the reaction determines the course of the oxidation process. From the given scheme it is clear that the conversion mechanisms in fuel combustion systems are very complicated.

Figure 1.4:

The most important reaction steps in the methane oxidation [ 2 ].



(M indicates an arbitrarily chosen gas molecule).

Detailed information of the combustion natural gas is given in the literature [ 3, 4, 5 ] and beyond the scope of this thesis.

### 1.1.1.2 Heat transfer from the flames

The heat transfer from the combustion chamber to the batch or glass melt involves mainly the radiation of the flames towards the colder surfaces of the melt or the batch. The heat of radiation from the flames to the raw batch materials or the glass melt is approximated by relation (1.2):

$$H_R = A \cdot \epsilon_{\text{eff}} \sigma \cdot (T_F^4 - T_m^4) \quad (1.2)$$

where:

- $H_R$  = heat of direct radiation from the flame (W)
- $\epsilon_{\text{eff}}$  = effective emissivity of the combustion system
- $\sigma$  = Boltzmann's constant ( $\text{W m}^{-2} \text{K}^{-4}$ )
- $T_F$  = absolute flame temperature (K)
- $T_m$  = glass melt or batch temperature (K)
- $A$  = surface area of radiation ( $\text{m}^2$ ).

This very simple relation shows that high flame emissivities and temperatures result in an enhancing heat exchange. Radiation from the flame towards side walls and the crown and radiation from the superstructure of the furnace towards the melt also plays a role in the total heat exchange. Michelfelder [6], De Waal [7] and Cooper [8] have given different approaches for the radiative heat transfer from the combustion chamber in glass furnaces.

The emissivity value is strongly dependent on the chemical composition of the flames, for instance:

- soot particles;
- carbon dioxide;
- water vapor;
- and radicals enhance the radiation from the hot gases.

The radiating soot particles oxidize further in the flame resulting in mainly carbon dioxide formation. Radiation of a short flame is enhanced by the high temperature as previously stated in figure 1.3.

Approximately 95% of the heat input to the glass melt is due to the radiation of the flames and the combustion chamber. Convective heat transfer is enhanced by:

1. higher flame velocities
2. reactions of the unburned fuel residues in the boundary layer across the glass melt surface
3. positioning of the burner towards the glass surface.

### **1.1.1.3 The gas flow in the combustion chamber**

The velocities of the gases from an oil flame are higher than those velocities in case of natural gas firing. The flue gas velocities in glass melting tanks vary from 0.5 to 15 m/s. The gas velocity near the glass melt surface for a horizontally positioned burner amounts 0.5-1.0 m/s. Gas velocities increase till 4.0 m/s near the glass surface when the burner is directed towards the melt. The impulse of oil flames is generally higher than the impulse of natural gas flames. Therefore, mixing the exhaust gases from oil burners with the gas in the combustion chamber is more intensive than the mixing capacity of a natural gas flame.

The residence time of the main part of the exhaust gas from a natural gas flame in the furnace is rather short. In case of regenerative side-port firing 60 to 80% of the burner gases are transported directly to the opposite parts of the regenerative furnace.

The remaining part is mixed with the contents of the combustion chamber.

#### 1.1.1.4 $\text{NO}_x$ -formation in the combustion chamber

$\text{NO}_x$  is mainly produced in the oxidizing parts of the flame. Direct mixing of the combustion air with the fuel results in minor soot formation and high conversions of nitrogen with oxygen into nitrogen oxides as  $\text{NO}$  and  $\text{NO}_2$  in the flame, according to investigations of Abbasi et al [9].

Lack of complete mixing results in high  $\text{NO}_x$  formation in the oxidizing exhaust gases. The mixing process has come much more to completeness in end-port fired furnaces resulting in lower local air excesses.

Besides these disadvantages of a directly mixed fuel-air flow, a slight decrease in the maximum flame temperature is expected, especially in cases with high excess air combustion. The combustion air is preferably added to the reducing flame step-wise, to avoid the disadvantages of direct mixing of the complete air flow with the fuel. The air excess should be as low as possible because of mainly three reasons:

- An increase in the air excess results in an increasing volume of exhaust gases and so increases heat losses through the stack.
- The flame temperature decreases at high excesses of air.
- Low oxygen contents are preferable to decrease the most important reactant for nitrogen oxide formation.

The concentrations of  $\text{H}_2$ ,  $\text{CO}$ ,  $\text{CO}_2$ ,  $\text{O}_2$  and  $\text{NO}_x$  in a natural gas flame and a mineral oil flame are given in figure 1.5a and 1.5b respectively for an end-port furnace, (presented by figure 1.5c).

More information is given by Wakamatsu et al [10].

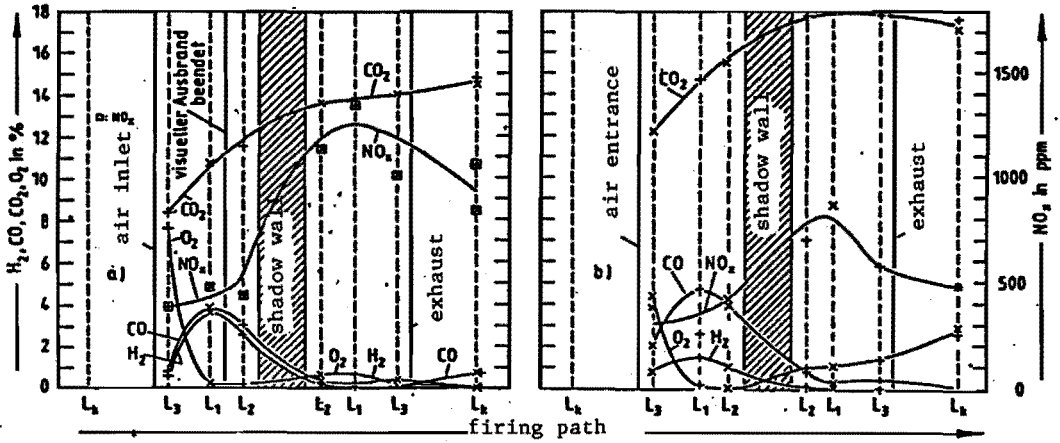


**Figure 1.5a:**  
 Concentrations of  $CO_2$ ,  $CO$ ,  $H_2$ ,  $O_2$  and  $NO_x$  as a function of the flame path length in a natural gas flame from reference [11].

**Figure 1.5b:**  
 Composition of heavy oil flame as a function of the flame path length reference [11].

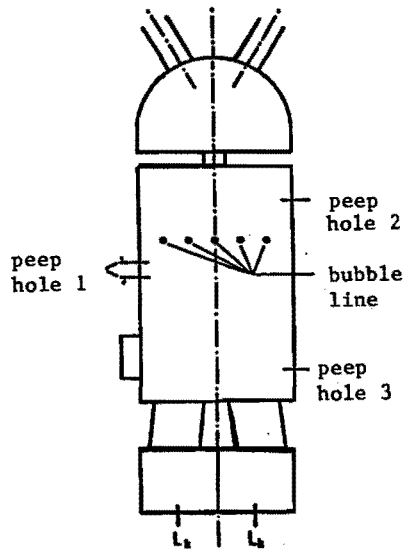


**Figure 1.5c:** End-port furnace with indicated flame pattern and positions for UV-observations.

### 1.1.1.5 Other aspects of mineral fuel combustion .

The maximum temperature of the flames is limited by the heat resistivity of the superstructure of the glass melting tank. The amount of burners of the furnace depends on the furnace dimensions and furnace type (side fired, end-port fired, regenerative or recuperative).

Exhaust gas compositions of a natural gas and a mineral oil fired glass furnace are given in table 1.3.

Table 1.3: Typical exhaust gas composition\*) for natural gas and mineral oil fired furnaces (air excess = 10%).

component	natural gas vol.%	mineral oil with 1.5% - sulphur vol.%
N <sub>2</sub>	71 - 73	73 - 74
CO <sub>2</sub>	9.0 - 10.0	11.5 - 12.5
O <sub>2</sub>	2.0	2.0
H <sub>2</sub> O	18.0 - 19.0	11 - 13
SO <sub>2</sub> + SO <sub>3</sub>	< 0.0005	0.04

\*) without fuel impurities and batch volatiles.

From this table it is shown that formation of sulphur oxides is an additional problem especially in case of oil combustion.

Sulphur oxides play an important role in:

- corrosion mechanisms in heat exchangers;
- salt formation in exhaust gases;
- gaseous emissions of glass furnaces.

The sulphur concentration in natural gas varies from 0 to 0.02 weight-% and in the used oils from 0.5 to 2.0 weight-%. Sulphur dioxide is the main product and minor concentrations of sulphur trioxide are formed.

The reaction:



proceeds very slowly and the equilibrium moves to the right only at temperatures below 1000 K. At high temperatures the reaction:



may take place in the initial stages of the flame because of the dissociation of molecular oxygen enhanced by radiation or collision of oxygen molecules with activated carbon dioxide molecules:



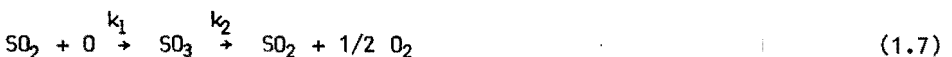
or



According to Hedley [12] these dissociations determine the oxidation process of sulphur dioxide to sulphur trioxide in oxygen rich environments. These reactions proceed reversely from the reactions to obtain equilibrium composition at these temperatures.

Hedley gives an explanation by assuming that the concentration of sulphur trioxide may exceed the equilibrium concentration during the first 100 msec. see figure 1.6.

The initial formation and reversely the proceeding dissociation as thermodynamically favoured, may be presented as:



\*) h.v indicates the energy supplied by radiation.

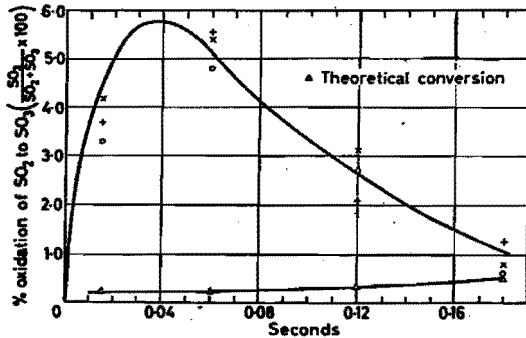


Figure 1.6: The concentration of SO<sub>3</sub> in an air rich flame during the initial stages according to reference [ 12 ].

The first reaction appears to be a first order reaction in the atomic oxygen concentration. The second reaction is a relatively slowly proceeding one. This results in temporary 'high' sulphur trioxide concentrations. So sulphur trioxide may be formed in the flame at temperatures above 1800 K see figure 1.6. Generally conversion of sulphur oxides is thermodynamically favoured at temperatures below 1200 K.

This process is limited by the slow kinetics at lower temperatures. However, silica dust and vanadium oxides enhance sulphur dioxide oxidation in regenerators or recuperators.

The combustion of natural gas is a cleaner process than that of fossil oil. However, nitrogen oxide formation is slightly increased by the combustion of natural gas according Kircher [ 13 ]. The impurities of fossil oils are mainly: sulphur, vanadium, nickel and sodium, see table 1.4.

Gaseous vanadium oxides have severe corrosive properties (Christof et al [ 14 ], Jones et al [ 15 ]) and may damage the bonding structure of the upper part of the regenerator checkers. Both nickel and vanadium compounds may affect the glass making process or colour the glass melt.

In the glass industry mineral oils are sometimes preferred because of the higher emissivity of oil flames. However, the heavy metal impurities in mineral oils will be an important disadvantage for the use of oil, unless newly developed filter installations are applied to clean the exhaust gases of the furnaces.

Table 1.4: Metal/Sulphur impurities in fossil oils in ppm (mg/kg).

	Venezuela oil	US oil	Middle East
Vanadium	0 - 30	0.7 - 2.0	3 - 100
Nickel	0.3 - 6.0	0.8 - 1.2	6 - 30
Sodium	10 - 30	3 - 40	0 - 1.0
Total ash	< 1000	< 500	< 250
Sulphur	0.55 - 2.5%	0.25 - 0.35%	1.5 - 2.5%

### 1.1.2 Volatilization from the glass melt

In the last twenty years a lot of attention has been paid to the vaporization of glass components from the glass melt. Formerly it was thought that the dust emitted from the exhaust originates from batch carry-over particles. Although particles from the batch are entrained in the turbulent exhaust gases, the main part of the deposits and dust is formed from the volatilized matter vaporized from the batch or the melt. In soda-lime glass melting tanks, sodium and sulphur compounds are the most important vapors from the melt. Lead oxides vaporize from lead glass tanks and boron compounds are volatile in borosilicate melters.

The concentrations of the chemical elements in the exhaust gases of glass furnaces exclusively combustion products ( $O_2$ ,  $N_2$ ,  $H_2O$ ,  $CO_2$ ) are given in table 1.5 for several glass furnaces.

The concentration of a certain element in the exhaust gas exit of the combustion chamber can be calculated with formula (1.8):

$$P_i = \frac{(x_i * B + Z_i * F + a_i * A - y_i * G)}{M_i * E * 40} \quad (1.8)$$

where:

$P_i$  = partial pressure of element i in the exhaust gas (atm.)

$x_i$  = weight fraction of element i in the batch

$y_i$  = weight fraction of element i in the produced glass

$a_i$  = weight fraction of element i in the combustion air

$z_i$  = weight fraction of element i in the fuel

$E$  = exhaust gas flow ( $m_n^3/hr$ )

$B$  = batch input (kg/hr)

$G$  = glass output (kg/hr)

$A$  = combustion air input (kg/hr)

$F$  = fuel input in kg/hr

$M_i$  = molecular mass of element i (kg/mol).

\*  $P_i$  is assumed for the calculations as the partial vapor pressure of the total concentration of element i, assumed as a gaseous atomic compound.

Table 1.5: Exhaust gas compositions from different glass furnaces, mentioned in table 1.6 (from industrial reports and from several literature sources) concentrations\*) in volume ppm.

furnace	As	S	Cl	Na	K	Pb	B	F
A	-	1200	60	100	10	-	-	-
B	20	160	60	100	10	-	-	-
C	-	190	50	100	-	-	-	-
D	-	1200	-	30	80	-	900	600
E	-	1340	-	-	-	160	-	-
F	-	-	5	16	25	120	-	-
G	-	160	10	500	100	-	600	-
H	-	-	-	5	40	-	70	-

\*) assumed as gaseous elements in combustion gases.

Table 1.6: Glass furnace types and glass compositions for the exhaust compositions of table 1.5.

Furnace	Description
A	container glass - side-port fired 71% SiO <sub>2</sub> - 1.5% Al <sub>2</sub> O <sub>3</sub> - 0.3% Fe <sub>2</sub> O <sub>3</sub> regenerative furnace, 10% CaO - 1% MgO - 14% Na <sub>2</sub> O - fuel: oil 1% K <sub>2</sub> O
B	container glass - side-port fired 71% SiO <sub>2</sub> - 1.5% Al <sub>2</sub> O <sub>3</sub> - regenerative furnace, 0.3 % Fe <sub>2</sub> O <sub>3</sub> 10% CaO - 1% MgO - fuel: natural gas 14% Na <sub>2</sub> O - 1% K <sub>2</sub> O
C	flat glass - side-port fired 72% SiO <sub>2</sub> - 1.5% Al <sub>2</sub> O <sub>3</sub> - regenerative furnace, 8% CaO - 3% MgO - 14% Na <sub>2</sub> O - fuel: natural gas 1% K <sub>2</sub> O - 0.3% SO <sub>3</sub>
D	borosilicate glass - recuperative furnace, 5% B <sub>2</sub> O - 16% Al <sub>2</sub> O <sub>3</sub> - 20% CaO fuel: oil 54% SiO <sub>2</sub> - 0.5% K <sub>2</sub> O - 4.5% MgO
E	lead glass - side-port fired 37% PbO - 45% SiO <sub>2</sub> - 4.5% K <sub>2</sub> O regenerative furnace, 2.7% Al <sub>2</sub> O <sub>3</sub> - 2% CaO - 1.7% Na <sub>2</sub> O fuel: oil
F	lead glass - side-port fired 29.5% PbO - 56.3% SiO <sub>2</sub> - 7.2% K <sub>2</sub> O regenerative furnace, 1.3% Al <sub>2</sub> O <sub>3</sub> - 4.7% Na <sub>2</sub> O fuel: natural gas
G	sodium-borosilicate glass - recuperative furnace, 5% B <sub>2</sub> O <sub>3</sub> - 11% Na <sub>2</sub> O - 73% SiO <sub>2</sub> fuel: natural gas 2% Al <sub>2</sub> O <sub>3</sub> - 9% CaO
H	borosilicate glass - electrical melting 5% B <sub>2</sub> O - 16% Al <sub>2</sub> O <sub>3</sub> - 20% CaO furnace 54% SiO <sub>2</sub> - 0.5% K <sub>2</sub> O - 4.5% MgO

### 1.1.2.1 Volatilization and particulate entrainment in furnace atmosphere

Several investigators [16, 17, 18] studied the composition of batch carry-over and volatilization products in flue gases of industrial glass melting furnaces.

The used methods are:

1. analysis of deposition products on a water-cooled paddle positioned at the entrance of regenerator ports;
2. analysis of deposition products on a platinum deposition paddle kept at furnace temperature and positioned at the entrance of a regenerator port;
3. analysis of isokinetic sampled gas volumes from the exhaust gases in regenerator ports.

Busby and Sengelow [16] used the first and second method for the analysis of particulate matter and volatilized matter carried by the exhaust gases from soda-lime glass furnaces. The furnaces under investigation were side-port or end-port fired using either oil or natural gas as energy source. The samples from method 1 consist of deposited particulate and condensed volatile matter of the furnace atmosphere.

Samples from method 2 probably only consist of the particulate or liquid matter in the furnace gases. From Busby's investigations it is concluded that volatilization of sodium and sulphur compounds from the glass melt is the main vaporization process. Vaporization of sodium compounds from the soda of the raw material batch will result in rather high sodium contents as compared to the contents of sulphur compounds in the furnace atmosphere above the batch in case of natural gas firing.

However, from the results of the analysis of the deposits from method 1 in the regenerator port near the batch entrance, it appeared that the  $\text{Na}_2\text{O}/\text{SO}_3$  ratios were lower than 1. From this result it seems that vaporization of sodium compounds from the raw batch material has a minor effect on the vaporization process.

Chlorides, resulting from the vaporization of minor sodium chloride impurities in synthetic soda have been detected. Silica, calcium oxide, alumina and sodium compounds have been analysed as the major components in the deposits of the particulate matter, obtained by method 2. Vanadium oxides have been detected in considerable amounts in the particulate matter.

Lyke and Byars [18] investigated the dust and gas composition of isokinetically sampled gas volumes from glass furnace atmospheres. The most important components were sodium and sulphur (sodium sulphate) and in case of the use of synthetic soda ash also chlorides. Calcium, magnesium and water insoluble components, formed the remainder of the samples. The addition of water to the raw material batch caused a reduction of the total dust emission with 30%.

#### 1.1.2.2 Volatilization mechanism

Although a lot of research has been done into the nature of the processes that determine volatilization from batch material and glass melt, the vaporization mechanisms have not yet been fully understood. The need to understand the involved vaporization processes arises from four aspects:

1. vaporization may cause a lack of volatile compounds in the glass products.
2. the composition of the surface glass may be different from the bulk glass composition; surface glass may be folded into the melt causing inhomogeneities in the parent glass.
3. volatilized glass components may damage refractory materials of the regenerators.
4. volatilization is the main cause for the emission of dust particles from the exhaust of glass furnaces.

The transport of glass components from the parent glass melt to the gas atmosphere of the furnace proceeds successively via:

- diffusional transport in the glass phase towards the glass-gas interface through a surface layer with a varying composition;
- vaporization and/or reaction at the glass surface resulting in conversion of glass constituents in volatile components;
- transport of the gaseous components from the gas/glass interface towards the gas atmosphere of the furnace;

- convective transport of the volatiles in the flue gas flows in the combustion chamber.

Volatilization may be enhanced by reactions of glass components with components of the gas atmosphere.

Constituents of the furnace atmosphere may enhance or reduce vaporization rates for certain glass components. The atmosphere of an industrial glass melting furnace is never saturated with components evaporated from the glass melt. The transport of the chemical compounds from the glass melt surface to the convective gas flow in the combustion chamber is determined by the diffusion through a gaseous boundary layer formed on the combusted gases above the melt. In case this transport through this boundary layer is the rate-determining step, vaporization will increase with the relevant Sherwood number for the flow conditions under consideration [19]. The Sherwood number increases proportionally to the square root of the gas velocity near the surface of the glass melt. Higher gas velocities result in increasing vaporization rates. An increase of the fuel consumption per square meter of melting area enhances the vaporization, but normally will decrease the amount of volatilized matter per unit of exhaust gas volume.

From the investigated literature it is clear that the vaporization mechanism depends on:

- the glass composition;
- the gas flow rate along the glass surface;
- the composition of the gas phase;
- the temperature.

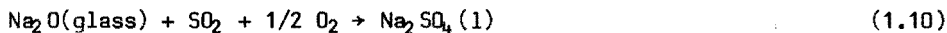
For the most relevant glass compositions these volatilization mechanisms are discussed in the following sections.

#### **a. Soda-lime glasses**

According to the investigations of Hanke and Scholze [22] vaporization of sodium components from soda-lime glasses is enhanced by the water vapor in the atmosphere.



The same conclusion is drawn by Conradt et al [19] from experiments with undersaturated gas flows above the glass melt. In the experiments of Conradt the gas flow was chosen at such a level that the vaporization rates are independent of the gas velocity. It is assumed that these experiments resemble the practical situation to a certain degree. Sanders et al [21] have shown that the volatilization of sodium compounds is increased by high partial sulphur dioxide pressures in an atmosphere above a well-stirred soda-lime glass melt. The sulphur oxide vapor pressures in their experiments exceeded the practical values till pressures up to 80 mbar. Dissolution of sulphur trioxide in the glass melt at these vapor pressures for sulphur dioxide resulted in increasing sodium sulphate activities in the melt. This effect is significantly lower in case of industrial glass melting furnaces where sulphur dioxide vapor pressures are below 5 mbar. Sodium sulphate in the well-stirred experiments of Sanders tends to volatilize molecularly. The total process may be explained by reactions (1.10) and (1.11):

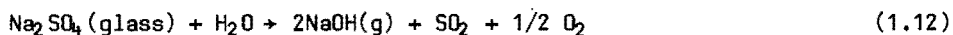


However, for a non-stirred glass in an undersaturated gas atmosphere, as is generally the situation in industrial glass melting furnaces, Conradt found a different behaviour: up to vapor pressures of 5 mbar sulphur dioxide hardly enhances vaporization from soda-lime glasses in a water containing atmosphere.

This behaviour was also found for soda-lime glasses with 0.22 weight-% sulphur trioxide. According to Conradt's investigations the reactions (1.10) en (1.11) are of minor interest for non-stirred melts. The sodium sulphate vaporization expected from the composition of the parent glass with 0.22%  $\text{SO}_3$  with high sodium sulphate chemical activities, was not significant for Conradt's experiments.

Reduced surface concentrations of sodium sulphates in the glass suppressed the vaporization expected from reaction (1.11). Only at high  $\text{SO}_3$  concentrations in the glass, a surface layer of sodium sulphate was separated from the glass melt.

This layer gave rise to a congruent sodium sulphate vaporization process as shown by reaction (1.11). The vaporization rates from these glasses were comparable with the volatilization rates from pure sodium sulphate, according to Conradt. Reaction kinetic limitations cause the inhibition of the reaction:



No increase in sodium sulphate vaporization was measured at increasing water vapor pressures. For practice this means that for commercial soda-lime glasses (sodium sulphate concentrations lower than 0.5 weight-%) the most important vaporization reaction is the formation of gaseous sodium hydroxides.

Sulphur oxides from the melt are presumably formed during the refining stage, see reaction (1.13):

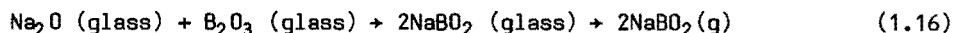


#### **b. Sodium-borosilicate glasses**

Wenzel and Sanders [23] studied the volatility of sodium-borosilicate glasses in water containing atmospheres. The used glass composition (16.5 mol.%  $\text{Na}_2\text{O}$ , 16.5 mol.%  $\text{B}_2\text{O}_3$ , 67 mol.%  $\text{SiO}_2$ ) with the sodium metaborate stoichiometry, is expected to vaporize nearly congruently. The reactions (1.14) and (1.15) are believed to be of minor interest for this system.



The activities of the sodium metaborates in the stirred glass melt are relatively high compared to the sodium oxide or borium oxide activity. The main reaction is given by (1.16):



With high water concentrations in the furnace atmosphere the sodium vaporization decreased, no explanation was given for this fact. Although reaction (1.16) is predominant, the amount of vaporised boron slightly exceeds the amounts of vaporised sodium components, probably as a result of  $\text{Na}_2\text{B}_4\text{O}_7(\text{g})$  formation.

Conradt [19] concluded from his study that at high water vapor pressures a surface film is formed in the industrial glass melts. The surface film thickness will grow to a certain degree resulting in decreasing vaporization rates from the melt of this kind of glass.

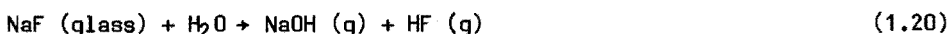
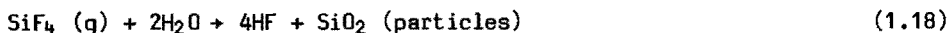
After a certain time the volatilization becomes time-independent. The decreasing vaporization rate of sodium-borosilicate glasses as the water vapor pressure increases is due to the strongly influenced diffusion of sodium or boron compounds through the layer. Formation of surface films with strongly changing compositions relative to the parent glass is enhanced by the water vapor content of the furnace atmosphere.

The volatilization rate of boron and sodium components from borosilicate glasses decreases considerably at increasing silica contents and decreasing sodium contents. An increase of the melting temperature with 50 K increases the total vaporization rate of borosilicate glasses with equivalent boron and sodium concentrations, with a factor 2. For high  $\text{B}_2\text{O}_3$ -concentrations relative to  $\text{Na}_2\text{O}$ -concentrations, vaporization of boron components as  $\text{HBO}_2$  is expected, according to Wenzel et al [23].

### c. Glasses with fluorides

Fluorine containing components are sometimes added to the glass batch to accelerate the melting process and to decrease the viscosity of the glass melt. Fluorides are also applied as opacifying agents for opal glasses. The scattering particles in these glasses are often  $\text{NaF}$ ,  $\text{BaF}_2$  or  $\text{CaF}_2$ . The fluoride retention factor in opal glasses varies from 50% to 70%, as determined by Parker et al [26]. The volatilization of fluorides is obvious and this not only increases fluoride concentrations in the exhaust gases but also silicium and sodium concentrations increase, due to reactions (1.17) to (1.20).





The vaporization rate of sodium fluorides and silicium fluorides at temperatures below 1300 K is mainly determined by the diffusion in the glass through a rather thick surface layer.

However, at higher melting temperatures this surface layer is mixed with the parent glass due to surface tension gradients and density gradients. This enhances the vaporization rates of fluorine containing species from industrial glass melts.

However, sodium fluorides as impurities in the raw materials may also vaporize from the batch material. Fluoride emissions from glass melts containing 1 weight-% fluorides may exceed values of 400 volume ppm in the exhaust gases. According to Scholze et al [26], reaction (1.20) has been proven to be the vaporization determining step. Rather high silicium oxide concentrations in the dust of the exhaust gases from fluoride rich glass melting furnaces are expected due to reaction (1.18).

#### **d. Lead glasses**

Matousek et al [27] investigated vaporization of potassium and sodium containing components from  $\text{Na}_2\text{O} - \text{K}_2\text{O} - \text{PbO} - \text{SiO}_2$  glass melts with different compositions.

However, their experiments were carried out in a Knudsen effusion cell; the influence of the composition of the gaseous atmosphere was not under investigation. From their results Matousek concluded that elemental sodium and potassium evaporates at temperatures above 1200 K. Lead oxides vaporize from glass melts in vacuum especially above 1300 K.

In practice water vapor enhances vaporization of alkali components from alkali-lead glasses. Conradt [19] has shown the influence of the water vapor on lead vaporization from lead glass melts in experiments carried out under conditions that resemble the practical situation.

From his experiments Conradt expected that lead oxides or lead hydroxides are the predominant constituents of the vapor phase above the glass melt of a 15  $K_2O$  . 25  $PbO$  . 60  $SiO_2$  glass melt in a water containing atmosphere. Matousek and Hlavac [27] studied the volatilization mechanism of a 24%  $PbO$  glass in a nitrogen atmosphere.

The vaporization rates are determined by the diffusion of  $PbO$  through the melt and the vaporization at the surface. The glass under study contained also 10 weight-%  $K_2O$  and 4.5 weight-%  $Na_2O$ . More than 90% of the volatilized matter consisted of lead oxides.

The addition of water to the atmosphere enhanced the lead oxide vaporization and lead oxide impoverishment of the glass surface. In industrial lead glass furnaces volatilization from lead oxides is mainly controlled by the diffusion in the glass melt. The retention factor for the added lead oxides in the glass is approximately 95% in industrial glass furnaces.

### 1.1.2.3 Conclusions

The vaporization mechanisms in industrial glass melting furnaces depend primarily on the glass composition and the composition of the furnace atmosphere. Water vapor increases alkali vaporization from soda-lime and alkali lead glasses, and also enhances the vaporization of lead components. Vaporization of sodium-borosilicate melts is hardly increased by water vapor in the atmosphere. Sulphur oxides in the furnace atmosphere are of minor importance for the vaporization of alkali components from commercial glass compositions. Reactions with constituents of the furnace atmosphere at the glass surface may enhance or reduce volatilization processes.

The vaporization rates are partly controlled by the diffusion of sodium oxide in the glass melt of soda-lime glasses in industrial furnaces. This diffusion limited vaporization is of major importance for borosilicate glasses and rather important for lead oxide vaporization from lead oxide glasses. Fluorides are generally very volatile in opal glass melts.

### **1.1.3 Heat exchanging devices in the glass industry**

The total heat input in the glass melting furnace via fossil fuels is normally reduced by the use of heat regenerating or heat recuperating systems. Combustion air is preheated by the hot exhaust gases leaving the combustion chamber of the furnace. Heat exchanging efficiencies up to 40% have been achieved by the use of metallic radiation recuperators and up to 70% in regenerative systems.

The furnace design is strongly dependent on the heat exchanger type. In this paragraph a description of the different heat exchanging devices is given as a base for the study of the condensation and the deposition behaviour in exhaust gas channels.

#### **1.1.3.1 Regenerative systems**

Regenerators are commonly used in the glass industry. A regenerative glass furnace is always equipped with two regenerators, a regenerator is normally divided into chambers. The incoming combustion air passes through one regenerator filled with hot refractory bricks and is heated up to 1400 K to 1600 K. This air is then introduced to the combustion chamber of the furnace where it is mixed with the fuel.

Two types of regenerative furnace systems are schematically presented in figures 1.1 and 1.2b. The regenerator of a side-port fired furnace generally consists of 3 to 8 chambers, each chamber has been connected to the furnace by a port. A lattice of refractory bricks in a regenerator chamber is heated by the exhaust gases and subsequently cooled by the combustion air.

The temperature of the exhaust gas at the regenerator entry is 1650 to 1850 K. The temperature and mass flow of the exhaust gases in the chambers near the hot spot location of the furnaces are higher than in the other parts of the regenerator.

In the regenerator the exhaust gases are cooled down to 700 K - 850 K. Figure 1.7 shows the temperature distribution of the exhaust gas, the air and the bricks of a regenerator.

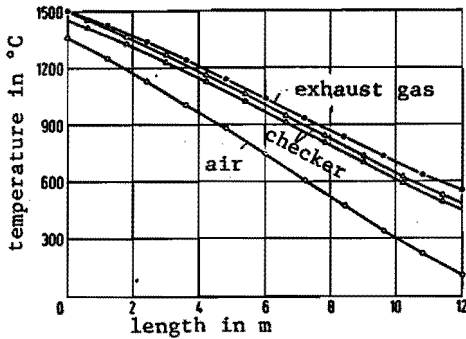


**Figure 1.7:** Distribution of the temperatures of the exhaust gas, combustion air and checker bricks in the exhaust gas flow direction of the regenerator [ 1 ].

According to results of mathematical calculations the temperature variation of the exhaust gas during the regenerator heating period at a certain location is approximately 25 K to 35 K [ 1, 28, 29 ]. The same difference of the local air temperature of 25 K to 35 K is calculated between the beginning and the end of the air preheat period. According to Barklage-Hilgefort [ 29 ] the local temperature differences between air and the surface of the brick is 100 K to 350 K. Temperature differences between the local exhaust gas and brick surface are considerably lower: approximately 30 K to 100 K.

The relatively low temperature differences between the brick surface and the local exhaust gas temperatures are a result of the heat exchange coefficient between exhaust gas and brick being higher than those between the brick and the air. The temperature variations in a regenerator brick are dependent on the thickness of the brick, the heat capacity and heat conductivity of the brick.

The temperature difference between the surface and the centre of the brick varies between 20 K and 40 K in most cases. The mean heat transfer rate of a regenerator system mainly depends on:

- regenerator volume
- total heat exchanging area
- heat conductivity and capacity of the refractories
- geometry of the checker
- geometry of the bricks.

The different types of regenerator checkers commonly used in the glass industry are given in figure 1.8.

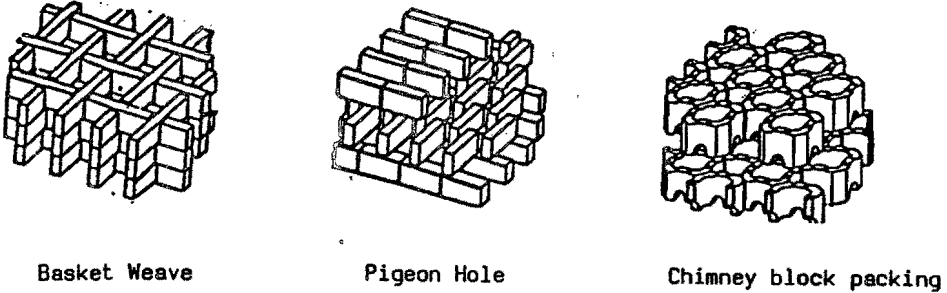


Figure 1.8: Different regenerator packings for the glass industry [30].

The passage-width in the checker work varies from 100 x 100 mm to 200 x 200 mm, but may also be rectangular. The exhaust gas velocities and combustion air velocities for a typical glass furnace regenerator are 0.4 to 1 m/s (1013 mbar, 295 K).

The flow conditions (characterized by the Reynolds number) determine the heat transfer in the regenerator, see figure 1.9.

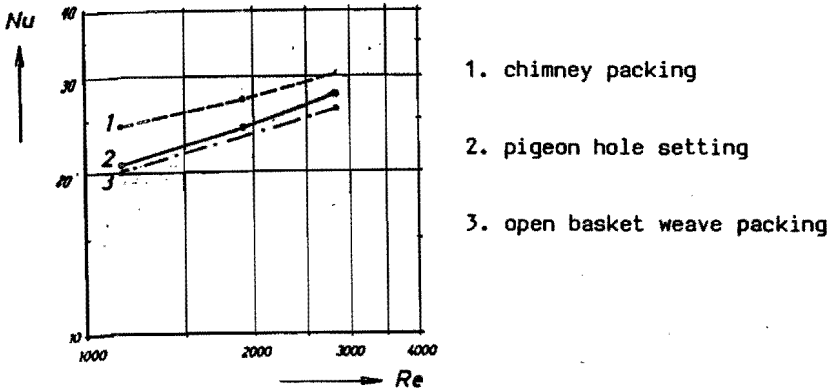


Figure 1.9: The dimensionless presentation of the heat transfer from the exhaust gas to the air by the checker work as function of Reynolds [31].

The increase in the Nusselt number is approximately proportional to the increase in the Reynolds number for the gas flow in the regenerator channels, relation (1.22). The Nusselt and the Reynolds number are related to the hydraulic diameter of the passages.

$$Nu = A + B \cdot Re \quad (1.22)*$$

\* In a more correct approach the Reynolds number is given by (1.22a):

$$Re = Re_f + a \cdot \frac{Gr}{Re} \quad (1.22a)$$

where:

$Re_f$  = Reynolds number based on the gas velocity.

$Gr$  = Grashof number

$a$  = empirical factor.

A detailed description for the Nusselt number as a function of the flow characteristics is given by Gramatte et al [31].

The same approach may be used for the description of the dimensionless Sherwood number for mass transport:

$$Sh = A' + B' \cdot Re \quad (1.23)$$

The factors  $A$ ,  $A'$ ,  $B$  and  $B'$  depend mainly on the geometry of the checker work. The Reynolds numbers for regenerator situations vary from 1000 to 5000. The Nusselt number varies from 10 to 30. Deposition of material condensed from the exhaust gases of the glass furnaces results in a decreasing heat transfer.

According to Trier [1] the thermal efficiency of a regenerator will decrease annually by 2 to 4%, by deposition of salt components from the exhaust gases.

### 1.1.3.2 Recuperative systems

Glass furnaces with glass melting capacities lower than 100 tons/day are often equipped with a recuperator. A recuperative furnace is continuously fired, the exhaust gases preheat the combustion air in mostly metallic recuperators.

The air preheat temperatures are limited by the maximum admissible metal temperature. The exhaust gases and the combustion air are separated by a metallic pipe or tube. One recuperator type is presented by figure 1.10.

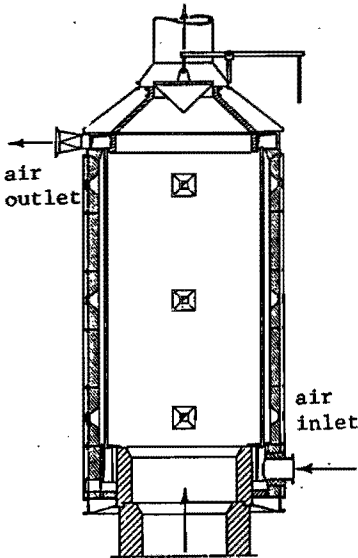


Figure 1.10: Radiator recuperator.

The recuperator is often a double-wall tube with an inner diameter of 0.5 - 1.0 m. The exhaust gases flow through the inner tube and the combustion air passes the space between the inner and outer tube in counter flow or in the same direction as the exhaust gas flow.

The heat transfer from the hot exhaust gas is partly radiative and partly convective, depending on exhaust gas temperature and exhaust gas velocity. Exhaust gases are cooled from 1450 K - 1600 K to 1000 K - 1150 K and the air is preheated to 850 K - 1100 K.

The flue gas velocities in the recuperator vary from 1 to 3 m/s (1013 mbar, 295 K). The heat transfer may slightly decrease during the furnace campaign, caused by deposition of exhaust gas condensates.

### 1.1.4.3 Waste heat boilers

Glass producers may often require steam for secondary manufacturing processes. Exhaust gases from regenerators but particularly from recuperators contain large amounts of sensible heat.

However, recovery of this heat by means of steam or warm water generation in heat exchangers may be troublesome because of fouling and corrosion of the heat exchanger materials by the exhaust gases. Figure 1.11 shows a waste heat reboiler system behind a recuperative furnace.

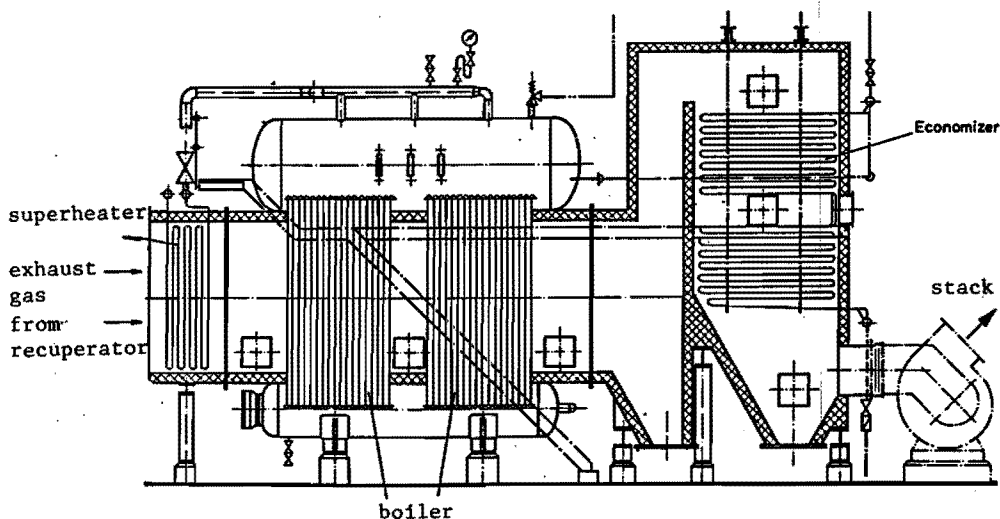


Figure 1.11: Waste heat boiler behind a recuperator, Kölsch [33].

The corrosion of waste heat boilers below the dew point of the acids in the exhaust gases of oil-fired furnaces may be a severe problem and limits the heat exchanger temperature to values above 450 K.

Waste boiler systems are described in detail in the relevant literature [32, 33, 34].

## 1.2 Exhaust gas emissions from the glass industry

### 1.2.1 Introduction

The exhaust gases consist of combustion products, air components, volatilized matter from the melt and batch carry-over material. Dust formation of condensed matter from the exhaust gas constituents results in emission of solid particles at stack gas temperatures between 500 K and 700 K. This dust may contain hazardous components like lead, boron or fluorides depending on glass and batch composition. Gaseous constituents from the stack of glass furnaces may be:

- nitrogen oxides;
- sulphur oxides;
- chloric acid;
- boric acid;
- fluoric acid.

These components are harmful for vegetation, animals and human life because they accumulate in the ambient air and in the soil. However, the glass industry is a minor pollutant as compared to power plants, steel industries, chemical industries, oil refineries and automobiles. The chemical elements in the exhaust gases, with the exclusion of the combustion products have been given by table 1.5 of section 1.1.3.

### 1.2.2 Gaseous emissions from glass melting furnaces

#### Nitrogen oxides

The combustion of fossil fuels in the glass melting furnace is a high temperature process, flame temperatures of 2000 K are common in the combustion chamber. These high temperatures cause formation of nitrogen oxides in the flame, see paragraph 1.1.1.4. The nitrogen oxide compounds are mainly NO and minor amounts of NO<sub>2</sub>. Kircher [13] has measured nitrogen oxide concentrations in the exhaust gases of different glass melting furnaces, see figure 1.12.

Denitrification of the stack gases is possible by injection of ammonia and hydrogen in the exhaust gases at temperatures of 950 K - 1200 K, reaction (1.24):



Catalytic denitrification processes were recently developed for temperatures of approximately 600 K.

### Sulphur oxides

The presence of sulphur oxides in the exhaust gases of glass furnaces is caused either by dissociation of the sulphates in the glass melt or the combustion of sulphur containing fuels.

At high temperatures, above 1100 K sulphur dioxide is the most stable sulphur containing component. Sulphur trioxide is produced in the flame as a metastable compound, but the dissociation into sulphur dioxide and oxygen is a rather slowly proceeding process (see section 1.1.1.5).

Below 1100 K sulphur oxides react with:

alkali hydroxides, lead oxides or other inorganic compounds resulting in formation of sulphates. The remainder may react with oxygen to sulphur trioxide, but normally only 5% - 10% of the sulphur oxides in the stack gases consists of sulphur trioxide. This sulphur trioxide reacts with water at temperatures between 400 K and 500 K resulting in formation of the corrosive sulphuric acid. High concentrations of gaseous sulphur compounds have been measured in exhausts of oil-fired furnaces.

### Chloric acid

The emission of gaseous chloride components rarely exceeds concentrations of 40 volume-ppm. Sodium chloride is an impurity in synthetic soda ash or is added to the glass melt as refining agent. Condensation of alkali chloride compounds from exhaust gases only takes place in cases where the amounts of sulphur oxides are insufficient to convert all the alkali containing species into sulphates.

This is not the case for most glass melting furnaces. The main part of the chlorides vaporized from the batch or the melt is converted into chloric acid (HCl) and in that form emitted from the stack.

### Fluoric acid

Fluoric acid may cause severe damages to the health of vegetation, animal life and human life. Fluoride containing components like  $\text{CaF}_2$  improve the melting rate and lower the viscosity of the melt.

These components are very volatile and retention factors vary from 0.5 to 0.7, in for instance opal glass melts, as mentioned previously. Fluorine containing components are converted mainly to HF, in these stack gases.

#### Boric acid

The vaporised boron compounds,  $\text{NaBO}_2$  or  $\text{HBO}_2$  are converted to condensed phases of  $\text{NaBO}_2$  and  $\text{Na}_2\text{B}_4\text{O}_7$ . The non-condensed boron is present in the stack gas as boric acid ( $\text{H}_3\text{BO}_3$ ). The concentrations of  $\text{H}_3\text{BO}_3$  in the stack gases vary from 0 to 200 volume ppm.

### **1.2.3 Dust formation and emission from the stack of glass melting furnaces**

Batch carry-over particles or liquid droplets partly remain in the regenerator or recuperator but the largest amount is transported to the chimney by the exhaust gases. These particles mainly exist of silica dust, alumina, feldspar and limestone.

However, condensation of gaseous compounds is the major cause of dust formation, resulting in emission of alkali sulphates, alkali borates, lead oxides, or other particulate matter.

Lead, fluorine and boron containing dust may be hazardous for the environment and the emission of these components has to be limited by use of filter installations.

The most important solid components in non-filtered stack gases of several glass furnaces are listed in table 1.7. The lead glass furnace produces glass of the following composition (in weight-%):

48  $\text{SiO}_2$  - 35  $\text{PbO}$  - 10  $\text{K}_2\text{O}$  - 2  $\text{CaO}$  - 2  $\text{Na}_2\text{O}$  - 3  $\text{Al}_2\text{O}_3$

The composition of the sodium borosilicate glass is approximately:

66  $\text{SiO}_2$  - 14  $\text{Na}_2\text{O}$  - 2  $\text{K}_2\text{O}$  - 3  $\text{Al}_2\text{O}_3$  - 6  $\text{B}_2\text{O}_3$  - 7  $\text{CaO}$

The values given in this table are rough estimates from the studied literature or from own measurements.

Alkali, lead, silicium and calcium components exist only as small particles or dust in the stack gases of the furnaces. The emission of dust particles is mainly caused by vaporization of sodium or lead components from the glass melt as described in 1.1.2.

Table 1.7: Dust emission from glass furnaces in mg/m<sup>3</sup> (based on 8 vol.% O<sub>2</sub> in stack gas).

	oil-fired container glass [ 14]	gas-fired container glass [ 14]	gas-fired flat glass	oil fired lead glass	gas-fired borosilicate glass [36]
Na <sub>2</sub> SO <sub>4</sub>	140	180	100	nihil	< 100
NaHSO <sub>4</sub>	140	3	-	-	-
NaCl	-	-	20	-	-
K <sub>2</sub> SO <sub>4</sub>	5	5	100	100	20
PbO	-	-	-	300	-
PbSO <sub>4</sub>	-	-	-	1500	-
NaBO <sub>2</sub>	-	-	-	-	1000
Na <sub>2</sub> B <sub>4</sub> O <sub>7</sub>	-	-	-	-	500
CaSO <sub>4</sub>	20	20	20	-	10
Al <sub>2</sub> O <sub>3</sub>	nihil	nihil	5	nihil	nihil
SiO <sub>2</sub>	nihil	nihil	5	nihil	nihil

The size of sodium sulphate particles varies from 0.05 µm to 20 µm. Reduction of particulate emissions is possible by:

- Changes in melting behaviour, a temperature increase of 50 K corresponds with a 30% higher dust emission from soda lime furnaces.

- Batch pretreatment, like agglomeration of raw materials by means of pelletizing may reduce the entrainment of fines in the exhaust gases.
- Filtering processes, separating a large amount of the dust, mainly the coarse fraction, from the exhaust gases.
- The use of less volatile glass constituents, particularly in case of hazardous evaporating compounds.

#### **1.2.4 Filter installations**

Regulations to protect the environment of glass factories, have promoted the installation of dust filtering devices. The use of installations to separate hazardous gaseous components from flue gases is only occasionally applied in the glass industry. Below, a short description is given of several filter installations applied in the glass industry.

##### **- Electrostatic filters**

Particulate matter is electrically charged by a cathode. The positively charged particles are deposited on negatively charged plates, separating the dust stream from the exhaust gas.

The advantage is the small pressure loss of the exhaust gas by passing the electrostatic precipitator and the high permissible gas temperatures till 650 K. A disadvantage is the bad performance for poorly electrically conductive dust, (Noll [35]) and the electricity consumption of this installation.

##### **- Cyclones**

The separation of coarse particles may be carried out by the use of cyclones, well known for industrial applications. The disadvantage of such a system is the low separation efficiency for fine particles.

##### **- Filtering by fabrics**

The use of fabrics to separate particles from the exhaust gases is limited to cases of dry, non-sticking dust. The maximum temperature for which this method may be applied is 450 K. The separation efficiency for dust from soda lime glasses varies from 99.5 to 99.8%. In spite of this high efficiency, blockage and the pressure drop over the filter reduce the application possibilities of these filters in the glass industry.

## Literature references chapter 1

- [ 1] Trier W.;  
'Glasschmelzöfen'.  
Springer Verlag Berlin-Heidelberg-New York-Tokyo (1984).
- [ 2] Bechtel J.H., Blint R.J., Cameron J. Dash, Weinberger D.A.;  
'Atmospheric pressure premixed hydrocarbon - air flames: Theory and Experiment'.  
Combustion and Flame 42 (1981) 197-213.
- [ 3] Jensen D.E., Jones G.A.;  
'Reaction rate coefficients for flame calculations'.  
Combustion and Flame 32 (1978) 1-34.
- [ 4] Coffee T.P.;  
'Kinetic Mechanisms for Premixed, Laminar, Steady State Methane/  
Air Flames'.  
Combustion and Flame 55 (1984) 161-170.
- [ 5] Spalding D.B.;  
'Combustion and Mass Transfer'.  
Pergamon Press (1979).
- [ 6] Michelfelder S.;  
'Methoden zur Vorausberechnung von Feuerungen'.  
Glastechn. Ber. 50 (1977) 193-200.
- [ 7] De Waal H.;  
'De insmeltsnelheid van een glasgemeng'.  
Klei Glas Keramiek 3 (1982) 222-225.
- [ 8] Cooper A.R.;  
'Melting Kinetics'.  
Intern. Summerschool on continuous glassmaking, Cleveland 1980.
- [ 9] Abbasi H.A., Khinkis M.J., Fleming D.K., Kurzynske F.R.;  
'Reduced NO<sub>x</sub> emissions from gas-fired glass melters'.  
Wärme Gas International 34 (1985) 325-329.
- [ 10] Wakamatsu M., Shimizu S., Terada K., Kunugi M.;  
'Formation and decay of nitric oxide in the test furnace system  
from 1800 °C down to 500 °C'.  
XIII International Congress on Glass, Hamburg 1983, 221-226.

- [ 11] Barklage-Hilgefort H., Mergler K.W.;  
'Vergleichende UV - Beobachtungen an erdgas- und schwerölbeheizten U-Flammenwannen'.  
Glastechn. Ber. 54 (1981) 231-241.
- [ 12] Hedley A.B.;  
'A kinetic study of sulphur trioxide formation in a pilot scale furnace'.  
The mechanism of corrosion by fuel impurities from Johnson; Littler; Butterworths London (1963) 204-215.
- [ 13] Kircher U.;  
'Staub- und Schadgasemissionen von Glasschmelzwannen'.  
Glastechn. Ber. 51 (1978) 139-146.
- [ 14] Christof G., Rostami F.;  
'Schmelzmullitsteine gegen  $V_2O_5$ -Angriff in der Glasofengitterung'.  
XXVIII International Colloquium on Refractories Aachen (1985) 92-148.
- [ 15] Jones M.C.K., Hardy R.L.;  
'Petroleum ash components and their effect on refractories'.  
Trans. Brit. Soc. (1959), 3.
- [ 16] Busby T.S., Sengelow W.M.;  
'Sampling regenerator carryover'.  
Glass Technology 19 (1978) 47-53.
- [ 17] Moss J.F.;  
'Measurement of glass furnace carryover'.  
Am. Ceram. Soc. Bull. 44 (2) (1965), 163-166.
- [ 18] Lyke L.R., Byars J.B.;  
'Isokinetic sampling of glass batch carryover'.  
The Glass Industry (1981) 10-31.
- [ 19] Conradt R., Scholze H.;  
'Zur Verdampfung aus Glasschmelzen'.  
Glastechn. Ber. 59 (1986) 34-52.
- [ 20] Sanders D.M., Haller W.C.;  
'Effect of water vapor on sodium vaporization from two silica-based glasses'.  
Journal of the Am. Cer. Soc. 60 (1977) 138-141.

- [ 21 ] Sanders D.M., Wilke M.E., Hurwitz S., Haller W.K.;  
 'Role of water vapor and sulfur compounds in sodium vaporization during glass melting'.  
 Journal of the Am. Cer. Soc. 64 (1981) 399-404.
- [ 22 ] Hanke K.P., Scholze H.;  
 'Einfluss der Ofenatmosphäre auf die Verdampfung aus Glasschmelzen'  
 Glastechn. Ber. 50 (1977) 271-275.
- [ 23 ] Wenzel J.T., Sanders D.M.;  
 'Sodium and boron vaporization from a boric oxide and a borosilicate glass melt'.  
 Physics and Chemistry of Glasses 23 (1982) 47-52.
- [ 24 ] Oldfield L.F., Wright R.D.;  
 'The volatilization of constituents from borosilicate glass at elevated temperatures'.  
 Advances in Glass Technology Part I (With International Congress on Glass, Washington DC (1962) 35-51.
- [ 25 ] Parker J.M., Al-Dulaimy J.A.M., Q.A. Juma'a;  
 'Volatilisation from fluoride opal melts'  
 Glass Technology 25 (1984) 180-187.
- [ 26 ] Scholze H., Tünker G., Conradt R.;  
 'Verdampfung von Fluor aus Glasschmelzen und beim Einschmelzprozess'.  
 Glastechn. Ber. 56 (1983) 131-137.
- [ 27 ] Matousek J., Hlavac J.;  
 'A study of the volatilisation of lead glass'.  
 Glass Technology 12 (1971) 103-106.
- [ 28 ] Lenoir Ch., Meunier H.;  
 'A new mathematical model for the calculation of the regenerator in the glassworks furnaces'.  
 XXVIII International Colloquium on Refractories Aachen (1985)  
 263-273.
- [ 29 ] Barklage-Hilgefert H.;  
 'Zum Wärmübergang in Regeneratorgitterungen'.  
 XVIII International Colloquium on Refractories' Aachen (1985)  
 213-228.

- [ 30] Scheiblechner G.P.;  
'The case for Chimney Block Packing'  
Glass Industry (1984) 16-38.
- [ 31] Gramatte W., Horak J., Mögling g., Triesnig A.;  
'Messung des Konvektiven Wärmeübergangskoeffizienten an  
verschiedener Besatzsystemen für Regeneratoren von Glaswannen'.  
XXVIII International Colloquium on Refractories Aachen (1985)  
229-247.
- [ 32] Kölsch E.;  
'Abhitzeverwertung bei einer rekuperativ beheizten Glasschmelzwanne  
mit Abhitzekessel'.  
Glastechn. Ber. 52 (1979) 192-196.
- [ 33] Ehrich W.;  
'Abhitzekessel hinter Regeneratoren und Glasschmelzwannen'.  
Glastechn. Ber. 48 (1975) 173-180.
- [ 34] Webb R.L., Marchiori D., Durbin R.E., Wang Y.J., Kulkarni A.;  
'Heat Exchangers for Secondary Heat Recovery from Glass Plants'.  
Heat Recovery Systems 4 (1984) 77-85.
- [ 35] Noll C.G.;  
'Electrostatic precipitation of particulate emissions from the  
melting of borosilicate and lead glasses'.  
Glass Techn. 25 (1984) 91-97.

## NOMENCLATURE CHAPTER 1

$a_i$	weight fraction of element in the combustion air
$a$	empirical factor in relation 1.22a
$A$	empirical factor in relation 1.22
$A'$	empirical factor in relation 1.23
$A$	surface area of radiation ( $m^2$ ) relation 1.2
$A$	combustion air input (kg/hr) relation 1.8
$B$	batch input (kg/hr)
$B$	empirical factor in relation 1.22
$B'$	empirical factor in relation 1.23
$C_e$	concentration of fuel at stoichiometric mixing point ( $kg/m^3$ )
$C_o$	concentration of fuel at injection point ( $kg/m^3$ )
$D$	characteristic length or diameter (m)
$D$	diffusivity ( $m^2/s$ )
$d_o$	nozzle diameter (m)
$E$	exhaust gas flow (kg/hr)
$F$	fuel input (kg/hr)
$G$	glass output (kg/hr)
$h$	Planck's constant ( $= 6.62 \cdot 10^{-34}$ J.s)
$Gr$	Grashof number
$H_r$	heat of direct radiation from the flame (W)
$k_1, k_2$	reaction rate coefficients ( $s^{-1}$ or $m^3 \cdot mol^{-1} s^{-1}$ )
$L_f$	total flame length (m)
$k$	mass transfer coefficient ( $m \cdot s^{-1}$ )
$M_i$	molecular mass of element $i$ (kg/mol)
$Nu$	Nusselt number ( $\alpha D/\lambda$ )
$P_i$	partial pressure of element $i$ in the exhaust gas (atm.)
$Re$	Reynolds number on basis of gas velocity ( $v \cdot \rho \cdot D/\mu$ )
$Re'$	Reynolds number defined by relation 1.22a
$Sh$	Sherwood number ( $k \cdot D/D$ )
$T_f$	absolute flame temperature (K)
$T_m$	glass melt or batch temperature (K)
$T$	temperature (K)
$x_i$	weight fraction of element $i$ in the batch
$y_i$	weight fraction of $i$ in the produced glass
$z_i$	weight fraction of element $i$ in the fuel

### Greek symbols

$\alpha$	heat transfer coefficient ( $\text{W.m}^{-2}.\text{K}^{-1}$ )
$\lambda$	heat conductivity ( $\text{W m}^{-1} \text{K}^{-1}$ )
$\nu$	frequency of light or radiation ( $\text{s}^{-1}$ )
$\sigma$	Stefan Boltzmann's constant $5.6703 \cdot 10^{-8} \text{ W.m}^{-2} \text{ K}^{-4}$
$\epsilon$	emissivity of the combustion system
$\rho$	fluid density ( $\text{kg/m}^3$ )
$\rho_0$	fuel density at injection point ( $\text{kg/m}^3$ )
$\rho_c$	density of combustion air ( $\text{kg/m}^3$ )
$\mu$	dynamic viscosity ( $\text{kg.m}^{-1}.\text{s}^{-1}$ )

## 2. LITERATURE SURVEY OF THERMODYNAMIC PARAMETERS AND MASS TRANSPORT PROCESSES IN EXHAUST GASES OF GLASS FURNACES

### 2.1 Introduction

During the cooling of the exhaust gases doped with glass melt volatiles, various chemical reactions take place. The nature of these gaseous reactions mainly depends on the elemental composition of the gaseous phase. The temperature dependence of the thermodynamic functions of the constituting flue gas components leads to conversions in the gaseous phase or to condensation processes at decreasing temperatures. In most cases the conversions proceed very quickly especially at high exhaust gas temperatures. For that reason it may be assumed that the exhaust gas composition in recuperators or regenerators approaches the equilibrium situation for most locations.

However, in the boundary layers of submerged obstacles or inner walls, temperature gradients may be so high that the conversions are limited by reaction kinetic aspects.

The heat of the exhaust gases is transported through these boundary layers towards the surface of regenerator bricks or the recuperator walls. Concentration gradients over the boundary layer result in diffusional transport processes, transferring gaseous molecules and very small particles, towards these surfaces. The accumulation of the transported molecules leads to saturation of certain vapors resulting in deposition at the heat exchanging surfaces.

The deposition rates for the condensed salt components are generally dependent on mass transport rates for salt constituting elements through the boundary layers. The most important chemical reactions involved in the exhaust gases are presented in this chapter for several glass furnace types or glass compositions. The evaluation of these reactions has been based on analytical measurements, thermodynamic considerations and experimental observations.

Condensation and deposition of salt or metal oxide components from flue gases has been evaluated on the basis of literature data. Attention has been paid to the literature on the analytical procedures to determine exhaust gas compositions in various combustion systems.

## 2.2 Evaluation of reactions in glass melter atmosphere and exhaust gases

This paragraph deals with the reactions occurring in the cooling exhaust gases of several glass furnaces. The next section is divided into seven parts, each part describing the reactions for a specific case.

### 2.2.1 Flue gases with sulphur, chloride and sodium compounds

The chemical reactions in flue gases of a natural gas fired flat glass furnace have been studied by Kirkbride [1] on a thermodynamic basis. The most important components in the furnace atmosphere are listed in table 2.1.

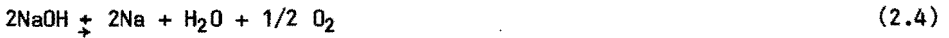
Table 2.1: Chemical components in furnace atmosphere of a gas-fired flat glass furnace.

sodium components	Na, NaCl, NaOH*
chloride components	HCl, NaCl*
sulphur components	SO <sub>2</sub> *, SO <sub>3</sub>

\* indicates the major component.

Kirkbride neglected the element sodium as a gaseous component in the furnace atmosphere. However, in spite of the oxidizing circumstances in the combustion chamber, sodium gas is a relatively important constituent of the gas phase above 1500 K. The reactions between gaseous components that take place during the cooling process are given below.



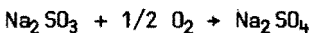


\* all components in the gaseous phase.

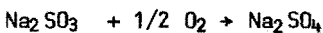
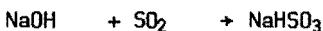
Reaction number 2 proceeds to the right at decreasing temperatures, resulting in increasing sodium sulphate concentrations. The scheme presents only the equilibrium reactions, the reaction mechanisms for these conversions are generally very complex.

For example, sodium sulphate may be formed from reactions of sodium chlorides with sulphur oxides, or from reactions of sodium hydroxides with sulphur oxides. Possible reaction mechanisms for sodium sulphate formation have been proposed by Durie et al [2] (mechanism I) and Mulcahy in ref. [3] (mechanism II and III).

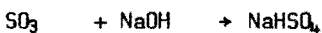
Mechanism I (ref. [2]):



Mechanism II (ref. [3]):



Mechanism III (ref. [3]):

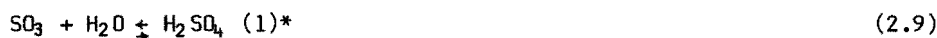
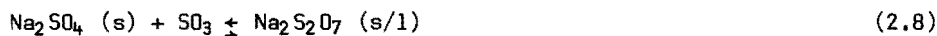
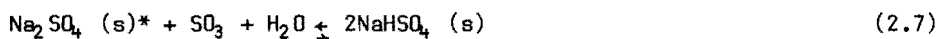


Fryburg et al [4] have indicated the possibility of  $\text{NaSO}_2$  and  $\text{NaSO}_3$  formation as precursors of sodium sulphate in flames.

The reaction scheme presented by reactions (2.1) to (2.6) is sufficient to calculate the thermodynamic equilibrium compositions for the most important components in the gaseous phase.

At temperatures below 1350 K, condensation of sodium sulphate may take place as a result of increasing sodium sulphate concentrations in the gaseous phase during cooling. In sulphur lean flue gases, sodium chloride or sodium carbonate may condense.

In sulphur rich flue gases, pyrosulphates, bisulphates or sulphuric acid may be formed below 600 K [5].

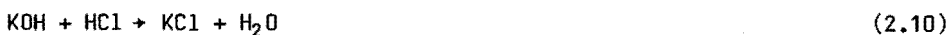


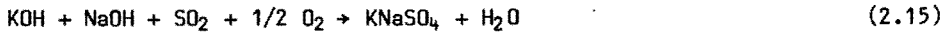
\* (1) indicates the liquid state

(s) indicates the solid state

## 2.2.2 Flue gases with sulphur, chlorides, potassium and sodium

Flue gases from container glass or flat glass furnaces may contain potassium in addition to sodium. Although potassium oxide is a minor component in these glass melts as compared to sodium oxide, potassium components are generally more volatile than sodium components. The most important equilibrium reactions in the flue gases are reactions (2.1) to (2.6) and:





\* all reactions include only gaseous components.

The chemical equilibrium reactions for the potassium components in exhaust gases of glass furnaces are similar to the mentioned reactions of sodium compounds in these atmospheres. The mixed alkali sulphate  $\text{KNaSO}_4$  is a deposition product often found in regenerators.

The potassium/sodium ratio in container glass furnace atmospheres rarely exceeds 10%. Potassium sulphate has a melting point of 1342 K, and the formation of liquid potassium sulphate deposits is mostly excluded in exhaust gases of glass furnaces. Potassium hydroxide is the main potassium containing component at temperatures above 1300 K and sulphur dioxide is the most important sulphur component at these temperatures. The mechanisms of the reactions for the formation of potassium sulphates from potassium hydroxide (or potassium chloride) and sulphur dioxide are poorly understood. Judging from the similarity between the potassium and sodium behaviour in exhaust gases, the mechanism of potassium sulphate formation may be analogous to sodium sulphate formation.

At low temperatures, formation of  $\text{KHSO}_4$  or  $\text{K}_2\text{S}_2\text{O}_7$  in the condensed state may take place in sulphur rich stack gases.

### **2.2.3 Flue gases with sodium, calcium, sulphur and chlorides**

Exhaust gases from soda-lime glasses contain minor amounts of calcium oxide dust entrained in the furnace gases from the batch. However, these very low concentrations of calcium components in the flue gases hardly influence the chemical behaviour as mentioned in 2.2.1.

In oil-fired glass tanks the concentration of sulphur containing compounds may exceed the stoichiometric value relative to sodium for sodium sulphate formation. The excess of sulphur, mainly as sulphur dioxide may be converted, by injection of limestone dust, into calcium sulphate (gypsum).

Introduction of calcium containing components results in reactions like:



(s) indicates the solid state, all other components are assumed to be gaseous.

Reaction (2.18) and reaction (2.2) involve the conversion of sulphur oxides into solid material. This may preclude formation of sticky sodium bisulphates or sodium pyrosulphates below 600 K.

The condensation of sulphuric acids below 450 K is also suppressed by addition of limestone in sulphur rich flue gases.

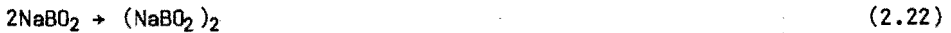
#### 2.2.4 Flue gases with sodium and boron

From sodium-borosilicate glass melts, sodium metaborates volatilize in the glass furnace [6]. At temperatures above 1200 K, sodium metaborate, sodium tetraborate and metaboric acid are the main boron containing components [7].

The sodium containing substances are sodium hydroxide, occasionally sodium chloride (in the presence of chlorine), and the two mentioned sodium borates. At lower temperatures  $\text{HBO}_2$  may be converted into  $\text{H}_3\text{BO}_3$ . The relevant reactions are given in the next scheme:



and according to Büchler et al [8]:



For completeness sake the following reactions may be postulated:

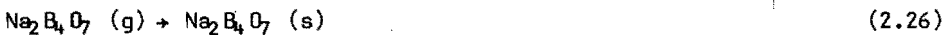


\* all reactions include only gaseous components.

However, reactions (2.23) and (2.24) are evidently of minor importance in oxidizing or wet atmospheres.

Addition of sulphur to these flue gases causes reactions between sodium and sulphur oxides as given in 2.2.1. No reactions between sulphur and boron compounds are to be expected in such flue gas compositions. On the basis of thermodynamics the formation of  $\text{BCl}_3$  or other boron chloride combinations is not expected.

The main condensation products from flue gases only doped with boron and sodium components are  $\text{NaBO}_2$  and  $\text{Na}_2\text{B}_4\text{O}_7$  commonly as solid products:



### 2.2.5 Flue gases with potassium, sulphur, boron and fluorides

E-glass melts contain low concentrations of alkali oxides but the presence of boron enhances the vaporization of the small amounts of alkali in the melt, according to Wenzel [6]. Potassium metaborates preferably volatilize from E-glass melts due to the high chemical activity of the metaborates in the melt and the high vapor pressure for  $\text{KBO}_2$ . Fluorides, which are sometimes added to these glass melts (see paragraph 1.1.2) are very volatile and contribute to the emissions of these furnaces.

In this flue gas, equilibrium reactions (2.10) to (2.14) and the following reactions between gaseous components take place:



From thermodynamic calculations it is known that components like  $\text{K}_2\text{SiF}_6$ ,  $\text{SiF}_4$  and  $\text{BF}_3$  are instable in flue gases with oxygen concentrations higher than 1.0 volume-%.

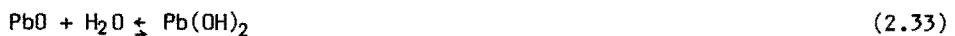
Silicium fluorides vaporizing from fluoride containing glass melts react with water in the furnace atmosphere according to Scholze et al [9]:

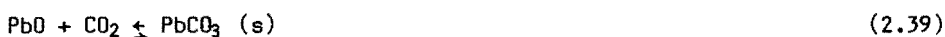
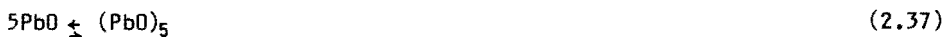
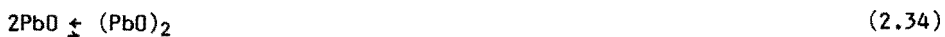


This reaction is only relevant for the volatilization process close to the glass melt surface, and enhances the vaporization of fluorides.

### 2.2.6 Flue gases only doped with volatilized lead

Lead, as shown in paragraph 1.1.2 vaporizes from lead glass melts as  $\text{PbO}$  or  $\text{Pb}(\text{OH})_2$ . In case that no sulphur compounds are added to the raw material batch of a natural gas fired lead glass furnace, lead oxide seems to be the most important component in the exhaust gases. The equilibrium reactions in flue gases of such furnaces are predominantly:





The reactions (2.34) to (2.38) are polymerisation reactions as postulated by Drowart et al [10].

Deposition or condensation of lead compounds from these flue gases is mainly achieved by reactions (2.40) and (2.41).



### 2.2.7 Flue gases with lead and sulphur

Precipitated dust from oil-fired lead glass furnaces contains lead sulphate as the main condensation product. Lead sulphate is produced by reaction (2.42):



The formation of gaseous lead sulphates has not been studied as far as we know from the available literature sources. However, gaseous metal sulphates are commonly minor components constituting the impurities in the flue gases.

In our investigations combinations of condensed lead oxide and lead sulphate have been found in deposits of flue gases doped with sulphur and lead compounds, (see section 3.3):



Thermodynamic calculations carried out in our studies, also indicate the conversion to  $2\text{PbO} \cdot \text{PbSO}_4$  and  $3\text{PbO} \cdot \text{PbSO}_4$ :



### 2.3 Thermodynamic properties of flue gas components: Equilibrium Constants and Vapor Pressures

In the previous section, paragraph 2.2 the most important reactions that may take place during cooling of exhaust gases from glass furnaces were presented. Assuming that the flue gases are always in equilibrium composition at the considered gas temperature, one can calculate the gaseous composition making use of the equilibrium constants of the relevant reactions.

The equilibrium constant is a function of the absolute temperature and may be determined from the difference in Gibbs' Free Energy between reactants and products:

$$K_T = \exp (- \Delta G/RT) \quad (2.47)$$

For a reaction between gaseous components only:



where

$a_i$  stoichiometric coefficient for reactant  $R_i$

$b_j$  stoichiometric coefficient for product  $P_j$ .

$$\Delta G = \sum_j b_j G_j - \sum_i a_i G_i \quad (2.49)$$

$G_j$  is Gibbs' Free Energy for one mole of gaseous product  $j$  at a pressure of 1 atmosphere.

$G_i$  is Gibbs' Free Energy for one mole of gaseous reactant  $i$  at a pressure of 1 atmosphere.

The reaction between the equilibrium vapor pressures  $P_{R_i}$  or  $P_{P_j}$  given in atmospheres, and  $K_T$  is given by formula (2.50):

$$K_T = \frac{\prod_j (P_{P_j})^{b_j}}{\prod_i (P_{R_i})^{a_i}} \quad (2.50)$$

In formula (2.50) the chemical activity has to be used instead of the partial pressure for condensed components in liquid or solid form, that may be included in the reaction equation. In case of a vapor-condensed phase equilibrium like:



$$K_T = \frac{1}{P_T^*} = \exp \left( - \frac{G_{A(s/l)} - G_{A(g)}}{R * T} \right) \quad (2.52)$$

Table 2.1: Equilibrium Constants of Flue gas reactions.

in  $K_T = A \cdot T + B + C/T$  temperature range 600-1800 K.

Reaction number mentioned in section 2.2	A	B	C	literature sources
2.1	1.38 $10^{-3}$	-33.93	1.58 $10^4$	11
2.2	3.44 $10^{-3}$	-39.28	6.82 $10^4$	11, 12, 13
2.3	6.84 $10^{-3}$	-39.89	4.23 $10^4$	11, 14
2.4	1.405 $10^{-4}$	15.65	-4.78 $10^4$	11
2.5	7.08 $10^{-4}$	-20.26	2.72 $10^4$	11
2.6	1.87 $10^{-4}$	-11.49	1.19 $10^4$	11
2.7	-	-	-	no data available
2.8	-	-	-	no data available
2.9	4.827 $10^{-3}$	-35.427	2.08 $10^4$	11
2.10	-4.15 $10^{-5}$	- 0.385	1.59 $10^4$	11
2.11	4.325 $10^{-3}$	-39.05	6.989 $10^4$	11, 15, 16
2.12	1.202 $10^{-2}$	-42.742	3.36 $10^4$	11, 17
2.13	1.54 $10^{-4}$	15.23	-4.83 $10^4$	11
2.14	7.63 $10^{-4}$	-19.75	2.34 $10^4$	11
2.15	-	-	-	no data available
2.16	-5.27 $10^{-4}$	25.57	-9.72 $10^4$	11, 18
2.17	-1.50 $10^{-3}$	11.36	-3.23 $10^4$	11, 19
2.18	-4.55 $10^{-3}$	-24.38	5.21 $10^4$	11, 20
2.19	-6.354 $10^{-3}$	+15.669	-2.17 $10^4$	7
2.20	8.934 $10^{-3}$	-65.08	1.229 $10^5$	8, 7
2.21	3.25 $10^{-4}$	-16.74	2.304 $10^4$	11
2.22	-3.97 $10^{-5}$	-13.53	2.66 $10^4$	8
2.23	1.98 $10^{-5}$	0.674	-6.35 $10^3$	11
2.24	2.83 $10^{-4}$	9.604	-3.82 $10^4$	11
2.25	4.97 $10^{-6}$	-19.82	3.67 $10^4$	8
2.26	1.18 $10^{-2}$	-45.44	4.95 $10^4$	7, 11
2.27	-1.67 $10^{-4}$	- 1.028	-9.48 $10^3$	11, 21
2.28	-	-	-	no data available
2.29	-4.87 $10^{-6}$	15.32	-8.91 $10^3$	11, 21
2.30	9.63 $10^{-5}$	- 0.625	7.87 $10^3$	11
2.31	2.28 $10^{-2}$	64.86	5.17 $10^3$	11
2.32	4.001 $10^{-4}$	10.789	-1.263 $10^4$	11
2.33	-	-	-	no data available
2.34	-4.12 $10^{-5}$	-16.23	3.14 $10^4$	10
2.35	-3.26 $10^{-5}$	-35.96	6.47 $10^4$	10
2.36	-1.49 $10^{-4}$	-54.22	1.004 $10^5$	10
2.37	-8.76 $10^{-5}$	-71.97	+1.28 $10^5$	10
2.38	-2.005 $10^{-5}$	-91.188	+1.65 $10^5$	10
2.39	-2.10 $10^{-5}$	-31.13	3.68 $10^4$	22
2.40	-4.73 $10^{-5}$	-16.01	3.084 $10^4$	11, 10
2.41	-1.81 $10^{-2}$	-23.46	8.34 $10^4$	10
2.42	2.35 $10^{-4}$	-47.81	7.65 $10^4$	10
2.43	7.75 $10^{-3}$	-84.21	1.20 $10^5$	10
2.44	8.43 $10^{-3}$	-130.44	2.05 $10^5$	10
2.45	-3.766 $10^{-4}$	-84.42	1.42 $10^5$	10
2.46	-1.66 $10^{-3}$	-105.23	1.77 $10^5$	10

where:

$P_T^*$  = saturation pressure at temperature T given in atmospheres

R = Boltzmann constant (8.31432 J/mol.K)

T = absolute temperature (K).

The equilibrium constants as functions of the absolute temperature are given in table 2.1. These thermodynamic values have been calculated from data given in the literature.

One of the assumptions of the thermodynamic equilibrium model for calculating exhaust gas compositions is the restriction that the vapor pressures may not exceed the saturation values. Components that may condense from exhaust gases are listed in table 2.2.

The relations for the saturation pressures dependent on temperature are presented in this table for the components mentioned.

Table 2.2: Vapor pressure - temperature relation, for exhaust gas components.  $\ln (P_{\text{saturation}}/\text{atm}) = A/T + B + C/T$ .

Component only monomer gas molecules	A	B	C	literature sources
NaCl	-4.46 $10^{-3}$	23.75	-2.90 $10^6$	11
NaF	-1.32 $10^{-3}$	20.294	-3.44 $10^6$	11
Na <sub>2</sub> SO <sub>4</sub>	-4.94 $10^{-3}$	26.33	-4.41 $10^6$	12, 13
Na <sub>2</sub> CO <sub>3</sub>	-5.61 $10^{-6}$	9.136	-2.65 $10^6$	14
NaBO <sub>2</sub>	-4.97 $10^{-6}$	19.819	-3.67 $10^6$	8
Na <sub>2</sub> B <sub>4</sub> O <sub>7</sub>	-4.525 $10^{-3}$	30.942	-6.253 $10^6$	7
KCl	-3.47 $10^{-3}$	20.934	-2.64 $10^6$	11
KF	-2.35 $10^{-3}$	19.014	-2.72 $10^6$	11
KBO <sub>2</sub>	-7.93 $10^{-3}$	41.741	-5.07 $10^6$	21
K <sub>2</sub> B <sub>4</sub> O <sub>7</sub>	-	-	-	no data available
K <sub>2</sub> SO <sub>4</sub>	-2.478 $10^{-3}$	23.418	-4.18 $10^6$	16
K <sub>2</sub> CO <sub>3</sub>	-1.13 $10^{-2}$	21.343	-4.13 $10^6$	17
PbO	1.38 $10^{-5}$	16.099	-3.089 $10^6$	10
CaO	-7.995 $10^{-6}$	21.268	-6.885 $10^6$	18
H <sub>2</sub> BO <sub>3</sub>	-3.32 $10^{-3}$	26.738	-1.250 $10^6$	11
H <sub>2</sub> SO <sub>4</sub>	-3.85 $10^{-3}$	15.929	-8.33 $10^6$	11

saturation vapor pressure (log p<sub>i</sub>/atm.)

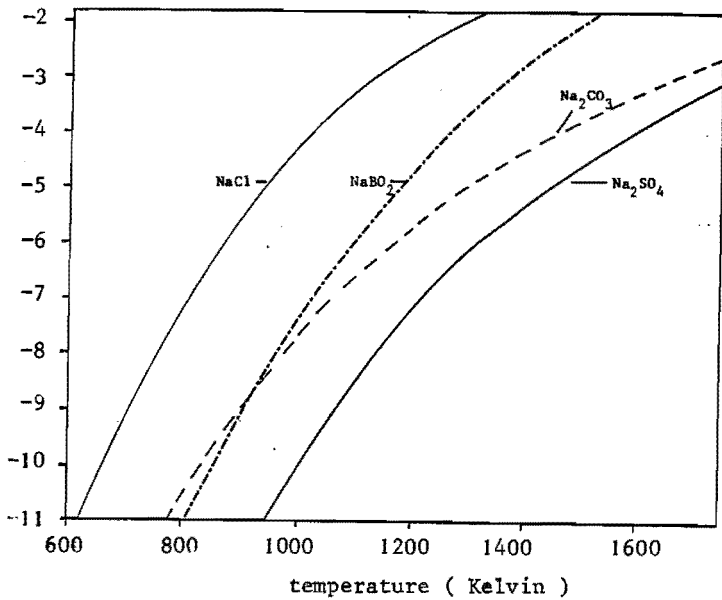
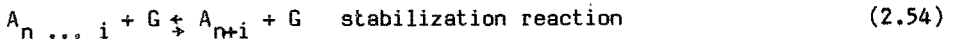
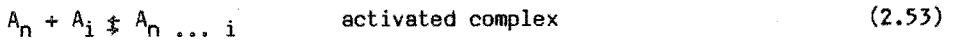


Figure 2.1: Saturation pressures of sodium salts.

#### 2.4 Condensation and deposition from exhaust gases doped with inorganic components

Condensation of saturated components in the gaseous phase may happen in the bulk gas phase resulting in dust formation. According to Bauer and Frurip [23] homogeneous nucleation of molecules in supersaturated gases takes place by initial formation of dimers, trimers etc.

The released collision energy has to be extracted from the activated n-i-mer by collision with a third molecule, to avoid splitting up of the new formed polymer. This reaction model as postulated by Amdur and Hammes [24] is presented by:



where:

$A_n$  = n-mer of molecule A

G = arbitrary gaseous molecule.

For low values of  $n+i$ , the activated complex is very instable, the initial stages of nucleation proceed very slowly. At high supersaturation values the formation of polymerised molecules with high  $n$ -values is favoured and stable nuclei are formed.

Thus the homogeneous nucleation process is accelerated by high supersaturation values where nuclei with  $n$ -values larger than  $n_{critical}$  are formed. The nuclei may grow further resulting in the formation of dust particles. The complete description of this theory and the modelling of the involved kinetic processes is beyond the scope of these investigations.

Although homogeneous nucleation may play a role in the condensation processes it is reasonable to assume that in the exhaust gases from the melting furnace, heterogeneous condensation processes are dominant. This work has been focussed on the chemical equilibrium reactions in the main gas flow and on the deposition of salt components from flue gases in regenerators or recuperators.

Deposition in the heat exchanging systems occurs at the inner walls of recuperators or at the surface of the bricks constituting the checker works of regenerators. The deposition rates are determined by the transport rates of gaseous material through the boundary layers at the deposition surfaces, resulting in supersaturated salt vapors near these surfaces. Brown [25] made the supposition that condensation processes within the boundary layer reduce deposition of sodium sulphate from exhaust gases doped with sulphur and sodium containing species.

Jackson and Duffin [26] studied the deposition of sodium chloride from flue gases on surfaces below 1300 K. No deposits from gases doped with  $170 \text{ mgr/m}_n^3$  sodium chloride were found above 980 K. The deposition of sodium chloride increased at surface temperatures decreasing from 980 K to 850 K, below 850 K the deposition rates remained constant according to Jackson et al.

From Jackson's laboratory investigations it was concluded that the deposition rate is approximately proportional to the dopant concentration in the flue gas. The oxygen concentrations in these flue gases had only a very slight effect on the deposition behaviour of sodium chloride.

The measured dew point increased from 910 K for a  $34 \text{ mgr/m}_n^3$  doped flue gas to 1038 K for a flue gas with  $1700 \text{ mgr/m}_n^3$  sodium chloride.

Jackson and Duffin found higher dew point temperatures for flue gases doped with the same amount of sodium sulphate instead of sodium chloride. However, at low temperatures (below 900 K) sodium sulphate deposition rates were considerably lower than sodium chloride deposition rates for similar conditions.

Raask [27] studied deposition of sodium chloride and sodium sulphate (and also potassium sulphate) deposited at surface temperatures below 1150 K. The exact flue gas composition is not given in Raask's paper.

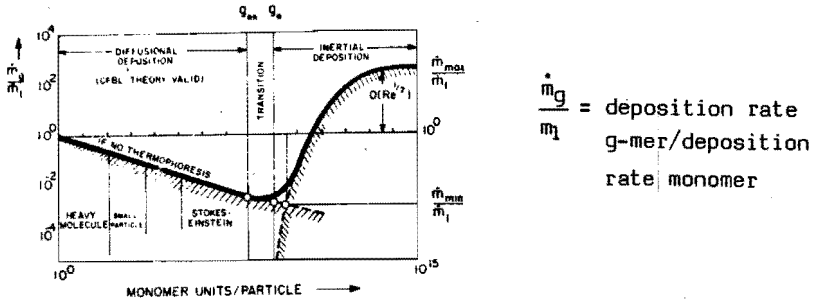
Condensate deposition from combustion gases has been studied intensively by Rosner and co-workers [30 - 33]. These investigators postulated relations describing the diffusional molecular transport of chemical species through gaseous boundary layers, preceding the condensation at the surface.

They distinguished between situations where only gaseous components are transported through the boundary layer and situations where also particles are transported to the surface.

For particles containing less monomer units than a certain value  $n^*$  the particles behave like heavy molecules. The formation of these small particles reduces the deposition rate for this component. For particle sizes larger than  $n^{**}$ , all the upstream particles within the projected region of the obstacle or target in the flue gas flow, will be caught by the surface and may adhere there, causing increasing deposition rates.

The deposition rates for these particles are proportional to  $\sqrt{\text{Re}}$  (Re = Reynolds number).

The effect of particle size on deposition behaviour is presented in figure 2.3 from Rosner et al [32].



$$\frac{\dot{m}_g}{\dot{m}_m} = \frac{\text{deposition rate g-mer}}{\text{deposition rate monomer}}$$

Figure 2.3: Changing deposition rates for single sized particles as a function of monomer units per particle.

The theoretical description of the proposed boundary layer model by Rosner is presented in chapter 4 of this thesis. The investigations of Rosner and co-workers clearly showed that the deposition rates depend on the Sherwood number for the flow conditions near the deposition surface and the diffusional parameters like the molecular diffusivity  $D_i$  and thermophoretic diffusivity  $\alpha_i$ .

Deposition rates are roughly proportional to the square root of the gas velocity and proportional to the diffusion coefficients. High temperature differences between locations near the surface and in the host gas flow cause steep concentration gradients across the boundary layer and so increase the driving force for diffusional mass transport.

Sodium sulphate is the most important deposition product from exhaust gases of glass furnaces. According to Kohl et al [33] in this case the transported molecules are sodium, sodium hydroxide, sodium sulphate, sodium chloride and sulphur dioxide.

Kohl measured sodium sulphate dew points of 1260 K for a flue gas doped with 11.3 ppm sea salt (69% NaCl and 11.5%  $\text{Na}_2\text{SO}_4$ ). The oxygen and water vapor concentrations in their flue gases were respectively 6.6 and 10 volume-%. Deposition studies for alkali borates or lead compounds are not known from the available literature.

## **2.5 Analytical procedures for measurements of gaseous components in the exhaust of glass melting furnaces**

Literature data for the gaseous composition of the exhaust of glass furnaces at elevated temperatures are very rare. Up to now, no accurate procedure has been developed for the chemical analysis of flue gas compositions in regenerators, recuperators or furnace atmospheres. On laboratory scale a method has been developed to investigate the chemical composition of simulated flue gases by means of mass spectrometric techniques. A rough indication of the elemental composition of condensing flue gas components in the furnace atmosphere can be obtained by chemical analysis of condensation products collected on a water cooled paddle. In this section further attention has been paid to the literature on the analysis of furnace atmospheres or simulated flue gas compositions.

### **2.5.1 Deposition on water cooled paddles in hot exhaust gases**

The collection of condensing materials on water cooled paddles in the regenerator ports of soda-lime glass furnaces was done by Busby and Sengelow [34]. Although this method may give information on the vaporization of alkali, sulphur, chlorine or other volatiles from the melt, no data can be obtained to calculate the absolute values of vapor pressures for these components. Table 2.4 presents the results of the measurements performed by Busby and Sengelow.

**Table 2.4:** Chemical analysis of water cooled paddle deposits from different ports of a regenerative side port furnace with oil firing, from reference [34].

Glass: Soda-lime glass.

*Condensate carryover analyses (samples from first or end ports)*

	Furnace											
	A	B	C	E	F	G	H	I	J	K	L	M
H <sub>2</sub> O in batch (%)	2.8	2.7	1.3	2.3	2.2	3.2	3.0	4.4	2.2	2.2	1.7	1.6
Carryover (g/24 h)	3.3	4.0	3.8	2.7	8.1	3.8	5.1	8.9	7.7	12.6	2.7	7.1
Glass melted (t/24 h)	184	231	124	27.5	74.9	227.5	275	167	70	105.5	184	124
Fuel	Oil	Oil	Gas	Gas	Oil	Oil	Oil	Oil	Oil	Oil	Oil	Gas
<b>Analysis of carryover (wt %)</b>												
SO <sub>2</sub>	49.5	53.3	36.2	45.5	45.8	48.7	45.4	48.6	51.3	44.9	54.2	38.9
Na <sub>2</sub> O	30.9	36.4	27.5	23.1	34.0	30.4	29.6	22.8	33.4	34.0	36.6	30.3
K <sub>2</sub> O	2.4	2.5	2.4	2.1	3.7	3.4	2.8	4.2	5.2	3.4	1.8	1.2
Fe <sub>2</sub> O <sub>3</sub>	0.4	0.3	0.2	0.6	0.4	0.2	0.2	0.4	0.3	0.5	0.2	0.3
SiO <sub>2</sub>	10.1	4.1	21.6	19.0	3.0	7.6	13.2	5.3	2.7	4.5	0.9	11.0
Cr <sub>2</sub> O <sub>3</sub>	0.05	0.2	0.05	0.3	0.2	0.2	0.2	0.03	0.1	1.5	0.2	0.1
MgO	0.3	0.1	0.2	0.01	0.05	0.2	0.1	5.2	0.1	0.5	0.2	0.2
CaO	1.5	1.5	6.7	5.6	5.6	3.6	3.4	10.8	2.9	5.4	1.6	11.4
NiO	0.5	0.3	0.01	0.06	0.5	0.5	0.4	0.3	0.3	0.3	0.3	0.05
V <sub>2</sub> O <sub>5</sub>	2.0	1.1	0.01	0.05	1.6	2.5	2.3	1.07	0.8	1.0	1.3	0.03
Al <sub>2</sub> O <sub>3</sub>	0.5	0.3	1.4	1.3	0.6	0.4	0.6	0.6	0.3	0.5	0.4	1.0
-Cl	0.4	0.2	3.8	0.1	3.6	0.02	0.02	0.5	0.04	2.7	0.1	5.2

*Change in composition of condensate carryover along the length of a furnace*

	Furnace							
	H		I		I		Fourth	
	First port	Second port	Third port	First port	Second port	Third port	Fourth port	
<b>Analysis of carryover (wt %)</b>								
SO <sub>2</sub>	45.5	52.7	54.3	48.6	50.2	52.0	56.2	
Na <sub>2</sub> O	29.6	34.6	35.1	22.8	28.3	29.9	28.3	
K <sub>2</sub> O	2.8	3.5	3.3	4.2	6.0	5.6	5.9	
Fe <sub>2</sub> O <sub>3</sub>	0.2	0.2	0.3	0.4	0.3	0.7	0.2	
SiO <sub>2</sub>	13.2	2.8	1.7	5.3	2.8	2.5	1.5	
Cr <sub>2</sub> O <sub>3</sub>	0.2	0.3	0.4	0.03	0.02	0.05	0.01	
MgO	0.1	0.1	0.05	5.2	2.1	1.1	0.4	
CaO	3.4	1.1	0.6	10.8	4.9	2.4	1.0	
NiO	0.4	0.4	0.4	0.3	0.4	0.7	0.5	
V <sub>2</sub> O <sub>5</sub>	2.3	2.6	2.3	1.07	1.3	2.1	1.9	
Al <sub>2</sub> O <sub>3</sub>	0.6	0.3	0.2	0.6	0.3	0.2	0.2	
-Cl	0.02	0.04	0.08	0.5	0.2	0.1	0.1	
Weight of carryover (g/24 h)	5.1	4.5	4.8	8.9	4.8	4.0	3.2	

### 2.5.2 Mass spectrometric in situ analysis of exhaust gas compositions

Vaporization processes may be studied by coupling a mass spectrometer system to a Knudsen Effusion Cell. With this method vaporization processes in equilibrium situation have been studied in vacuum for various types of glasses.

However, this method is not applicable whenever interaction of the furnace atmosphere with the glass melt has to be investigated, nor has this method any significance for the determination of the composition of flue gases under atmospheric pressure. The development of a high pressure, free jet expansion sampling system by Milne and Greene [35] has led to the application of mass spectrometric analysis of flames and hot atmospheric gases on laboratory scale.

In this system a sample from an atmospheric gas flow (a flame or exhaust gas) passes a nozzle and expands in a vacuum chamber. Generally this expansion has to be carried out in two or three pressure reduction steps. Stearns et al [36] described this system developed for the mass spectrometric investigations of 'high temperature molecules'. From their study they concluded that the gaseous pressure in the sample reduces with a factor  $10^5$  within  $5 \cdot 10^{-6}$  seconds.

The formation of a free expanding jet of molecules leads to a molecular beam of gas molecules from the atmospheric gas flow. Interactions of the molecules in this beam are rare and chemical reactions or condensation is avoided in this stage. Several investigators [35, 36, 37, 38, 40] have used this technique to prevent chemical reactions during the sampling and pressure reduction in the analytical instrument.

The composition of the molecular beam, representing the flue gas composition, can be derived by means of conventional mass spectrometric instruments. The formation of gaseous sodium sulphate and potassium sulphate in a flame has been studied by Fryburg et al [39] by means of the mentioned mass spectrometric system. Their equipment is presented by figure 2.4 including the free-jet expansion sampling system, and an example of a flame analysis.

Although this system seems to be helpful in the determination of flue gas compositions one of the drawbacks may be the disturbance of the gas flow or the temperature profile in the flame by the sampling cone.

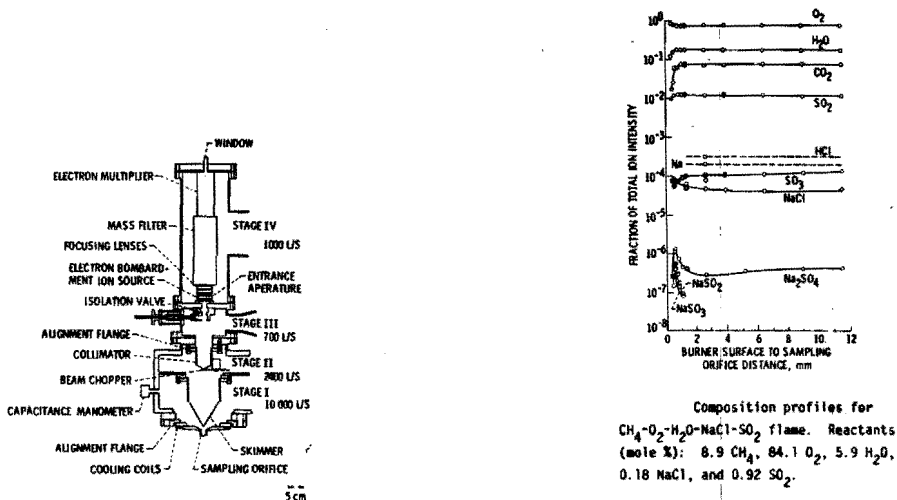


Figure 2.4: Analysis of flame composition with High Pressure Molecular Beam Mass Spectrometric Sampling, Fryburg [39].

Taking this into account Fryburg concluded from the comparison of the analytical measurement with thermodynamic calculations that the latter method gives reasonable results for the determination of equilibrium compositions in sodium (or potassium) and sulphur doped flames of 2100 K. According to Fryburg's analytical observations the reaction time to achieve the equilibrium situation in flames of 2100 K was approximately 1 to 2 msec.

Hastie et al [38] used the molecular beam sampling system to study the composition of evaporating gases during transpiration measurements for KOH and KCl melts.

Bonnel and Hastie [40] described this apparatus to investigate the volatilization from glass melts in an atmospheric gas flow of variable composition. Several literature references for the application of molecular beam sampling systems to study high temperature and high pressure gases by means of a mass spectrometer have been given by Stearns et al [36].

## Literature references chapter 2

- [ 1] Kirkbride B.J.;  
'The chemical changes occurring during the cooling of hot gases from flat glass furnaces'.  
Glass Technology 20 (1979) 174-180.
- [ 2] Durie R.A., Milne J.W., Smith M.Y.;  
'The deposition of salts from hydrocarbon flames containing sodium and sulphur species'.  
Combustion and Flame 30 (1977), 221-230.
- [ 3] Johnson H.R., Littler D.J.;  
'The mechanism of corrosion by fuel impurities'.  
Comment in discussion p. 133 Int. Conf. 1963, Butterworths-London.
- [ 4] Fryburg G.C., Miller R.A., Stearns C.A., Kohl F.J.;  
'Formation of  $\text{Na}_2\text{SO}_4$  and  $\text{K}_2\text{SO}_4$  in flames doped with sulphur and alkali chlorides and carbonates'.  
from: 'High temperature metal halide chemistry'; D.L. Hildenbrand and D.D. Cubicciotti vol. 78-1 (1978) 468-483.
- [ 5] Webb R.L., Marchiori D., Durbin R.E., Wang Y.J., Kulkarni A.K.;  
'Heat exchanger for secondary heat recovery from glass plants'.  
Heat Recovery Systems 4 (1984) 77-85.
- [ 6] Wenzel J.T., Sanders D.M.;  
'Sodium and boron vaporization from boron oxide and a borosilicate glass melt'.  
Physics and Chemistry of Glasses 23 (1982) 47-52.
- [ 7] Cole S.C., Taylor N.W.;  
'Vapor pressures of sodium metaborate and sodium diborate between 1150 °C and 1400 °C'.  
J. Am. Ceram. Soc. 18 (1935) 82-86.
- [ 8] Büchler A., Berkowitz-Mattuck J.B.;  
'Gaseous metaborates I: Mass-Spectrometric Study of Vaporization of Lithium and Sodium Metaborates'.  
The Journal of Chemical Physics 39 (1963) 286-291.
- [ 9] Scholze H., Tünker G., Conradt R.;  
'Verdampfung von Fluor aus Glasschmelzen und beim Einschmelzprozess'.  
Glastechn. Ber. 56 (1983) 131-137.

- [ 10 ] Drowart J., Colin R., Exsteen G.;  
'Mass-Spectrometric Study of the Vaporization of Lead-Monoxide'.  
Trans. Faraday Soc. 61 (1965) 1376-1383.
- [ 11 ] 'Janaf Thermochemical Tables', Stull D.R. and Proplet H., (1971)  
NSRDS-NBS 37.
- [ 12 ] Cubiciotti D., Keneshea F.J.;  
'Thermodynamics of Vaporization of Sodium Sulphate'.  
High Temperature Science 4 (1972) 32-40.
- [ 13 ] Halle J.C., Stern K.A.;  
'Vaporization and Decomposition of  $\text{Na}_2\text{SO}_4$  Thermodynamics and  
Kinetics'.  
J. Phys. Chem. 84 (1980) 1699-1704.
- [ 14 ] Kröger C., Stratman J.;  
'Dampf- und Zersetzungsdrücke einiger an der Glasschmelze  
beteiligter Alkaliverbindungen'.  
Glastechnische Berichte 34 (1966) 311-320.
- [ 15 ] Lau K.H.; Cubiciotti D., Hildenbrand D.L.;  
'Effusion Studies of the Vaporization/Decomposition of Potassium  
Sulphate'.  
J. Electrochem. Soc.-Solid-State Sc. and Techn. 126 (1979) 490-494.
- [ 16 ] Eliezer I., Howald R.A.;  
'Thermodynamics of the vaporization processes for potassium  
sulfate'.  
The Journal of Chem. Ph. 65 (1976) 3053-3062.
- [ 17 ] Simmons L.L., Lowden L.F., Ehlert T.C.;  
'A mass spectrometric study of  $\text{K}_2\text{CO}_3$  and  $\text{K}_2\text{O}$ '.  
The Journal of Phys. Chem. 81 (1977) 706-709.
- [ 18 ] Schick H.L.;  
'Thermodynamics of Certain Refractory Compounds'.  
Volume II Academic Press New York-London (1966).
- [ 19 ] Kalff P.J., Alkemade C.Th.J.;  
'Determination of dissociation energies for some alkaline earth  
(hydro-)oxides in  $\text{CO}/\text{N}_2\text{O}$  flames'.  
The Journal of Chem. Phys. 59 (1973) 2572-2579.
- [ 20 ] Lau K.H., Cubiciotti D., Hildenbrand D.L.;  
'Effusion studies of the thermal decomposition of magnesium and  
calcium sulfates'.  
The Journ. of Chem. Phys. 66 (1977) 4532-4539.

- [21] Gorokhov L.N., Gusarov A.V., Makarov A.V., Nikitor O.I.;  
'Mass spectrometric study of the evaporation of alkali  
metaborates'.  
High Temperature Science 9 (1971) 1082-1085.
- [22] Barin I., Knacke O., Kubaschewski O.;  
'Thermochemical properties of inorganic substances'.  
Berlin, Heidelberg, New York: Springer 1973-1977.
- [23] Bauer S.H., Frurip D.J.;  
'Homogeneous Nucleation in Metal Vapors 5. A self-consistent  
Kinetic Model'.  
The Journal of Physical Chemistry 81 (1977).
- [24] Amdur I., Hammes G.G.;  
'Chemical Kinetics'.  
McGraw-Hill New York (1966) p. 42.
- [25] Brown T.D.;  
'The deposition of sodium sulphate from combustion gases'.  
J. Inst. Fuel 39 (1966) 378-385.
- [26] Jackson P.J., Duffin H.C.;  
'Laboratory studies of the deposition of Alkali-Metal Salts from  
flue gas' inclusive discussions; from: 'The Mechanism of corrosion  
by fuel impurities'.  
Int. Conf. 1963 Butterworths-London 1963 p. 427-442.
- [27] Raask E.;  
'Reactions of Coal Impurities during Combustion and Deposition of  
Ash Constituents on Cooled Surfaces' from: 'The Mechanism of  
Corrosion by Fuel Impurities'.  
Int. Conf. 1963 Butterworths-London 1963 p. 145-154.
- [28] Fenimore C.P.;  
'Two modes of interaction of NaOH and SO<sub>2</sub> in gases from fuel-lean  
H<sub>2</sub>-air flames'.  
Fourteenth Symposium (Int.) On Combustion, The Combustion  
Institute, (1973) 955-963.
- [29] Kulkarni A.K., Wang Y.J., Webb R.L.;  
'Fouling and Corrosion in Glass Furnace Regenerators'  
Heat Recovery Systems 4 (1984) 87-92.

- [ 30 ] Rosner D.E., Chen Bor-Kuan, Fryburg G.C., Kohl F.J.;  
 'Chemically Frozen Multicomponent Boundary Layer Theory of Salt  
 and/or Ash Deposition Rates from Combustion Gases'.  
 Comb. Science and Techn. 20 (1979) 87-106.
- [ 31 ] Rosner D.E., Seshadri K., Fernandez de la Mora J., Fryburg G.C.,  
 Kohl F.J., Stearns C.A., Santoro G.J.;  
 'Transport, Thermodynamic and Kinetic Aspects of Salt/Ash  
 Deposition Rates from Combustion Gases'.  
 Nat. Bur. Standards Spec. Public. 561 (1979) Proc. 10<sup>th</sup> Mat.  
 Res. Symp. Characterization of High Temperature Vapor and Gases,  
 p. 1451-1474.
- [ 32 ] Rosner D.E., Seshadri K.;  
 'Experimental and Theoretical Studies of the Laws Governing  
 Condensate Deposition from Combustion Gases'.  
 Eighteenth Symposium on Combustion 1981 p. 1385-1394.
- [ 33 ] Kohl F.J., Santoro G.J., Stearns C.A., Fryburg G.C., Rosner D.E.;  
 'Theoretical and Experimental Studies of the Deposition of  $\text{Na}_2\text{SO}_4$   
 from Seeded Combustion Gases'.  
 J. Electrochem. Soc.-Sol. St. Science and Techn. 126 (1979)  
 1054-1061.
- [ 34 ] Busby T.S., Sengel W.M.;  
 'Sampling regenerator carryover'.  
 Glass Technology 19 (1978) 47-53:
- [ 35 ] Milne T.A.;  
 High-Pressure Sampling Conference Report (Midwest Research  
 Institute, 1965); AD-618566.
- [ 36 ] Stearns C.A., Kohl F.J., Fryburg G.C., Miller R.A.;  
 'High Pressure Molecular Beam Mass Spectrometric Sampling of High  
 Temperature Molecules'.  
 NBS Spec. Publ. 561 (1979) Proceedings of the 10<sup>th</sup> Materials  
 Research Symposium on Characterization of High Temperature Vapors  
 and Gases' p. 303-355.
- [ 37 ] Biordi J.C., Lazzara C.P., Papp J.F.;  
 'Chemical flame inhibition using Molecular Beam Mass Spectrometry  
 Bromotrifluoromethane in low pressure methane-oxygen-argon flames'.  
 US Bureau of Mines Report of Investigations 7723 (1973) 1-39.

- [ 38] Hastie J.W., Imbov K.F., Bonnell D.W.;  
'Transpiration Mass Spectrometric Analysis of Liquid KCl and KOH  
vaporization'.  
High Temperature Science 17 (1984) 333-364.
- [ 39] Fryburg G.C., Miller R.A., Stearns C.A., Kohl F.J.;  
'Formation of  $\text{Na}_2\text{SO}_4$  and  $\text{K}_2\text{SO}_4$  in Flames doped with sulfur and  
alkali chlorides and carbonates'; from 'High Temperature Metal  
Halide Chemistry'. Hildenbrand D.L., Cubicciotti D.D.  
The Electrochem. Soc. Soft. Proc. Vol. 78-1 (1978) p. 468-483.
- [ 40] Bonnel D.W., Hastie J.W.;  
'Transpiration Mass Spectrometry of High Temperature Vapors'.  
NBS Spec. Publ. 561 (1979) Proceedings of the 10<sup>th</sup> Materials  
Research Symposium on Characterization of High Temperature Vapors  
and Gases' p. 357-409.

## NOMENCLATURE CHAPTER 2

$a_i$	stoichiometric coefficient for reactant $i$
A	component A in equation 2.51
A	gaseous polymer in equation 2.53 or 2.54
$b_j$	stoichiometric coefficient for product $j$
$\Delta G$	change in Gibbs Free Enthalpy ( $\text{J/mol}^{-1}$ )
$G_j$	standard Gibbs Free Enthalpy at 1 atmosphere ( $\text{J/mol}$ ) for product $j$
$G_i$	standard Gibbs Free Enthalpy at 1 atmosphere ( $\text{J/mol}$ ) for reactant $i$
G	arbitrary chosen gaseous molecule in equation 2.54
$K_T$	reaction equilibrium constant
$P_j$	product $j$
$P_T$	saturation pressure at temperature $T$ in (atm)
$R_i$	reactant $i$
R	constant of Boltzmann $8.3143 \text{ (J mol}^{-1} \text{,K}^{-1}\text{)}$

### Subscripts

c	condensed state
g	gaseous state
l	liquid state
s	solid state
n	indicates a n-mer in equation 2.53
i	indicates a i-mer in equation 2.53

### 3. CONDENSATION PRODUCTS AND GASEOUS COMPONENTS IN COOLING EXHAUST GASES

#### 3.1 Introduction

During the cooling process of the exhaust gases from glass melting furnaces several chemical conversions take place between 1700 K and 500 K. Gaseous components react to other gaseous compounds or to condensed material.

The kinetics of these chemical conversions are strongly dependent on temperature.

At temperatures above 1200 K almost all reaction rates are high enough to retain chemical equilibrium in the gas flow providing the temperatures do not change too quickly in the regenerators or recuperators. However, in the boundary layers near submerged obstacles in the flow regions of the exhaust gases, the high temperature gradients may result in limited conversions due to the finity of the reaction kinetics. At temperatures below 1200 K cooling rates may exceed reaction rates so that the local exhaust gas compositions in these temperature regions may differ from the equilibrium compositions.

The exhaust of glass furnaces entrains many different gaseous components and particulates in minor concentrations. These substances may catalyse the chemical conversion at low temperatures.

In this chapter the assumption is made that the exhaust gas composition equals the equilibrium composition in the entire temperature region between 1700 K and 600 K and this composition is calculated as a function of temperature with the aid of a thermodynamic model. Experiments have been carried out to evaluate this assumption and to investigate the reliability of this approach.

## 3.2 Thermodynamic approach to evaluate changing compositions during the cooling of the exhaust gases from glass furnaces.

### 3.2.1 The thermodynamic equilibrium model

In chapter 2 a comprehensive survey has been given for the most important gaseous reactions taking place in exhaust gases of various glass furnaces. Williams and Pasto [1], Kirkbride [2] and Roggendorf [3] have presented results of thermodynamic calculations for exhaust gas compositions for soda-lime glass furnaces.

In principle there are two methods of calculation:

1. Minimizing the total Gibbs' Free Energy for the components of the system at a certain temperature [4, 5].
2. Equilibration of all the relevant reactions (mentioned in chapter 2) at a certain temperature.

These two methods are essentially identical and give the same results, they only differ in the method of computation. Method 1 is preferably applied in very complex systems with more than 20 components. The calculations involve a non-linear minimization program. Method 2 may be used for calculations of rather simple systems and the computations can be executed with a small computer or with pocket calculators.

Besides the assumption of chemical equilibrium conditions in the gaseous phase, two other considerations have to be taken into account in this model:

- The concentrations of the gaseous constituents of the exhaust gases may not exceed the saturation pressure at the temperature under consideration. Condensation takes place for components reaching the saturation pressure and the partial pressure of these components will be equal to that pressure.
- The mass conservation laws have to be considered for each chemical element in the constituting gaseous or condensed components.

For a system with  $n$  different chemical elements,  $m$  different gaseous components and  $p$  different condensing components,  $(m-n)$  independent chemical reactions are involved, leading to  $(m-n)$  equilibrium equations.

The mass conservation laws lead to  $n$  equations and the amount of saturation pressure equations is equal to the value of  $p$ .

The total amount of equations is:  $(m-n) + n + p = (m+p)$ .

The total amount of gaseous and condensed compounds also equals  $(m+p)$ . Thus the applied equilibrium model always results in only one solution for the chemical composition of the exhaust gases in equilibrium situations.

An example for the calculations according to method 2 for an exhaust gas of a soda-lime glass furnace is presented in figure 3.1.

### **3.2.2 Chemical compositions of the exhaust gases from different glass furnaces**

Thermodynamic equilibrium calculations have been carried out to investigate the chemical nature of the gaseous components and condensed material in exhaust gases from soda-lime glass furnaces, borosilicate glass furnaces and lead glass furnaces. By means of thermodynamic equilibrium calculations the influences of changing temperatures, changing fuel composition, and changing vaporization behaviour of the melt on the chemical conversions and condensation processes in the exhaust gases have been determined.

#### **3.2.2.1 The calculation of flue gas compositions in soda-lime glass furnaces**

The conversions of gaseous components in soda-lime glass furnace exhausts may be described by reactions (2.1) to (2.9) of chapter 2. The most important constituent of the deposits in regenerators of these furnaces is sodium sulphate. According to Kirkbride [2] sodium carbonate and sodium chloride are expected to condense in sulphur lean flue gases. In this section the influence of variations in the elemental compositions on the condensation behaviour of exhaust gases from soda-lime glass furnaces is presented.

The first situation to be studied, involves an exhaust gas to be expected from natural gas-fired glass furnaces. The composition is given in table 3.1, oxygen, water vapor, nitrogen and carbon dioxide are the major constituents and their concentrations are assumed to be independent of temperature. The minor constituents are given in this table as chemical elements in gaseous form.

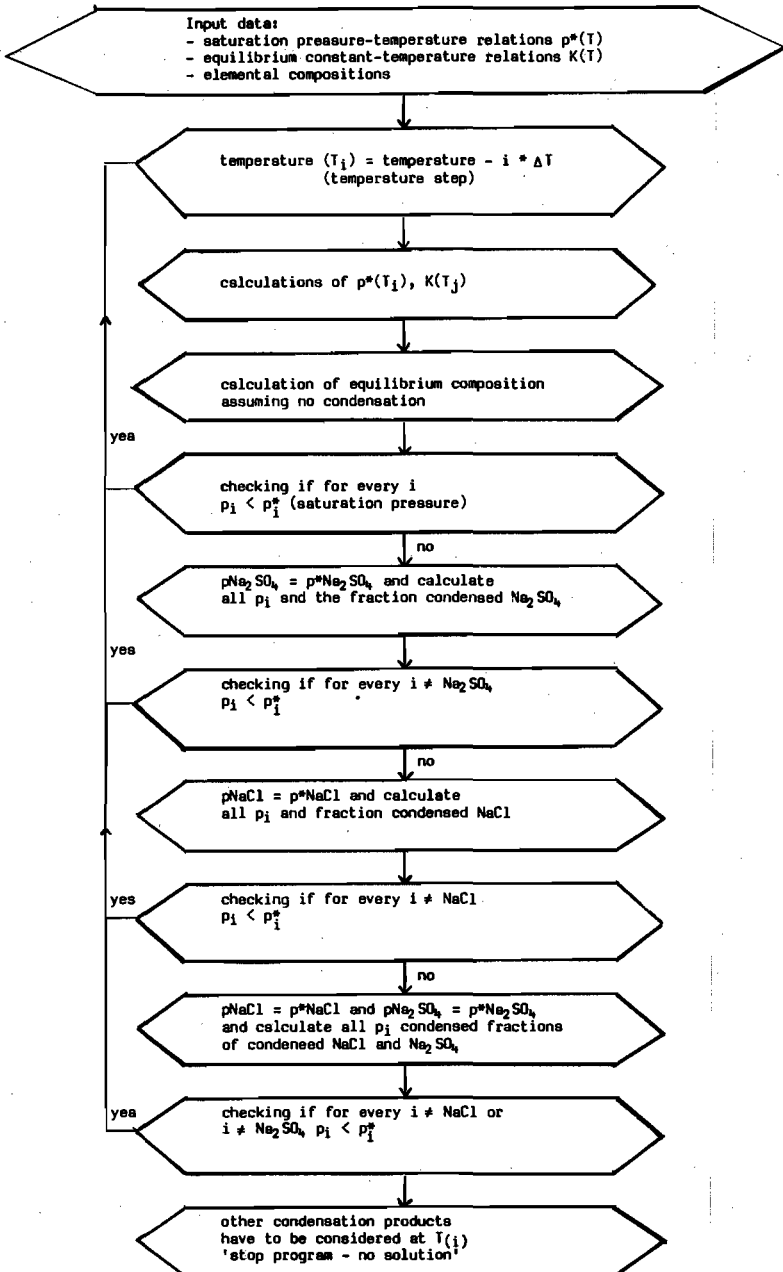


Figure 3.1: Schematic presentation of calculation process for the equilibrium composition of the exhaust gases from soda-lime glass furnaces, assuming only NaCl and Na<sub>2</sub>SO<sub>4</sub> condensation.

**Table 3.1:** Typical overall composition of the exhaust gas from a natural gas fired glass furnace producing soda lime glass.

major components	volume-%	minor elements	volume-%
N <sub>2</sub>	72.8	Na	1.25 10 <sup>-2</sup>
O <sub>2</sub>	4.4	S	2.5 10 <sup>-2</sup>
Ar	0.8	Cl	6.25 10 <sup>-3</sup>
CO <sub>2</sub>	9.0		
H <sub>2</sub> O	13.0		

Carbon dioxide is formed by the combustion reactions and by dissociation of the soda and limestone batch materials.

Chlorides mainly vaporize as sodium chloride (NaCl), an impurity in synthetic soda ash. Sodium vaporizes as sodium hydroxide from the glass melt and as sodium chloride from the soda ash.

Sulphur is released from the glass melt during the melting and refining period probably as sulphur dioxide (SO<sub>2</sub>). The chemical equilibrium composition for the most interesting gaseous components is presented by figure 3.2a and 3.2b. Gaseous sodium hydroxide, sodium chloride and sodium react to gaseous sodium sulphate at temperatures decreasing from 1700 K to 1400 K. This causes an increase in the concentration of Na<sub>2</sub>SO<sub>4</sub> at decreasing temperatures, as can be seen from figure 3.2a. Sodium carbonate concentrations and the concentrations of the dimer of sodium hydroxide (NaOH)<sub>2</sub> initially increase in the exhaust gases at decreasing temperatures.

However, below the dew point temperature of sodium sulphate, all the concentrations of the sodium- containing gaseous components decrease at further cooling. This is caused by formation of liquid or solid sodium sulphate.

In figure 3.2c the fraction of the total sodium amount is given, present in the flue gas as condensed sodium sulphate. At 1200 K, more than 90% of the available sodium is converted into liquid Na<sub>2</sub>SO<sub>4</sub>. Thus the condensation of sodium sulphate below the dew point of approximately 1380 K results in quickly diminishing concentrations of gaseous sodium components like NaCl, NaOH, Na, Na<sub>2</sub>SO<sub>4</sub>, Na<sub>2</sub>CO<sub>3</sub> and (NaOH)<sub>2</sub>.

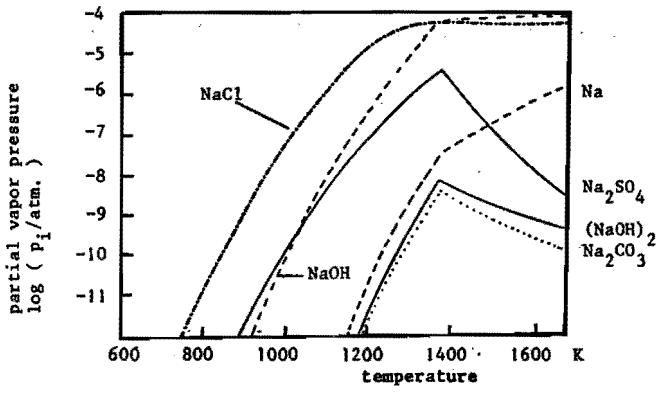


Figure 3.2a: Vapor pressures of sodium containing components in the exhaust gas according to equilibrium calculations for a natural gas fired soda-lime glass furnace.

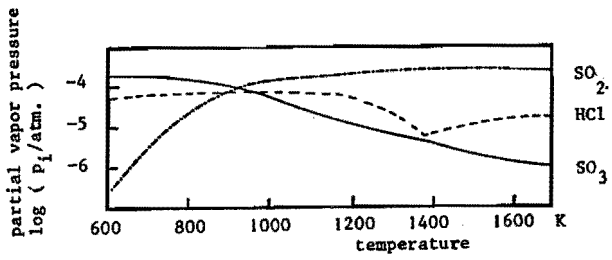


Figure 3.2b: Vapor pressures of sodium free components in the exhaust gas according to equilibrium calculations for a natural gas fired soda-lime glass furnace.

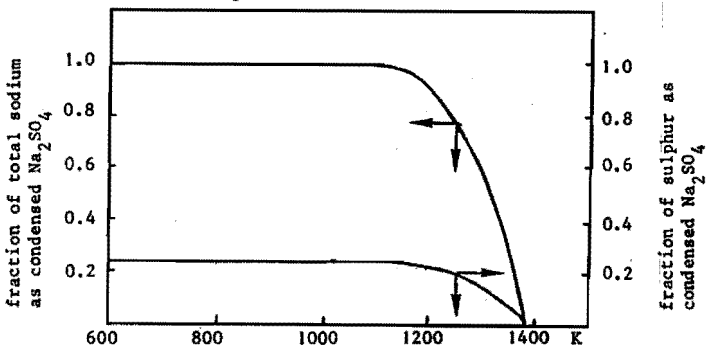


Figure 3.2c: Fractions of sodium and sulphur condensed as sodium sulphate in the exhaust gas from soda-lime glass furnace.

This effect is less obvious for the sulphur containing components like  $\text{SO}_2$  and  $\text{SO}_3$ . Because of the rather large excesses of sulphur containing components in the flue gas, the condensation of sodium sulphate has a relatively slight effect on the concentrations of sulphur dioxide and sulphur trioxide. In figure 3.2.c it is shown that only 25% of the total sulphur content is converted into condensed sodium sulphate. At decreasing temperatures the equilibrium of the reaction:



moves to the right, resulting in increasing  $\text{SO}_3$  concentrations, see figure 3.2b. According to these calculations sodium sulphate is the only stable product condensing from this exhaust gas between 1380 K and 1150 K as can be seen from figure 3.2c. Below 1150 K nearly all the gaseous sodium components are converted into this salt.

From additional calculations the conclusions may be drawn that no sodium chlorides and sodium carbonates condense from flue gases with sulphur/sodium ratios higher than the stoichiometric ratio of 0.5 in sodium sulphate. So, only with sodium concentrations four times higher or with sulphur concentrations four times lower than in this case, other sodium compounds will condense from these types of exhaust gases.

The dew point temperature (temperature for the onset of condensation) for sodium sulphate varies slightly with the water vapor concentration see figure 3.3 and varies only for low  $\text{O}_2$ -levels with the oxygen concentrations as shown in figure 3.4. The dew point increases to 1425 K for a sodium content twice that of the base situation as can be seen from figure 3.5. Thus for higher furnace temperatures or higher flame velocities with higher volatilization rates the onset of sodium sulphate condensation shifts to higher temperatures.

By changing the fuel from natural gas to heavy oil the carbon dioxide concentrations and sulphur concentrations will increase and the water vapor content will decrease slightly. The exhaust gas composition is almost independent of the carbon dioxide concentrations because of the very low sodium carbonate conversion in the flue gases. The sulphur concentration in case of oil-firing may reach values of  $4 \cdot 10^{-4}$  to  $1 \cdot 10^{-3}$  volume-%, the water concentration is approximately 10%.

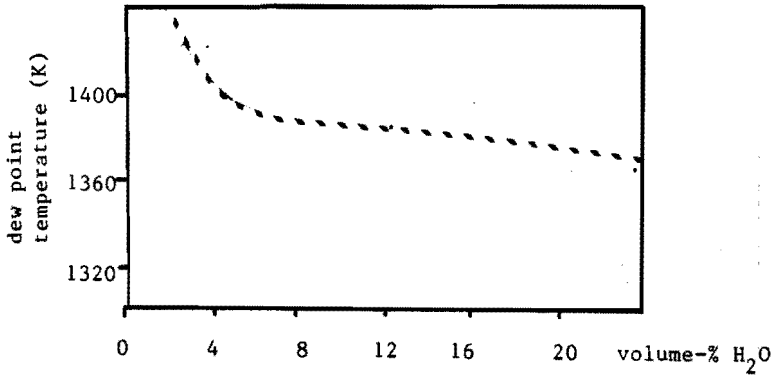


Figure 3.3: Thermodynamic dew point of sodium sulphate in exhaust gas for different water vapor levels.

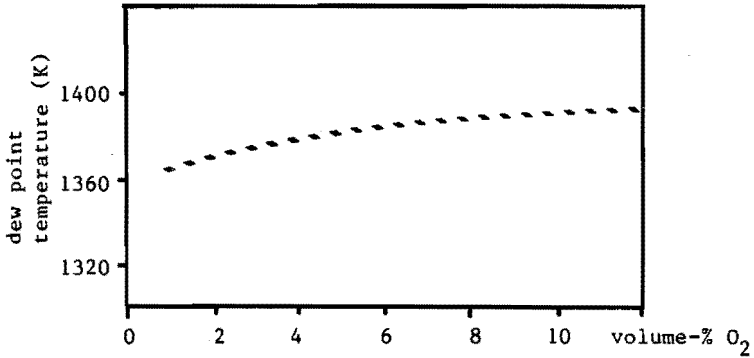


Figure 3.4: Thermodynamic dew point of sodium sulphate in exhaust gas for different oxygen levels.

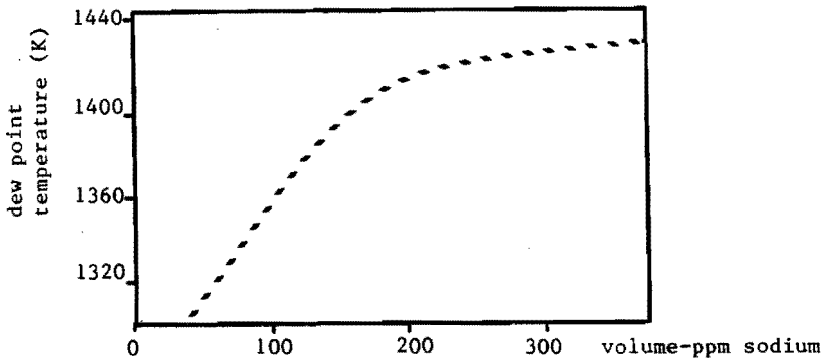


Figure 3.5: Thermodynamic dew point of sodium sulphate in exhaust gas for different sodium concentrations.

According to figures 3.3 and 3.6 the sodium sulphate dew point increases only 10 to 20 K when using mineral oils instead of natural gas. The dew point rises 25 K by using natural soda ash instead of synthetic soda ash due to the very low chloride levels in natural soda ashes. Figure 3.7 presents the relation between dew point and chlorine content in the flue gas. At high dew point temperatures a large amount of sodium sulphate condenses in the liquid phase above the melting temperature of 1157 K.

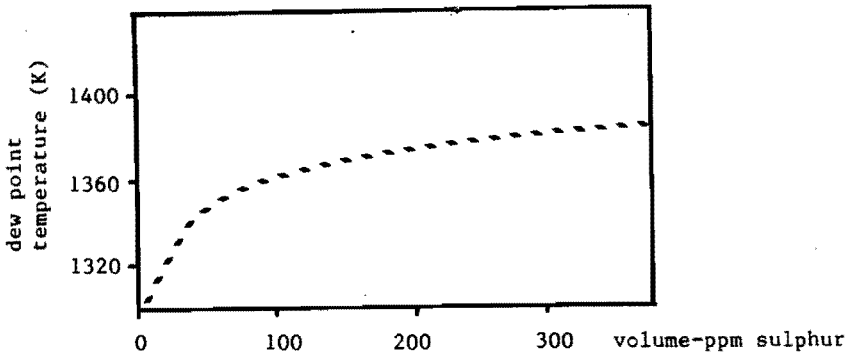


Figure 3.6: Thermodynamic dew point of sodium sulphate in exhaust gas, for different sulphur levels.

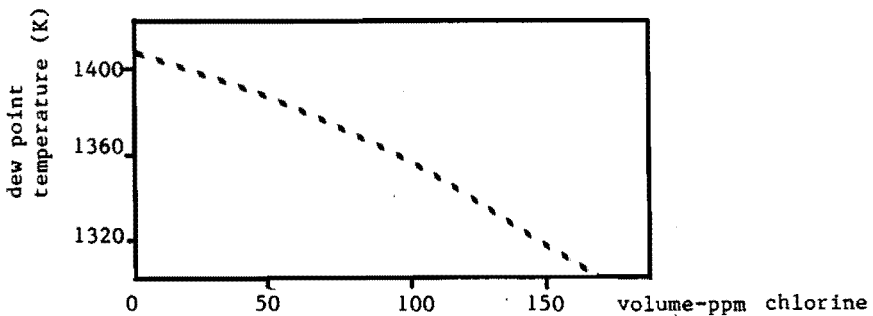


Figure 3.7: Thermodynamic dew point of sodium sulphate in exhaust gas, for different chlorine levels.

Liquid sodium sulphate is extremely corrosive and may damage the refractories of the checker works. Deposition of sodium sulphate on regenerator bricks just above the melting point temperature is extremely dangerous. During the air preheat period this deposited liquid salt may convert into solid sodium sulphate. The liquid sodium sulphate that might have penetrated the pores of the bricks mechanically damages their structure when becoming solid and therefore having a higher specific volume. For that reason it is important to prevent condensation or deposition of sodium sulphate near the melting point.

By means of the equilibrium calculations it is possible to predict the influence of flue gas additions on the temperature region where the condensation process takes place. The total amount of dust produced in the exhaust gases of soda-lime glass furnaces is mainly dependent on the volatilization rate of sodium containing components. According to the considerations of section 1.1.2 of this thesis the volatilization of sodium components increases with the water vapor pressure, the temperature and the flame velocity in the glass melting furnace. Although sodium hydroxide vaporization is enhanced by the higher water vapor concentrations in natural gas-fired furnaces as compared to those in oil-fired furnaces, this effect is countered by relatively low flame velocities in natural gas fired tanks. The sulphate content of the batch may be reduced by adding other refining agents than sodium sulphate.

Table 3.2: Overall composition of sulphur lean flue gas from a natural gas fired glass furnace producing soda-lime glass.

major components	volume-%	minor elements	volume-%
N <sub>2</sub>	72.8	Na	1.25 10 <sup>-2</sup>
O <sub>2</sub>	4.4	S	3.0 10 <sup>-3</sup>
Ar	0.8	Cl	6.25 10 <sup>-3</sup>
CO <sub>2</sub>	9.0		
H <sub>2</sub> O	13.0		

In the case that only small amounts of salt cake ( $\text{Na}_2\text{SO}_4$ ) are added to the batch, the sulphur concentrations in the flue gases can be reduced to  $3.0 \cdot 10^{-5}$  volume-% for a natural gas fired furnace.

The exhaust gas composition in this case is given by table 3.2, figure 3.8a represents the equilibrium compositions of such an exhaust gas between 1600 K and 600 K. Below 990 K sodium chloride condenses (figure 3.8b) and below 1030 K small amounts of sodium carbonate may condense.

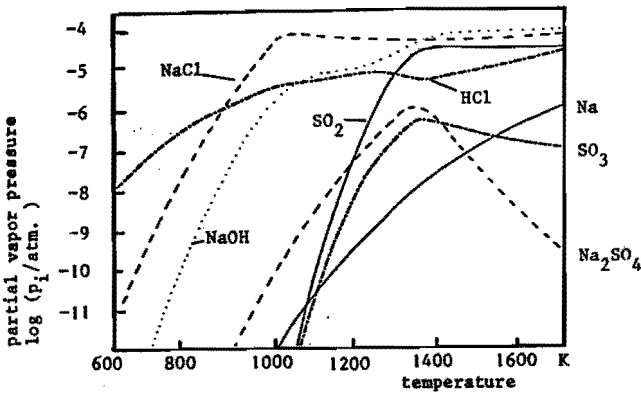


Figure 3.8a: Vapor pressures of constituents of sulphur lean exhaust gas, according to equilibrium calculations.

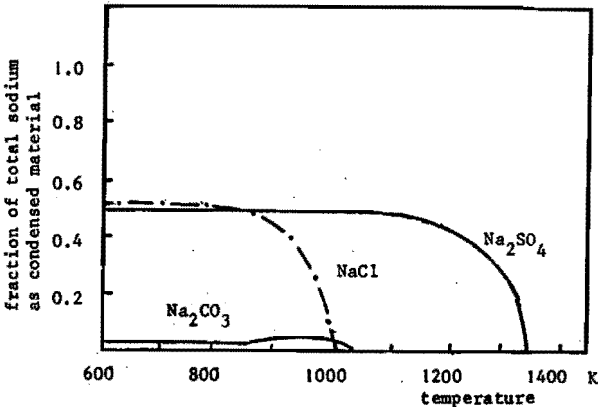


Figure 3.8b: Sodium distribution among condensed components from sulphur lean flue gas.

The dust in the gases contains 32 mol-% sodium sulphate, 66.7 mol-% sodium chloride and 1.3 mol-% sodium carbonate below temperatures of 800 K.

Finally, the case is considered when besides sodium also potassium components vaporize from the glass melt. Equilibrium calculations have been carried out for the overall gas composition listed in table 3.3.

Table 3.3: Overall flue gas composition of a soda-potash glass furnace with natural gas firing.

major components	volume-%	minor elements	volume-%
N <sub>2</sub>	72.8	Na	8.0 10 <sup>-3</sup>
O <sub>2</sub>	4.4	K	4.0 10 <sup>-3</sup>
Ar	0.8	S	2.50 10 <sup>-2</sup>
CO <sub>2</sub>	9.0	Cl	6.25 10 <sup>-3</sup>
H <sub>2</sub> O	13.0		

These calculations do not take the formation of condensed sodium-potassium sulphates into account. The thermodynamic properties of KNaSO<sub>4</sub> are not sufficiently known and formation of this compound is neglected in the model. The formation of KNaSO<sub>4</sub> hardly affects the results of our calculations, figure 3.9.a and 3.9.b give the results of these calculations.

The gaseous sodium sulphate as well as the gaseous potassium sulphate concentrations increase during cooling from 1700 K to 1400 K. Sodium sulphate condenses at 1360 K resulting in decreasing concentrations of the gaseous sodium components NaOH, NaCl and Na<sub>2</sub>SO<sub>4</sub> below this temperature. Below 1250 K (the dew point for K<sub>2</sub>SO<sub>4</sub>) the concentrations of gaseous potassium components decrease rapidly. The formation of condensed sodium sulphate and condensed potassium sulphate is presented in figure 3.9c. Below 1000 K nearly all the sodium and potassium are converted into respectively condensed Na<sub>2</sub>SO<sub>4</sub> and condensed K<sub>2</sub>SO<sub>4</sub> or condensed KNaSO<sub>4</sub> (not regarded in our calculations).

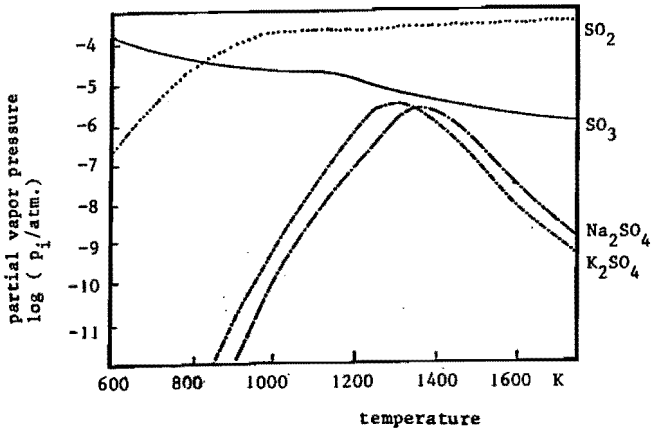


Figure 3.9a: Vapor pressures of sulphur containing components in exhaust gas, according to equilibrium calculations, exhaust gas from table 3.3.

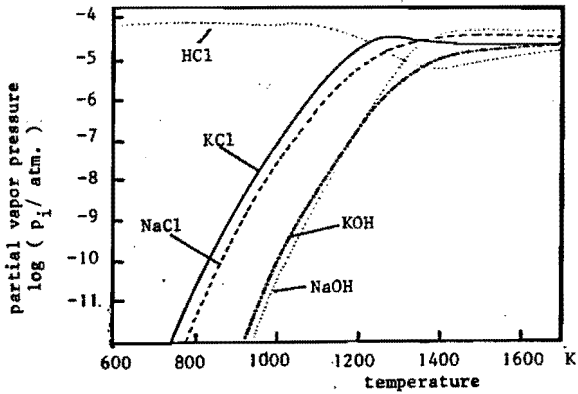


Figure 3.9b: Vapor pressures of sulphur free components in exhaust gas, according to equilibrium calculations, exhaust gas from table 3.3.

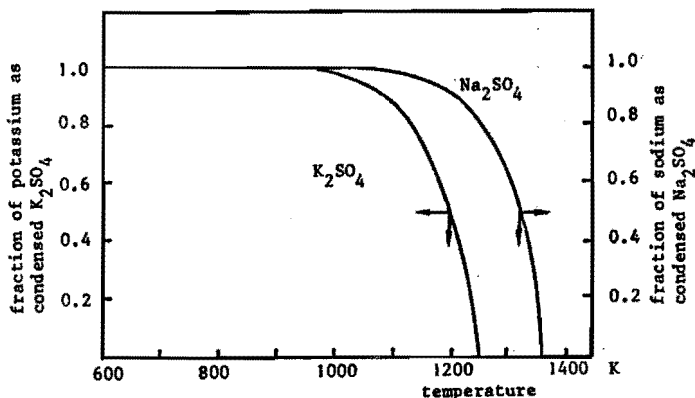


figure 3.9c: Fractions sodium and potassium from exhaust gas condensed as respectively  $Na_2SO_4$  and  $K_2SO_4$  according to equilibrium calculations for exhaust gas from table 3.3.

### 3.2.2.2 Calculations of flue gas compositions in borosilicate glass furnaces

Although several investigators have studied the equilibrium compositions of exhaust gases from soda-lime glass furnaces, very little information is available about the compositions of flue gases from other glass furnaces. The compositions of borosilicate glasses vary widely: alkali-borosilicate glasses with 4-6 weight-% sodium and potassium, or with alkali concentrations lower than 0.5 weight-% are produced on industrial scale.

Sodium oxides in the melt react with borium oxide resulting in the formation of volatile sodium metaborate. Concentrations of sodium and potassium containing components (primarily borates) may exceed the concentrations of these components in exhaust gases of soda-lime glass furnaces, although the glass may contain less alkali oxides. The exhaust gas composition of a typical sodium-borosilicate glass furnace is given in table 3.4.

Table 3.4: Exhaust gas composition for a natural gas fired sodium borosilicate glass furnace.

glass composition oxide weight-%	major components	volume-%	minor elements	volume-%
SiO <sub>2</sub>	N <sub>2</sub>	72.8	Na	5. 10 <sup>-2</sup>
Al <sub>2</sub> O <sub>3</sub>	O <sub>2</sub>	4.4	S	1.25 10 <sup>-2</sup>
Na <sub>2</sub> O 5.0	Ar	0.8	Cl	1.0 10 <sup>-5</sup>
K <sub>2</sub> O	CO <sub>2</sub>	9.0	B	5. 10 <sup>-2</sup>
CaO	H <sub>2</sub> O	13.0		
B <sub>2</sub> O <sub>3</sub>				
others				

According to the thermodynamic calculations sodium sulphate condensation starts below 1350 K. At temperatures approximately 80 K lower than the dew point of sodium sulphate, sodium metaborate condenses and at much lower temperatures sodium chloride may condense. The composition of this exhaust gas, dependent on temperature, is given in figure 3.10a and 3.10b.

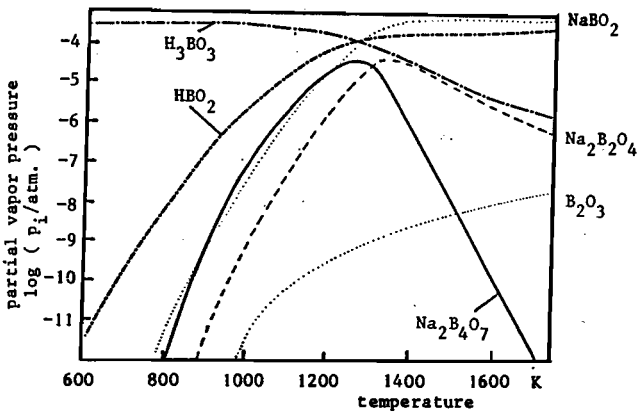


Figure 3.10a: Vapor pressures of boron containing components in exhaust gas, according to equilibrium calculations - exhaust gas from table 3.4.

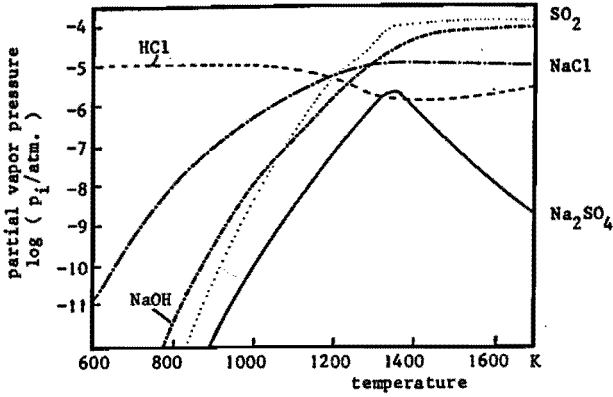


Figure 3.10b: Vapor pressures of boron free components in exhaust gas, according to equilibrium calculations - exhaust gas from table 3.4.

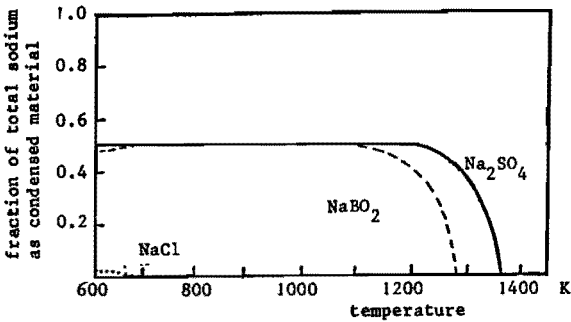


Figure 3.10c: Distribution of total sodium in exhaust gas among condensed components according to equilibrium calculations - exhaust gas from table 3.4.

Below the sodium sulphate dew point the concentrations of gaseous sodium components decrease rapidly. At temperatures lower than the dew point of sodium metaborate a decrease in the concentrations of gaseous metaboric and sodium metaborate takes place.

Figure 3.10c presents the condensation behaviour in the flue gas at different temperatures. Sodium metaborate below 1270 K and sodium sulphate below 1360 K, condense. Sodium metaborate, sodium hydroxide and sodium chloride are the most important gaseous sodium constituting components at temperatures above the sulphate dew point. Metaboric acid ( $\text{HBO}_2$ ) is converted to boric acid ( $\text{H}_3\text{BO}_3$ ) at temperatures below 1300 K. At all temperatures borium oxide ( $\text{B}_2\text{O}_3$ ) is a minor component in this exhaust gas and no condensation of  $\text{B}_2\text{O}_3$  is expected from the results of the calculations. Sodium tetraborate is an important gaseous constituent between 1150 K and 1350 K but no condensation of  $\text{Na}_2\text{B}_4\text{O}_7$  is expected from this flue gas.

However, the system  $\text{B}_2\text{O}_3$ - $\text{Na}_2\text{O}$  is very complex and minor important components like  $\text{Na}_2\text{O} \cdot (\text{B}_2\text{O}_3)_5$  or  $\text{Na}_2\text{O} \cdot (\text{B}_2\text{O}_3)_4$  may be formed, but these have not been included in our calculations. In figure 3.10 the vapor pressure curves for  $\text{Na}_2\text{CO}_3$ ,  $(\text{NaOH})_2$ , Na and  $\text{SO}_3$  are not given, these components appear to be of minor importance for the exhaust gas analysis.

### Sodium tetraborate condensation

Flue gases from furnaces melting borosilicate glass with high borium oxide concentrations, contain large amounts of metaboric acid or at low temperatures boric acid ( $\text{H}_3\text{BO}_3$ ).

These components react with sodium hydroxide or sodium metaborate to sodium tetraborate:



Instead of sodium metaborate condensation, sodium tetraborate deposition or dust formation may take place in these exhaust gases. Calculations have been carried out for an exhaust gas similar to the exhaust gas from table 3.4 with instead of  $5.0 \cdot 10^{-2}$  volume-% boron,  $1.0 \cdot 10^{-1}$  volume-% boron.

The condensation products (see figure 3.11) are sodium sulphate below 1300 K, sodium metaborate between 1200 K and 1260 K and also below 825 K and finally sodium tetraborate between 1240 K and 775 K.

At a temperature of 1260 K the condensation of sodium sulphate is not complete and the ratio between gaseous sodium compounds and gaseous boron compounds is approximately 0.4. When nearly all sulphur has reacted with sodium compounds to condensed sodium sulphate the ratio gaseous sodium compounds/gaseous boron compounds lowers to a value of 0.25.

Sodium tetraborate condensation is favoured by high concentrations of boron and sodium and also for low sodium/boron ratios.

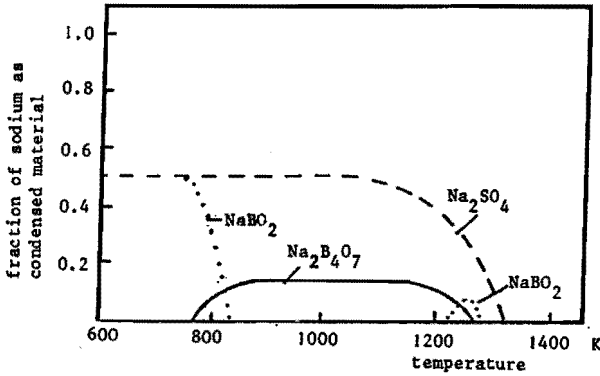


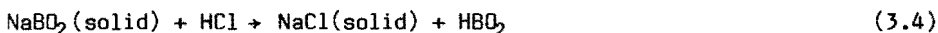
Figure 3.11: Distribution of the sodium from exhaust gas, among condensed compounds.

The complexity of the chemical behaviour in exhaust gases from borosilicate glass furnaces is shown by the condensation behaviour of these gases. The occurrence of two temperature regions for sodium metaborate condensation is caused by the different temperature dependence of the thermodynamic functions for condensed sodium metaborate and sodium tetraborate. The curve for sodium sulphate condensation is less steep than in the case of boron free exhaust gases. This effect is caused by the rather high gaseous sodium metaborate concentrations between 1200 and 1300 K.

### Sodium chloride condensation

The concentrations of chlorides in exhaust gases from borosilicate glass furnaces depend on the raw materials used. At chlorine concentrations of  $1.0 \cdot 10^{-3}$  volume-%, as is the case for the exhaust gas of table 3.4, only at temperatures lower than 700 K condensation of sodium chlorides may take place.

An increase from  $10^{-3}$  to  $5 \cdot 10^{-2}$  volume-% results in a 100 K higher condensation temperature for NaCl. In the temperature region where sodium chloride condensation takes place, a decrease in sodium metaborate condensation rates is observed. At these temperatures reaction 3.4 is important:



Sodium chloride condensation is not expected in regenerators of borosilicate furnaces because of the rather high temperatures and the relatively low sodium chloride dew points for these exhaust gases. Sodium metaborates only condense from exhaust gases with rather low sulphur concentrations. Sodium sulphate is the only condensed product thermodynamically stable in exhaust gases from oil-fired sodium-borosilicate glass furnaces with sulphur concentrations higher than  $3.0 \cdot 10^{-2}$  volume-%.

### Exhaust gases from glass furnaces producing alkali lean borosilicate glass

Borosilicate glasses like E-glass contain very low amounts of potassium oxide and sodium oxide. The furnace gases may contain boron concentrations of  $5 \cdot 10^{-2}$  till  $10^{-1}$  volume-%, potassium concentrations are in the order of  $2 \cdot 10^{-2}$  volume-% and sodium concentrations may vary from  $5 \cdot 10^{-3}$  to  $1 \cdot 10^{-2}$  volume-%. Especially potassium borates are very volatile resulting in rather high potassium amounts in the furnace atmosphere of borosilicate glasses with a  $\text{K}_2\text{O}$  concentration of 0.5 weight-%.

In natural gas fired furnaces and the application of refining agents other than sodium sulphate, condensation of sodium metaborate and potassium metaborate takes place, according to the calculation based on thermodynamic equilibrium. In oil-fired furnaces only sodium sulphate and potassium sulphate condense, boron is mainly emitted as gaseous boric acid ( $\text{H}_3\text{BO}_3$ ) in the stack gases.

### 3.2.2.3 Calculated flue gas compositions in lead glass furnaces

Lead glass furnaces are usually equipped with an electrostatic precipitator, since stack gases contain 700 to 1500 mg dust per cubic metre exhaust gas volume [6] (under normalized conditions, 295 K and 1013 mbar). More than 90% of this dust consists of lead components, like lead sulphate and lead oxides.

According to Matousek and Hlavac [7], the rate of volatilization of lead components from the glass melt is at least one order of magnitude higher than vaporization of alkali components from a glass with; 4.5 weight-%  $\text{Na}_2\text{O}$ , 10 weight-%  $\text{K}_2\text{O}$  and 24 weight-%  $\text{PbO}$ . The volatilization from lead glasses has been described in section 1.1.2.2 of this thesis.

Thermodynamic equilibrium calculations have been carried out for an exhaust gas from a natural gas fired furnace without sulphur components. This exhaust gas is presented by table 3.5.

Table 3.5: Sulphur free exhaust gas from a lead glass furnace.

major components	volume-%	minor elements	volume-%
$\text{N}_2$	72.8	Pb	$2 \cdot 10^{-2}$
$\text{O}_2$	4.4	K	nihil
Ar	0.08	Na	nihil
$\text{CO}_2$	9.0		
$\text{H}_2\text{O}$	13.0		

The flue gas composition is represented in figure 3.12a. The concentrations of the oligomers of  $\text{PbO}$  like  $\text{Pb}_2\text{O}_2$ ,  $\text{Pb}_3\text{O}_3$ ,  $\text{Pb}_4\text{O}_4$  increase during the cooling till approximately 1160 K. Below this temperature (see figure 3.12b) lead oxide condenses till 1000 K. The calculations neglect the formation of lead hydroxide because of insufficient thermodynamic data for this gaseous component. However, gaseous  $\text{Pb}(\text{OH})_2$  is a rather important constituent in these exhaust gases in a certain temperature region.

In spite of this, the calculations have been carried out and will be compared with experimental results presented later in this thesis. From this comparison the effect of neglecting the formation of lead hydroxide appears to be of minor importance for this treatment. Lead monoxide is converted into  $Pb_3O_4$  at temperatures below 700 K.

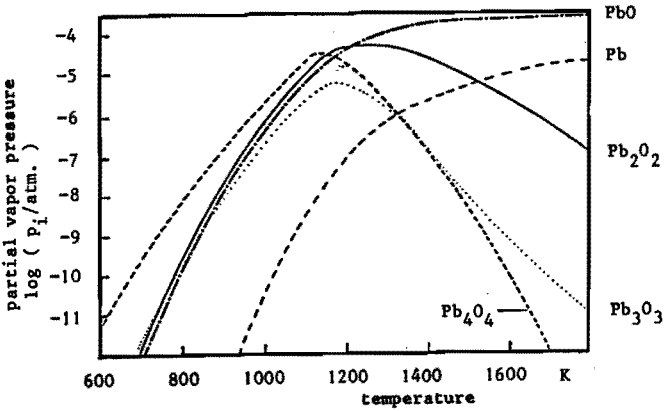


Figure 3.12a: Vapor pressures of lead compounds in exhaust gas according to equilibrium calculations for exhaust gas from table 3.5.

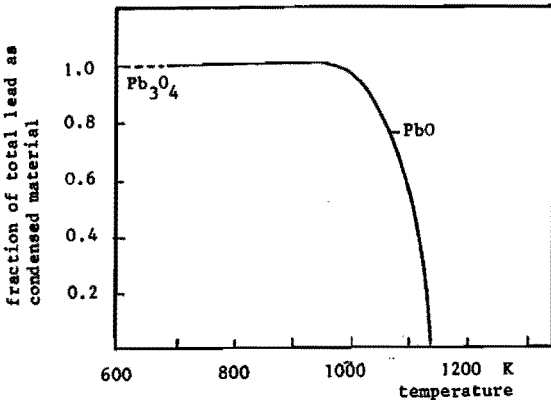


Figure 3.12b: Fraction of total lead from exhaust gas as condensed components according to equilibrium calculations.

Stack gases from oil-fired lead glass furnaces consist of large amounts of lead sulphate dust. Components like:

- $PbSO_4$  ;
- $PbO.PbSO_4$  ;
- $2PbO.PbSO_4$  ;
- $PbO$  ;

and  $Pb_3O_4$  may be present in the dust precipitated from these exhaust gases. The exhaust gas composition used for the equilibrium calculations is given in table 3.6.

Table 3.6: Exhaust gas from an oil-fired lead glass furnace.

major components	volume-%	minor elements	volume-%
$N_2$	72.8	Pb	$2.10^{-2}$
$O_2$	4.4	S	$3.10^{-3}$
Ar	0.8		
$CO_2$	9.0		
$H_2O$	13.0		

Figure 3.13 shows the temperature dependence of the exhaust gas composition. For flue gases with a lead/sulphur ratio higher than 1.0, also  $PbO$  and  $PbO.PbSO_4$  condensation is expected according to our calculations.

Other components like sodium or potassium hardly react with lead oxides. In exhaust gases containing alkali components like sodium or potassium besides lead and sulphur, the condensation of alkali sulphates is the first to set on. The sulphur oxides remaining in the gaseous phase after alkali sulphate condensation react with lead oxide resulting in lead sulphate ( $PbSO_4$ ) condensation.

Condensation of lead sulphate often takes place in combination with lead-oxide condensation, forming  $PbO.PbSO_4$ ,  $2PbO.PbSO_4$  or  $4PbO.PbSO_4$ .

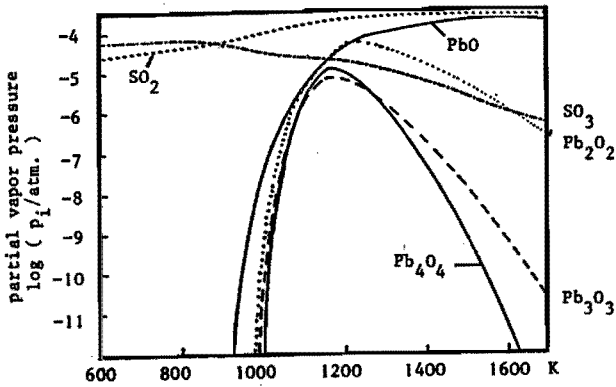


Figure 3.13a: Vapor pressures of sulphur and lead containing components in exhaust gas, according to equilibrium calculations for exhaust gas from table 3.6.

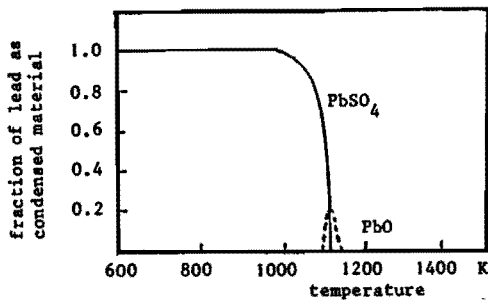


Figure 3.13b: Lead distribution among condensed phases according to equilibrium calculations for exhaust gas from table 3.6.

### 3.2.3 Restrictions of the thermodynamic equilibrium model

The reliability of the results of the thermodynamic calculations depends on many factors. The method presented here to investigate the composition of the gaseous and condensed products in exhaust gases from glass furnaces is the first step to determine the corrosive nature of the flue gases. However, a number of aspects have to be considered before the the model may be applied for practical situations.

#### 3.2.3.1 Reaction kinetic limitations

Exhaust gases are cooling down from 1700 K to approximately 800 K in 2 to 4 seconds in glass furnace regenerators. The limited reaction rates may inhibit the total conversion of exhaust gas components to the equilibrium composition when passing the checker work of the regenerator. To study the validity of the equilibrium calculations it is convenient to define first a characteristic reaction time  $\tau_c$ : the time needed to obtain a composition with concentrations within 10% of the equilibrium value. A practical way to apply this method is the introduction of the TSRT(n) (Temperature Step Reaction Time) for the reactivity of exhaust gases during the passage of the checker work. This TSRT(n) is the characteristic reaction time ( $\tau_c$ ) needed to obtain gas concentrations within 10% of the equilibrium values after a sudden temperature reduction of 100 K. For TSRT (100)-values lower than 100 milliseconds it is justified to assume that the exhaust gas components are in chemical equilibrium in the exhaust gases from glass furnaces. Reaction kinetic data for reactions in flue gases involving sodium, lead, boron or sulphur compounds are very rare. No data are available for the formation of gaseous sodium sulphate or lead oxides. Besides the lack of kinetic data the application of this method has some more drawbacks like the catalytic action of minor flue gas components (gaseous or particulate species) which may enhance the reactions in the gaseous phase. Nevertheless it seems worthwhile to carry out an evaluation of TSRT (100)-values for a hypothetical exhaust gas composition (without catalytic agents), for which data are available. This exhaust gas contains only sodium and chlorine as minor components. As an example we have taken the composition given in table 3.7.

Table 3.7: Exhaust gas composition for reaction kinetic calculations.

major components	volume-%	minor elements	volume-%
N <sub>2</sub>	73	Na	2.10 <sup>-5</sup>
O <sub>2</sub>	2.2	Cl	2.10 <sup>-5</sup>
Ar	0.8		
CO <sub>2</sub>	9		
H <sub>2</sub> O	13		

The TSRT (100)-values for different temperatures have been calculated with reaction kinetic data from Jensen and Jones [8] and are represented in figure 3.14.

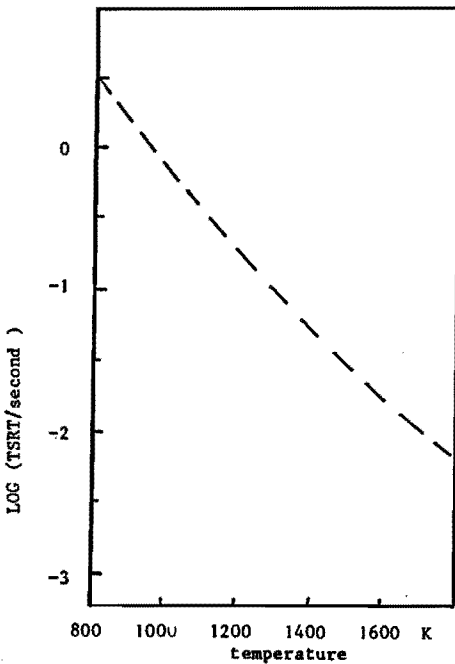


Figure 3.14: Dependence of characteristic reaction time TSRT (100) as function of temperature for exhaust gas from table 3.7.

This method provides a very rough estimation for reaction times in an exhaust gas doped with chlorides and sodium compounds, without taking into account the presence of catalysing agents. As can be seen for temperatures above 1200 K the requirement of a TSRT (100) larger than 100 milliseconds to obtain a chemical equilibrium in the exhaust gases, is fulfilled.

### **3.2.3.2 Condensation kinetic limitations**

In our equilibrium model the assumption has been made that condensation of components having partial vapour pressures equal to the saturation value takes place. In practice however, condensation may only set on after reaching a certain supersaturation at which the condensation rates are significant enough.

In exhaust gases containing supersaturated vapors two kinds of condensation processes may take place. Condensation may set on at already available condensed material or particulate matter in the exhaust gases. This is called heterogeneous condensation and is generally a relatively fast proceeding process.

In flue gases with little particulate matter, condensation starts only after a homogeneous nucleation process. Initially monomer molecules of the supersaturated component agglomerate into rather instable oligomers. These oligomers grow at increasing supersaturation values, resulting in the formation of more stable nuclei consisting of more than 100 monomer units. The complexity of the homogeneous and heterogeneous nucleation processes makes it difficult to study condensation in exhaust gases of glass furnaces theoretically.

### **3.2.3.3 Inaccuracies in the thermodynamic data**

The reaction constants for the most important conversions in flue gases from glass furnaces have been derived from the Gibbs' Free Enthalpy functions for the proper components. The values for these thermodynamic properties were taken from literature.

A comprehensive study has been carried out to validate these data and to choose the most reliable values. However, many of the available parameters had to be derived from less accurate determinations. The saturation pressures for sodium metaborate, sodium tetraborate and potassium borates for instance, could only be roughly estimated from the data available.

Extrapolation of thermodynamic data, measured in a limited temperature range, introduces rather large uncertainties at other temperatures. To study the effect of these inaccuracies, calculations have been carried out with a saturation pressure for sodium metaborate two times lower than the values used previously.

The exhaust gas composition from table 3.4 has been taken for these calculations. As a result of this altered parameter the dew point for sodium metaborate shifts to a 30 K higher temperature. At temperatures below 1000 K these changed saturation pressure values have a negligible influence on the compositions of gaseous and condensed products.

### **3.3 Experiments on the condensation of salt or metal oxide components from simulated flue gas compositions**

So far, the literature has come up with little evidence for the accuracy of the thermodynamic equilibrium models to evaluate the nature of exhaust gases from glass furnaces. In our study an experimental method has been applied to compare laboratory investigations of simulated exhaust gases with the results of the model.

Condensation of salt or metal oxide compounds from an exhaust gas doped with sodium, sulphur, lead, boron or other inorganic material has been studied experimentally.

The composition of the condensed components has been analysed and compared with the predictions of the equilibrium model.

#### **3.3.1 The experimental procedure**

Flue gases of several glass furnaces have been simulated on laboratory scale. The formation of condensed compounds during cooling down from 1700 K to 600 K has been investigated.

The equipment is presented schematically by figure 3.15.

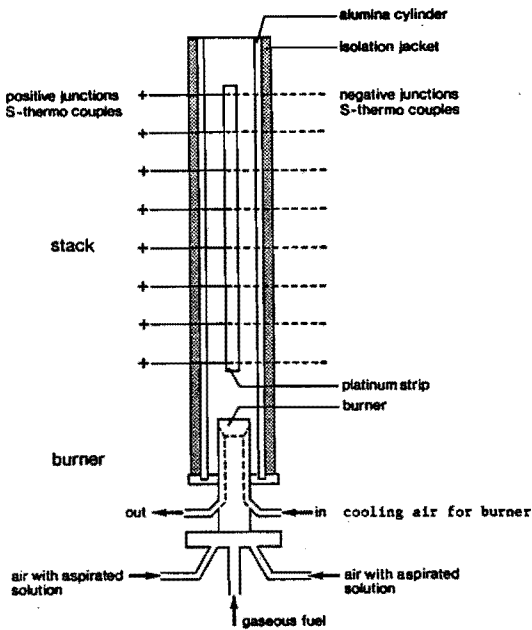


Figure 3.15: Schematic presentation of simulated flue gas channel with platinum strip.

An air cooled burner has been placed at the entrance of a vertical alumina cylinder with an inner diameter of 3.0 cm and a length of 60 cm. The air and the gaseous fuel are premixed in the burner chamber to obtain a homogeneous flame. A platinum strip with a total length of 50 cm is positioned in the centre axis of the alumina cylinder. The temperature distribution at the strip is measured by means of eight S-thermocouples welded to the surface. A solution of components containing the constituting elements of flue gases from glass furnaces is aspirated into the combustion air. The fuel used is propane resulting in a flame temperature of approximately 1750 K. The flows of air and fuel are controlled with rotameters and have been kept constant within 2%. The flue gases from the burner resemble the flue gases from glass furnaces with comparable compositions. These burner gases are conducted along the platinum strip through the alumina cylinder.

Condensed material from the exhaust gas may adhere to the platinum strip when supersaturation of certain components is reached. The total deposition at the inner surface of the alumina tube appeared to be rather small.

The amount of material from the flue gases deposited on the strip or on the cylinder surface hardly exceeds 10% of the dopants.

Gas velocities range from 3 m/s at 1700 K to 1.2 m/s at 600 K and these rates are comparable with exhaust gas velocities in regenerators of industrial furnaces. The composition of the deposits have been examined by means of X-ray diffraction to determine the nature of the crystalline phases. Generally more than 90% of the sample consisted of crystalline compounds.

A rough estimate has been made to determine the semi-quantitative composition of the deposit. The presence of a certain chemically identified phase is indicated on a scale of five as shown in figure 3.16. These experimental results are compared with the results from the equilibrium calculations.

The gas compositions of the applied flue gas simulations are given in table 3.8.

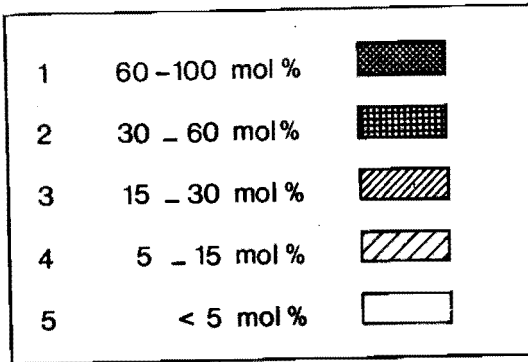


Figure 3.16: Scale of relative presence of components in deposition products.

Table 3.8: Flue gas compositions of the laboratory investigations.

composition	no.	I	II	III	IV	V	VI
O <sub>2</sub>	vol.%	4.5	4.5	4.5	4.5	4.5	4.5
N <sub>2</sub>	vol.%	72.7	72.7	72.7	72.7	72.7	72.7
H <sub>2</sub> O	vol.%	13.0	13.0	13.0	13.0	13.0	13.0
CO <sub>2</sub>	vol.%	9.0	9.0	9.0	9.0	9.0	9.0
Ar	vol.%	0.8	0.8	0.8	0.8	0.8	0.8
<u>dopants</u>							
Na	vol.-ppm	125	66	66	-	-	100
K	vol.-ppm	-	-	-	-	-	-
Ca	vol.-ppm	-	-	33	-	-	-
Mg	vol.-ppm	-	33	-	-	-	-
Pb	vol.-ppm	-	-	-	40	40	-
B	vol.-ppm	-	-	-	-	-	200
S	vol.-ppm	240	27	27	-	30	-
Cl	vol.-ppm	62.5	66	66	-	-	-

Flue gas I has a composition that resembles the composition of exhaust gases from gas fired flat glass furnaces. Addition of magnesium components to exhaust gases containing sulphur and sodium may change the condensation behaviour and the nature of the sulphate compounds. The combination of sulphur, chlorine, sodium and magnesium has been studied by the simulated flue gas II.

Calcium oxide has been added in flue gas III to investigate the formation of calcium sulphate (gypsum) together with sodium sulphate condensation. The flue gases II and III serve only to study the absorption of sulphur oxides by components other than sodium.

Formation of condensation products from a lead containing stack gas has been studied for a sulphur lean and a sulphur rich flue gas, respectively flue gas IV and flue gas V.

Flue gas VI represents sulphur lean flue gases in sodium-borosilicate furnaces.

### **3.3.2 Comparison of the results from the thermodynamic equilibrium model with the experimental investigations**

#### **I Flue gas composition with sodium, chlorine and sulphur**

The exhaust gas composition of flue gas I resembles the composition that Kirkbride [2] has given for gas fired flat glass furnaces. According to the thermodynamic equilibrium calculations only sodium sulphate ( $\text{Na}_2\text{SO}_4$ ) condensation is expected below 1340 K from this flue gas. However, no condensation products were found at temperatures above 1240 K. Below 1240 K sodium sulphate was indeed the only condensation product from this simulated flue gas. The discrepancy of 100 K between the experimentally determined dew point (1240 K) and the theoretically calculated dew point (1340 K) may be caused by reaction kinetic limitations. Especially in cases where the exhaust gas temperature decreases fast, the conversion to the equilibrium composition is limited by reaction kinetics. In our laboratory experiments temperatures decrease 100 K within approximately 40 milliseconds. Sodium sulphate is mainly produced from reactions between sodium hydroxide and sulphur oxides. This conversion consists at least of four steps, presented by mechanism I, II or III mentioned in section 2.2.1. A rough estimate of the reaction time in flue gases only doped with chlorides and sodium at 1300 K is approximately 10-20 milliseconds.

However, for reaction mechanisms more complex than gaseous sodium chloride formation, these reaction times are expected to be much longer. For sodium sulphate with a theoretically determined dew point of 1340 K, this implies a decrease of at least 50 K for condensation in the experimental case. Condensation kinetic limitations as well as errors in the thermodynamic values may be additional causes for the rather large deviations between theoretically and experimentally derived dew points.

#### **II Flue gas composition II, with sodium, chlorine, sulphur and magnesium**

Gas composition II differs from flue gas I in three ways:

- magnesium is an extra additive to the flue gas;

- the sodium content has been diminished by 50%;
- the sulphur content has been decreased to only 27 volume-ppm.

Three different condensed phases have been found in the deposits on the platinum strip. Above 1220 K only magnesium oxide condensed and at decreasing temperatures the samples contained increasing amounts of sodium sulphate.

Below 900 K deposition of sodium chloride was observed on the strip, see figure 3.17a. The composition of the condensed products as predicted by the thermodynamic equilibrium calculations is given in figure 3.17b.

According to the calculations sodium sulphate condensation is expected below 1275 K and sodium chloride should condense below 950 K.

Calculations with varying dopant concentrations show that for sodium/sulphur ratios higher than the stoichiometric ratio in sodium sulphate no magnesium sulphate is expected to condense from these flue gases.

The experimental results represented by figure 3.17a confirm this behaviour of magnesium oxide in a sodium rich flue gas. In this case sodium absorbs all the available sulphur components to form sodium sulphate. From figure 3.17a and 3.17b it appears that the agreement between the theoretically predicted behaviour and the experimental results is rather good, although the experimentally derived dew points are approximately 50 K lower.

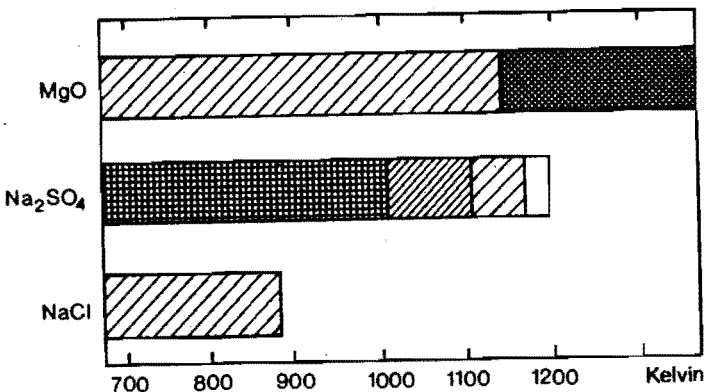


Figure 3.17a: Semi-quantitative distribution of deposition components in samples from flue gas II.

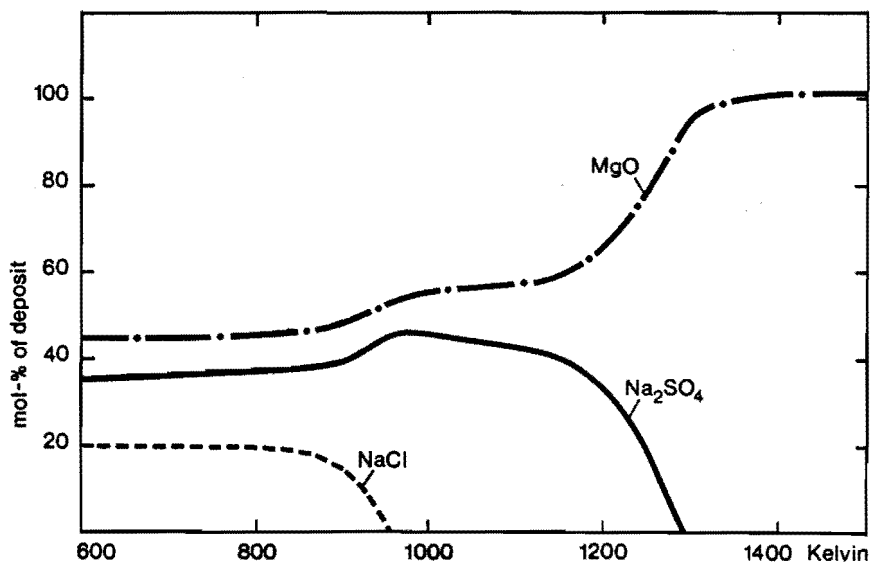


Figure 3.17b: Theoretical distribution of compounds in flue gas II deposits.

### III Flue gas composition III, with sodium, chlorine, calcium and sulphur

X-ray analysis of samples scraped from the platinum strip after experiments with flue gas III evidently prove the condensation of gypsum compounds ( $\text{CaSO}_4$ ) between 800 K and 1150 K. Other condensation products are (figure 3.18a):

- $\text{Na}_2\text{SO}_4$
  - NaCl
  - $\text{Na}_2\text{Ca}(\text{SO}_4)_2$
- and  $\text{Ca}_2\text{Na}_2(\text{SO}_4)_3$ .

The presence of these two last mentioned products has not been taken into account in the equilibrium model. In the model components like  $\text{Ca}_2\text{Na}(\text{SO}_4)_3$  and  $\text{Na}_2\text{Ca}(\text{SO}_4)_2$  are assumed to be only combinations of  $\text{CaSO}_4$  and  $\text{Na}_2\text{SO}_4$  and hardly differ in chemical behaviour. Thermodynamic data for  $\text{Ca}_2\text{Na}(\text{SO}_4)_3$  and  $\text{Na}_2\text{Ca}(\text{SO}_4)_2$  are very rare. In this model the assumption has been made that the sulphates condense as pure  $\text{CaSO}_4$  or  $\text{Na}_2\text{SO}_4$ . The results of the calculations are presented by figure 3.18b.

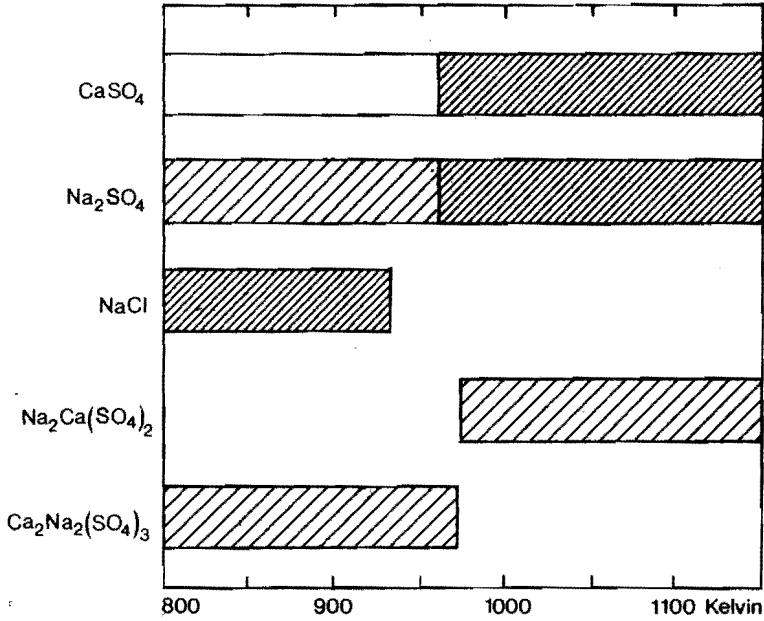


Figure 3.18a: Semi-quantitative distribution of deposition components in samples from flue gas III.

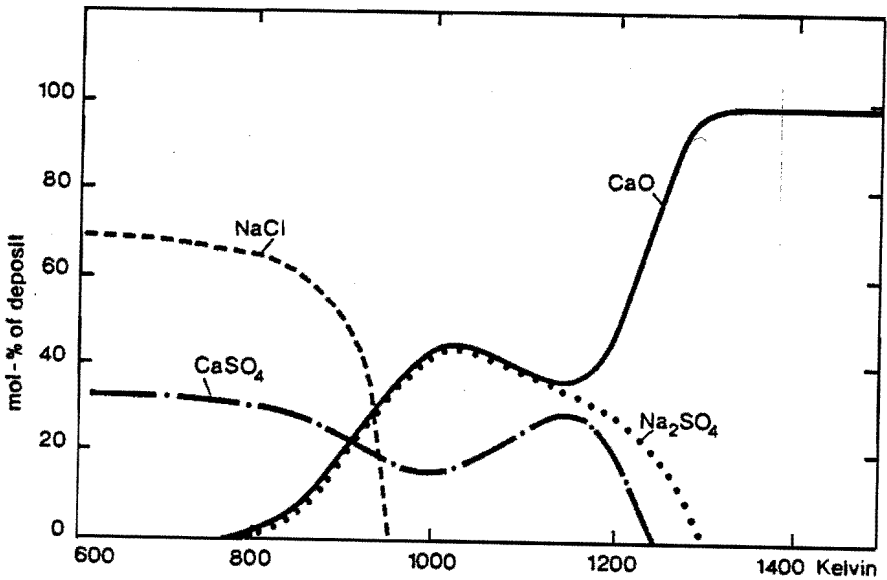


Figure 3.18b: Theoretical distribution of compounds in flue gas III deposits.

The discrepancy between the experiments and the theoretical predictions is obvious. According to these predictions considerable amounts of calcium oxide should condense above 850 K. However, this component was not found in the condensation products on the strip. It might be assumed that calcium oxide particles are formed in the flue gas at temperatures as high as 1750 K, since these particles hardly adhere to the surface of the strip, no calcium oxide deposition is observed.

According to the experiments and the theoretical approach sodium sulphate condensation is suppressed by solid sodium chloride formation at temperatures below 950 K. This experiment clearly shows the effectivity of the sulphur oxide capture by calcium oxide and sodium components in the temperature range between 800 and 1150 K. The amount of free sulphur oxides in this flue gas is negligible at temperatures below 900 K resulting in a decreasing sulphate condensation and increasing formation of condensed sodium chlorides (NaCl). Again the experimentally derived dew points for  $\text{Na}_2\text{SO}_4$  appear to be lower ( $\pm 100$  K) than the theoretical values.

#### **IV Flue gas composition number IV, with lead and without sulphur compounds**

Exhaust gases from lead glass furnaces contain large amounts of lead, existing in the furnace atmosphere mainly as gaseous lead oxides. Lead oxides, however, tend to polymerise in the gaseous phase resulting in formation of  $\text{Pb}_n\text{O}_n$ -molecules (the n-value ranges from 1 to 6) according to Drowart [9]. This polymerisation precedes the condensation of lead oxide phases at the strip at temperatures between 1100 K and 1250 K. Analysis by means of X-ray diffraction shows that the condensed product consists mainly of lead oxide below 1125 K. Minor amounts of lead hydroxide ( $\text{Pb}(\text{OH})_2$ ) or lead carbonate ( $\text{PbCO}_3$ ) have been found. These two compounds were probably formed during cooling and storing of the samples, caused by reaction with water vapor and carbon dioxide in the ambient air, since at temperatures above 700 K, these condensation products are not to be expected in these flue gases.

Calculations using the thermodynamic equilibrium model have been made, taking into account the polymerisation reactions of gaseous PbO which condenses at temperatures below 1100 K. This compound is converted into  $\text{Pb}_3\text{O}_4$  at temperatures lower than 700 K, chemical analysis of dust precipitated from stack gases of industrial lead glass furnaces confirm this.

### V Flue gas composition number V, with lead and sulphur

In case of oil-firing in lead glass furnaces considerable amounts of sulphur dioxide are introduced in the furnace atmosphere. Although gaseous lead sulphates may be of minor importance, lead oxides react with sulphur oxides resulting in the formation of solid lead sulphate. Flue gas number VI has been chosen as a gas simulating exhaust gases of oil-fired lead glass furnaces.

A survey of the analysed condensation products as a function of the temperature is given by figure 3.19a. Four different condensed phases have been found:

- $PbO.PbSO_4$ , below 1080 K;
  - $2PbO.PbSO_4$ , between 925 K and 1100 K;
  - $4PbO.PbSO_4$ , below 900 K;
- and  $PbSO_4$  at temperatures lower than 900 K.

The theoretical results of the equilibrium model are presented in figure 3.19b. Only  $PbO$ ,  $PbSO_4$  and  $PbO.PbSO_4$  phases are expected according to this approach. Chemical reactions of the deposition products during the cooling period after an experiment obviously influence the nature of the crystalline phases.

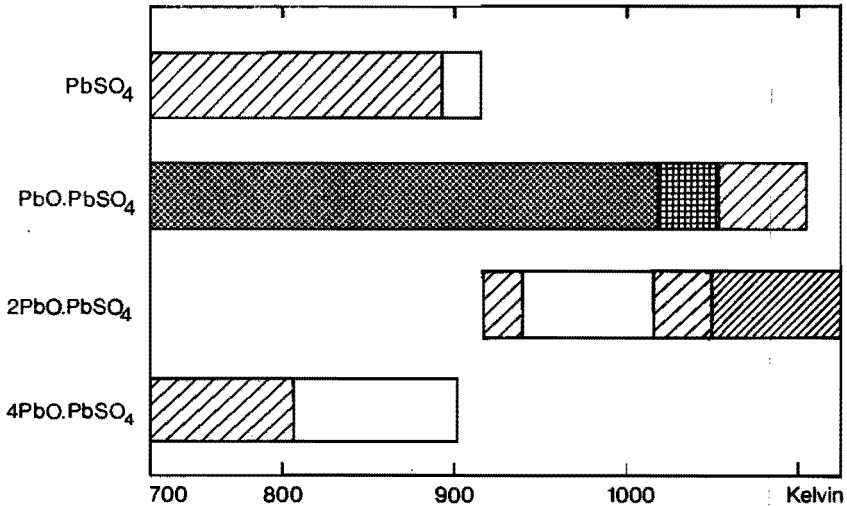


Figure 3.19a: Semi-quantitative distribution of deposition components in samples from flue gas V.

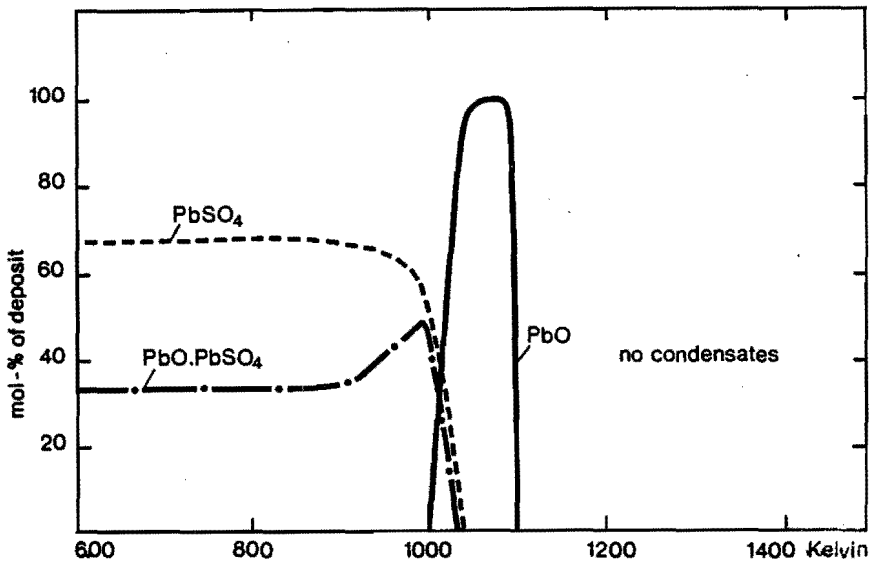


Figure 3.19b: Theoretical distribution of compounds in flue gas V deposits.

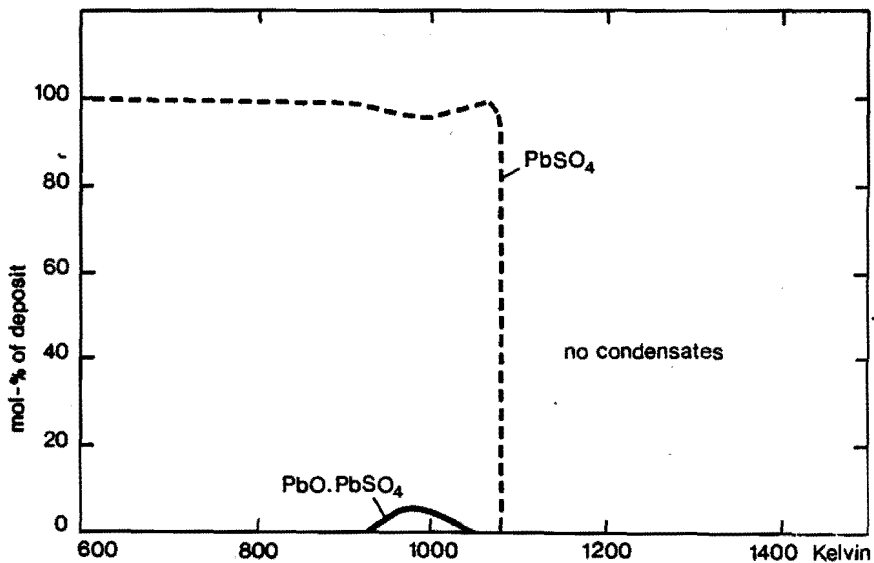


Figure 3.19c: Theoretical distribution of compounds in deposits from flue gas V with instead of 30 ppm sulphur, 40 ppm sulphur.

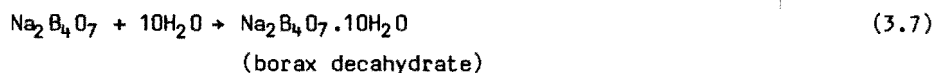
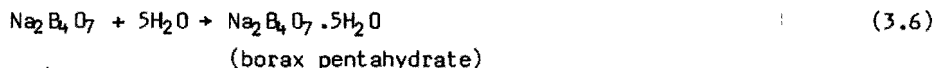
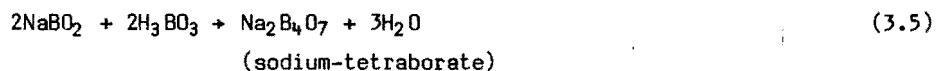
From the theoretical as well as the experimental results it can be seen that lead oxide and lead sulphate compounds condense below 1050 K - 1100 K. At increasing sulphur/lead ratios, a tendency to higher lead sulphate fractions in the condensed phases is expected as shown in figure 3.19c.

#### Flue gas VI, with sodium and boron

Exhaust gases from furnaces producing glass with sodium as well as borium oxide, contain boric acid, metaboric acid and large amounts of gaseous sodium borates. The gaseous sodium borates may react with sulphur oxides to form condensed sodium sulphate. From flue gases containing minor amounts of sulphur components, deposition of sodium metaborate takes place below 1190 K according to the experiments with flue gas number VI.

Sodium tetraborate condenses below 700 K, instead of the metaborates. Nearly the same behaviour was found from the results of the theoretical calculations. The sodium metaborate dew point for flue gas VI is calculated to be at 1240 K. Below 600 K condensation of sodium tetraborate  $\text{Na}_2\text{B}_4\text{O}_7$  is expected.

Although sodium metaborate dust can be obtained at temperatures above 600 K, reactions with  $\text{H}_3\text{BO}_3$  (3.5) or reactions with water, (3.6 and 3.7), may alter the nature of the dust in the stack.



The phase diagram for the system  $\text{Na}_2\text{O} - \text{B}_2\text{O}_3$  is partly presented by figure 3.20. Combinations like  $\text{NaBO}_2$ ,  $\text{Na}_2\text{B}_8\text{O}_{13}$ ,  $\text{Na}_2\text{B}_4\text{O}_7$ , may be obtained dependent on the ratios of sodium and boron in the deposit.

The experimentally obtained results deviate slightly from the theoretical predictions for this system. However, the thermodynamic data for gaseous  $(\text{NaBO}_2)_2$  and gaseous  $\text{Na}_2\text{B}_4\text{O}_7$  have been extrapolated from data for a limited temperature region, this may lead to some errors in the theoretical results.

$\text{Na}_2\text{O}-\text{B}_2\text{O}_3$

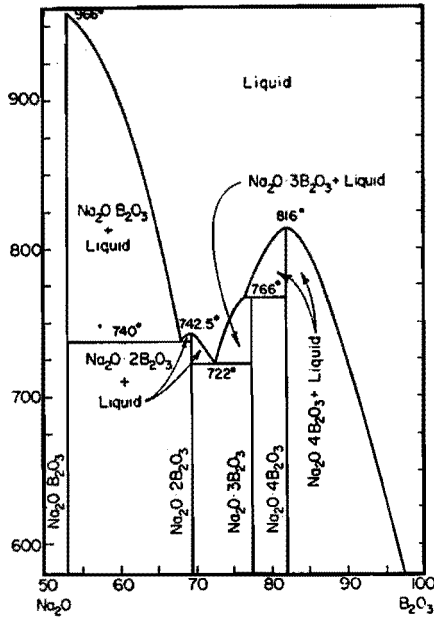


FIG. 188.—System  $\text{Na}_2\text{O} \cdot \text{B}_2\text{O}_3-\text{B}_2\text{O}_3$ .

G. W. Morey and H. E. Merwin, *J. Am. Chem. Soc.*, 58, 2252 (1936). In addition, the authors describe the compound  $2\text{Na}_2\text{O} \cdot \text{B}_2\text{O}_3$ ; melting point  $625^\circ\text{C}$ .

Figure 3.20: Phase diagram for system  $\text{Na}_2\text{O}-\text{B}_2\text{O}_3$  ref. [10].

**3.4 Conclusions**

Theoretical calculations based on thermodynamics to evaluate the condensation products expected in exhaust gases of glass furnaces have been compared with experimental studies of simulated flue gases on laboratory scale. In most cases the theoretical approach is consistent with the experimental observations.

The nature and presence of the condensation products estimated by thermodynamic calculations resemble in most cases the analysed condensation products obtained during the experimental studies. However, according to the theory the onset of condensation takes place at a 50 to 100 K higher temperature than observed experimentally.

The delay in condensation during the laboratory experiments is partly caused by reaction kinetic limitations. Especially in case of sodium sulphate condensation the experimental dew point deviates considerably (more than 100 K) from the theoretical dew point.

Sodium sulphate formation takes place in at least four steps, by reactions of NaOH with  $\text{SO}_2$  or  $\text{SO}_3$ . The reaction rates for this conversion seem to be rather slow resulting in a dew point lower than thermodynamically expected. The flue gases studied in this chapter are gases from different kinds of glass furnaces.

### 1. Soda-lime glass furnaces

Exhaust gases from soda-lime glass furnaces contain sodium, chloride and sulphur compounds. At flue gas temperatures above 1300 K - 1400 K these compounds exist mainly of gaseous sodium hydroxide, sodium chloride, sulphur oxides and hydrogen chloride. According to calculations with the thermodynamic model sodium sulphate condensation sets on at temperatures below 1300 K - 1400 K. The experimentally derived dew points for sodium-sulphate in these exhaust gases range between 1220 K and 1300 K. Higher sulphur concentration in case of firing with heavy oils increases the gaseous sulphur oxide concentrations and slightly increases the sodium-sulphate dew point.

High furnace temperatures and higher flame velocities enhance the volatilization of sodium compounds from the melt resulting in increasing concentrations of condensed sodium sulphate in the exhaust gases. The volatilized chlorides cause a decrease in the dew point temperature for sodium sulphate. Addition of lime stone influences the condensation of sulphates by formation of gypsum ( $\text{CaSO}_4$ ), magnesium oxides hardly react with flue gases from soda-lime furnaces. Sodium chloride and sodium carbonate may condense below 1100 K from sulphur lean flue gases.

### 2. Borosilicate glasses

From borosilicate melts containing large amounts of sodium oxide, components like sodium metaborate and metaboric acid volatilize rather fast. Sodium metaborate and other gaseous components are converted to condensed sodium sulphate during the cooling of the exhaust gases in case of oil-firing.

This condensation sets on at lower temperatures than in case of boron free flue gases. Boron keeps the sodium in the gaseous state as  $\text{NaBO}_2$  resulting in decreasing dew points for the other sodium components (like  $\text{Na}_2\text{SO}_4$ ). In flue gases of a gas-fired furnace sodium metaborate and occasionally sodium tetraborate condense at lower temperatures than sodium sulphate condensation normally sets on.

For high boron and sodium concentrations, condensation of sodium tetraborate is favoured in the temperature range between 800 K and 1200 K according to the equilibrium calculations. In sulphur lean flue gases with sodium and boron concentrations up to 250 volume-ppm, sodium metaborate condenses below 1150 K - 1250 K which is confirmed by the experiments. The remainder of boron not condensing as  $\text{NaBO}_2$  or  $\text{Na}_2\text{B}_4\text{O}_7$  is mainly present as gaseous metaboric acid ( $\text{HBO}_2$ ) above 1200 K but reacts to gaseous boric acid ( $\text{H}_3\text{BO}_3$ ) below this temperature.

Reactions between potassium and boron compounds are similar to the reactions between sodium components and boron species, causing condensation of  $\text{KBO}_2$  or  $\text{K}_2\text{B}_4\text{O}_7$ .

### 3. Lead glass furnaces

Exhaust gases of lead glass furnaces contain considerable amounts of gaseous lead components as lead oxide, atomic lead and lead hydroxide. In sulphur lean flue gases of natural gas fired furnaces lead oxide condenses mainly between 1180 K and 950 K. Polymerisation of gaseous  $\text{PbO}$  to  $\text{Pb}_n\text{O}_n$  ( $n = 2$  till 6) influences the condensation behaviour near the dew point (1100 K - 1200 K). Lead monoxide is converted into  $\text{Pb}_3\text{O}_4$  below approximately 700 K. Experimental studies confirm this conversion and the presence of these condensation products in simulated flue gases. Experimental work and calculations have shown that in sulphur rich flue gases from oil-fired lead glass furnaces, lead sulphate components or occasionally combinations between lead oxide and lead sulphate condense. The condensation of sulphates sets on at temperatures lower than  $\text{PbO}$  condensation, often below 1050 K. From simulated flue gases of lead glass furnaces with small amounts of sulphur oxides components like  $\text{PbO.PbSO}_4$  and  $2\text{PbO.PbSO}_4$  have been found.

Condensation of potassium sulphate or sodium sulphate generally takes place at higher temperatures than the formation of lead sulphates. In flue gases containing sulphur as well as lead and alkali components, lead possibly reacts with the excess of sulphur after formation of alkali sulphates. The remaining lead components are converted into lead oxides. The dust consists for this case of alkali sulphates, lead sulphate and lead oxides.

### Literature references chapter 3

- [ 1] Williams R.O.; Pasto A.E.;  
'High temperature Chemistry of Glass Furnace Atmospheres'.  
Journal of the American Ceramic Society 65 (1982), 602-606.
- [ 2] Kirkbride B.J.;  
'The chemical changes occurring during the cooling of hot gases  
from flat glass furnaces'.  
Glass Techn. 20 (1979) 174-180.
- [ 3] Roggendorf H., Waldecker G.G., Scholze H.;  
'Zusammensetzung der Abgase hinter Glasschmelzwannen'.  
Glastechn. Ber. 56 (1983) 218-227.
- [ 4] Gordon S., McBride B.J.;  
'Computer program for calculation of complex chemical equilibrium  
compositions, rocket performance, incident and reflected shocks and  
Chapman-Jirouquet detonations'. Report NASA SP-273 (1971).
- [ 5] Eriksson G.;  
'Thermodynamic studies of high temperature equilibria XII'.  
Che. Scr. 8 (1975) 100-103.
- [ 6] Scherer V.;  
'Abgase einer Glasschmelzwanne - Reinigung von blei- und/oder  
borhaltigen Stäuben'.  
Wasser Luft und Betrieb 22 (1978) 130-132.
- [ 7] Matousek J., Hlavac J.;  
'A study of the volatilization of lead glass'.  
Glass Technology 12 (1971) 103-106.
- [ 8] Jensen D.E., Jones G.A.;  
'Reaction rate coefficients for flame calculations'.  
Comb. and Flame 32 (1978) 1-34.
- [ 9] Drowart J., Colin R., Exsteen G.,  
'Mass-spectrometric study of the vaporization of lead-monoxide'.  
Trans. Faraday Soc. 61 (1965) 1376-1383.
- [ 10] Levin E.M., Robbins C.R., McMurdie H.F.;  
'Phase diagrams for ceramists'.  
The American Ceramic Society (1964).

### NOMENCLATURE CHAPTER 3

$K(T)$	equilibrium constant at temperature $T$
$p_i$	partial vapour pressure component $i$ (atm)
$p_i^*$	saturation pressure component $i$ (atm)
p.p.m.	volume fraction (assumed as gaseous elements) in $10^{-6} \text{ m}^3/\text{m}^3$
$T_i$	temperature at step $i$ (K)
TSRT	temperature step reaction time defined in section 3.2.3.1 (s)

#### Greek symbol

$\tau_c$	characteristic reaction time defined in section 3.2.3.1 (s)
----------	---

## 4. BOUNDARY LAYER MASS TRANSPORT IN DEPOSITION PROCESSES

### 4.1 Introduction

Thermodynamic equilibrium calculations can be carried out to determine the chemical composition of the main flue gas flow in regenerators or recuperators when kinetic limitations are neglected.

The equilibrium model, however, provides no direct information about the processes occurring at 'cool' surfaces along which the flue gases flow in regenerators or recuperators. In this chapter, the influence of the relatively cool surfaces (recuperator wall, tube surfaces or brick surfaces in regenerators) on chemical reactions and deposition processes is described with a model composed of mass transport equations and thermochemical equilibrium equations.

This model is based on a theory from Rosner et al [ 1, 2, 3 ] and is called the Chemically Frozen Boundary layer theory (CFBL-theory). By means of this model the nature of deposition products and the deposition rate for flue gas components condensing at the 'cool' surfaces in the flue gas channels is determined for different cases in this chapter.

The validity and applicability of this model has been studied in this chapter by comparing the theoretical results with experimental results for deposition from flue gases.

Two different kinds of laboratory set-ups are presented in this chapter. One set up was used to study the applicability and the restrictions of the CFBL-theory and the deposition of salt components on a cylinder positioned in cross flow configuration in a flame. The flame is doped with inorganic material to simulate certain flue gas compositions.

The second set-up consists of a channel for simulated flue gas to study the deposition behaviour at different locations in this channel.

The experiments have been carried out to simulate the situation in regenerators or recuperators on laboratory scale.

A model based on the CFBL-theory has been developed to calculate theoretically the deposition rates for these two experimental cases. An extension of these models to predict deposition rates in regenerators or recuperators of industrial glass furnaces is presented in chapter 5.

## 4.2 Theories describing mass transfer and deposition at cold surfaces

Several theories have been given in the literature to describe the deposition mechanism of salt components from flue gases of several combustion systems. Brown [4] suggested a method to establish deposition rates for sodium sulphate from combustion gases.

The transport rate of the condensing component was described by relation (4.1) for his collector geometry:

$$m = \frac{0.34 B}{Sc^{2/3} \cdot p_r^{1/3}} \cdot \left( \frac{V \mu \rho}{D} \right)^{1/2} \quad (4.1)$$

The driving force is presented as the dimensionless number B. Brown defined B as the difference between the sodium sulphate mass fraction in the main stream and the mass fraction in the gaseous phase near the deposition surface. According to Brown's interpretation condensation within the boundary layer caused a reduction of the value for B, resulting in decreasing deposition rates.

At temperatures below 650 °C the condensation took place mainly in the boundary layer, equation 4.1 fails to describe deposition rates for sodium sulphate below 650 °C. This model may be used as a first approach to determine deposition rates from exhaust gases, but there are some restrictions.

Brown assumed that all the sodium in the main gas flow existed as sodium sulphate and that the deposition rate was determined by the transport of  $Na_2SO_4$  only.

Thermodynamic calculations however, show that sodium sulphate is only a minor constituent of the sodium and sulphur containing species in these exhaust gases. The transport of the sodium sulphate constituting elements takes place by molecular transport of NaOH, Na,  $SO_2$  and  $SO_3$  mainly. Large temperature gradients within the boundary layers may influence the diffusion of molecules and small particles; for some situations these effects cannot be neglected. Srivastava [5] derived the relevant differential equations to describe the influence of thermal diffusion and variable properties of the gas phase (like  $\rho$ ,  $c_p$ ,  $\mu$ ) on mass transfer. The description of Srivastava's approach is beyond the scope of this dissertation but the main conclusions from his work were:

The species equation is of the form:

$$\rho u \frac{\delta Y_i}{\delta x} - \rho (v - v_s) \frac{\delta Y_i}{\delta y} = \rho D \frac{\delta^2 Y_i}{\delta y^2} + r_{i,eff}''' \quad (4.2)$$

where  $u$  and  $v$  are the velocities in  $x$  and  $y$  directions and  $Y_i$  the mass fractions of the diffusing component. The definition of  $v_s$  is given by (4.3) and the definition of  $r_{i,eff}'''$  by (4.4).

$$v_s = \frac{1}{\rho} \left[ \frac{\delta (\rho D)}{\delta y} + \rho D \alpha \frac{\delta \ln T}{\delta y} \right] \quad (4.3)$$

$$r_{i,eff}''' = \left\{ \frac{\delta}{\delta y} \left( \rho D \alpha \frac{\delta \ln T}{\delta y} \right) \right\} \cdot Y_i \quad (4.4)$$

$v_s$  may be seen as a suction-like effect on species transport, constituting of a part associated with thermal diffusion ( $\rho D \alpha \frac{\delta \ln T}{\delta y}$ ) and a part associated with the variety of  $\rho D$  in the boundary layer. For a positive value of  $v_s$ , the transport rate towards the wall is enhanced, therefore  $v_s$  is called a suction term.

The relation for  $r_{i,eff}'''$  may be seen as a source-term like terms occurring in differential equations for mass conservation with chemical conversions. These two effects,  $v_s$  and  $r_{i,eff}'''$  influence transport rates, according to Srivastava, especially in cases where high temperature gradients exist. More convenient for practical use is the CFBL-approach proposed by Rosner.

Rosner assumed in his model that no chemical reactions occur in the boundary layer itself. For situations where only gaseous molecules or very small particles (with molecular transport behavior) are transported to the deposition surface Rosner gave the following relation (4.5):

$$j_i = - \frac{D_{i,b}}{L} * \rho_b * Sh_i * F_i(\text{soret}) * F(\text{turb}) * \left\{ (c_{b,i} - c_{w,i}) + \frac{\tau_i * F_i(\text{nc}_p)}{F_i(\text{soret})} * c_{w,i} \right\} \quad (4.5)$$

where:

- $F_i(\text{soret})$  is a correction term for thermo-diffusional effects
- $F_i(\text{nc}_p)$  is a correction term for non-constant properties of the gaseous phase in the boundary layer
- $F_i(\text{turb})$  is a correction term for turbulences or recirculation in the boundary layer.
- $\tau$  a thermophoretic parameter (given by equation (4.6))
- $c_{b,i}, c_{w,i}$  are the mass fractions for component  $i$  at respectively bulk and wall positions
- $L$  characteristic length of submerged obstacle (m)
- $D_{i,b}$  diffusion constant for component  $i$  in the bulk flow ( $\text{m}^2/\text{s}$ )
- $\rho_b$  density of bulk gaseous phase ( $\text{kg}/\text{m}^3$ )
- $Sh_i$  Sherwood number for component (molecule)  $i$ .

The following assumptions are made in this model:

1. The boundary layer is chemically frozen, meaning no chemical conversions or condensation take place in the layer itself.
2. The gas phase at the outer edges of the boundary layer (in the main stream and at the deposition surface) is in chemical equilibrium; resulting in condensation of components with vapor pressures reaching the saturation value.
3. The ratio of the transport rates of the different chemical elements transferred by several gaseous components equals the ratio of these elements in the condensing material.

For example, in case of sodium sulphate ( $\text{Na}_2\text{SO}_4$ ) deposition, the net transport rate of sodium (transferred as  $\text{NaOH}$ ,  $\text{Na}$ ,  $\text{Na}_2\text{SO}_4$ ,  $\text{NaCl}$  etc.) has to be twice the net transfer of sulphur (transferred mainly as  $\text{SO}_2$ ,  $\text{SO}_3$  or  $\text{Na}_2\text{SO}_4$ ).

This method requires the simultaneous solution of the transport rates for each component and the evaluation of the equilibrium composition at the deposition surface and in the main gas flow, so that assumption 3 is met. The equilibrium composition has to be calculated according to the methods described in chapter 3.

Rosner's method is chosen to describe the deposition of salt components in flue gas channels, recuperators or regenerators of glass furnaces. His CFBL-theory describes deposition processes more completely than Brown, taking thermal diffusion and transport of gaseous components constituting the deposition products into account.

The derivation of the parameters used in Rosner's formula (4.5) is described in the next section. The assumption of a Chemically Frozen layer in Rosner's model appears to be adequate enough for our purposes. Srivastava's method is less convenient to describe deposition processes for our cases.

#### 4.2.1 Derivation of Mass Transport Parameters

The mass transport parameters occurring in equation (4.5), the diffusion coefficient  $D_i$ , the Sherwood numbers  $Sh_i$ , and the thermal diffusion parameters  $\tau_i$  and  $F_i$  (soret) have been derived by methods presented in this section.

##### Diffusion coefficients .

The numerical values for the diffusion coefficients of gaseous inorganic molecules like NaOH, NaCl, SO<sub>2</sub>, SO<sub>3</sub>, Na<sub>2</sub>SO<sub>4</sub> etc., in a gas g, may be estimated by the following Chapman-Enskog relation (Bird, Stewart and Lightfoot [6]):

$$D_{i,g} = 5.875 \cdot 10^{-21} * \frac{\sqrt{T^3 (1/M_i + 1/M_g)}}{p * \sigma_{i,g}^2 * \Omega_{i,g}} \quad (4.6)$$

where:

$p$  is the absolute pressure (P)

$\sigma_{i,g}$  Lennard-Jones (LJ) parameters, estimated by  $(\sigma_i + \sigma_g)/2$ , with  $\sigma_i$  the LJ-diameter of a gas molecule  $i$  and  $\sigma_g$  the LJ diameter of a average gas molecule  $g$

$\Omega_{i,g}$  is a dimensionless function of the temperature and of the inter-molecular potential field for one molecule  $i$  and one molecule  $g$ .

$M_i, M_g$  is the mass of one mole of respectively gas molecules  $i$  and the mean gas molecules  $g$ .

$T$  is the absolute temperature (K).

The diffusion coefficients for gaseous molecules in a combustion gas,  $g$  are given for three temperatures in appendix A as calculated by equation (4.6).

### Sherwood numbers

The dimensionless correlation factor for mass transfer, the Sherwood number, depends on the configuration of the gas flow around an obstacle. For well-defined geometries of these obstacles semi-empirical relations have been proposed by several investigators. Bird, Stewart and Lightfoot [6], gave relations between the Sherwood number and the number of Reynolds and Schmidt for cylindrical flow, flows around spheres and flows along flat surfaces under laminar and turbulent conditions.

### Thermodiffusion terms

The evaluation of the thermophoretic parameter  $\tau_i$  or the correction term  $F_i(\text{soret})$  is more complex. According to Rosner et al [2] the value for  $\tau_i$  may be estimated from relation (4.7):

$$\tau_i = \alpha_{i,w} * (Le_{i,w})^{0.4} * [(T_e - T_w)/T_w] \quad (4.7)$$

where:

$Le_{i,w}$  is the Lewis number (given by equation (4.7a)) at wall conditions  
 $\alpha_{i,w}$  is the thermal diffusion factor (given by equation (4.7b))  
 $T_e, T_w$  are respectively the main gas flow temperature and the temperature at the wall or deposition surface (K)

$$Le_{i,w} = D_{i,g} * \rho_w * c_{pw} / \lambda_w \quad (4.7a)$$

and

$$\alpha_{i,w} = \alpha_{\infty} * \left[ 1 + \frac{\alpha_{-1} / \alpha_{\infty}}{T_w} \right] \quad (4.7b)$$

The values for  $\alpha_{\infty}$  and  $\alpha_{-1}$  for several components are given in appendix B, these values are derived from [2] or from considerations given by Rosner [7].

$F_i(\text{soret})$  is a function of  $\tau_i$ . In the case of deposition from hot gases on colder surfaces, the value for  $r_{i,\text{eff}}''$  defined by equation (4.8) can be neglected.

Rosner [7] showed that for these situations  $F_i(\text{soret})$  may be approximated by:

$$F_i(\text{soret}) = \tau_i / (1 - \exp(-\tau_i)) \quad (4.8)$$

#### **Correction term for non-constant properties**

The differential equation of formula (4.5) consists of parameters that change in value across the boundary layer. The values of  $D_i$ ,  $\alpha$  and  $\rho$  depend on the gas temperature. It is clear that a correction term  $F(\text{ncp})$  has to be included in the mass transfer equation of formula (4.5). Rosner [7], however, concluded from exact calculations that for most cases this factor is close to one, for our purposes this correction can be neglected and  $F(\text{ncp})$  is approximately by unity.

#### **Correction term for turbulences in the boundary layer**

The deposition rates for salts from exhaust gases at cooler surfaces are generally enhanced by recirculations or free stream turbulences in the boundary layers.

$F(\text{turb})$  depends on the turbulence intensity and turbulence scale. Relations for  $F(\text{turb})$  are rare, but for smooth and only slightly curved surfaces,  $F(\text{turb})$  does not differ significantly from unity. For most cases the correction by  $F(\text{turb})$  is neglected in formula (4.5).

### **4.3 CFBL-predictions for deposition from exhaust gas on a relatively cool surface**

In this section the application of the model based on the CFBL-theory is shown for an experimental case. Deposition of different salts has been studied on a cylindrical surface positioned in cross flow configuration in a flame doped with inorganic material. The experimental results are compared with the theoretical calculations for several cases.

From this comparison the applicability and the restrictions of the model are derived and given in section 4.4. With the experimental data and the theoretical model the nature of the deposition products and the deposition rates are determined.

The application of the theoretical model to describe deposition processes in flue gas channels simulating regenerators or recuperators, is given and compared with experimental results in section 4.5.

#### 4.3.1. Experimental procedures

Evaluation of the proposed theory has been carried out by comparing CFBL-calculations with experimentally determined deposition rates on a platinum cylinder in cross flow configuration in a simulated flue gas or flame. The laboratory experiments have been carried out with an air-cooled cylinder in a propane-air flame doped with inorganic substances as shown in figure 4.1. To obtain a homogeneous surface temperature this cylinder is rotated around its axis at rotation speeds (the Reynolds number for the rotation velocity  $\ll$  Reynolds number for gas flow around cylinder) that hardly influence the flow characteristics of the exhaust gas. The diameter of the cylinder is 15 mm. The flame temperature is approximately 1750 K and the surface temperature has been varied between 800 and 1300 K. In all cases an air excess is adjusted to a value between 4 and 12% for the combustion of propane.

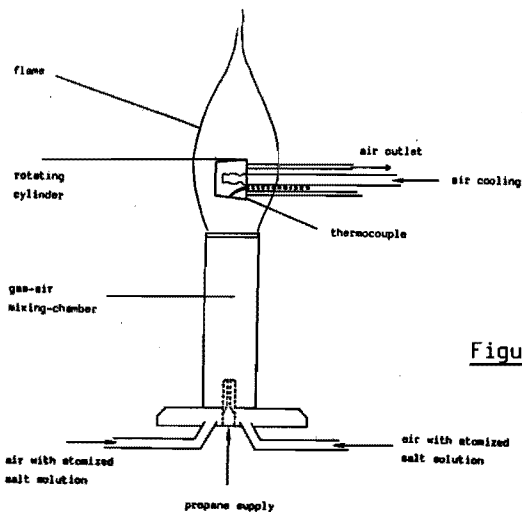


**Figure 4.1:** Experimental equipment to study deposition on cylindrical surface in cross flow direction.

Deposition of  $\text{Na}_2\text{SO}_4$ ,  $\text{NaBO}_2$ ,  $\text{NaCl}$ ,  $\text{K}_2\text{SO}_4$ ,  $\text{PbO}$  or  $\text{Pb}_3\text{O}_4$  and  $\text{PbSO}_4$  has been studied with this equipment. The flue gas compositions are given in table 4.1.

The following relation has been used for the value of the Sherwood numbers for this case [6]:

$$\text{Sh}_i = 0.40 + 0.54 * \text{Re}^{1/2} * \text{Sc}_i^{1/3} \quad (4.9)$$

#### 4.3.2 Comparison of experimental results with CFBL-predictions for the deposition on cylindrical surfaces in cross flow configuration.

Table 4.1: Flue gas composition in volume%.

Flue gas Composition	1	2	3	4	5	6	7	8
$\text{H}_2\text{O}$	15.2	15.2	15.2	15.2	15.2	15.2	15.2	15.2
$\text{O}_2$	2.3	2.3	2.3	2.3	2.3	2.3	2.3	2.3
$\text{N}_2$	71.5	71.5	71.5	71.5	71.5	71.5	71.5	71.5
Ar	0.9	0.9	0.9	0.9	0.9	0.9	0.9	0.9
$\text{CO}_2$	10.1	10.1	10.1	10.1	10.1	10.1	10.1	10.1
Na	$3 \cdot 10^3$	variable	$7.5 \cdot 10^3$	-	$2 \cdot 10^5$	$7.5 \cdot 10^3$	-	-
B	$6 \cdot 10^3$	-	-	-	-	-	-	-
S	-	variable	$3.75 \cdot 10^3$	$5 \cdot 10^3$	$3 \cdot 10^5$	-	-	$8 \cdot 10^3$
Cl	-	-	$3.75 \cdot 10^3$	-	-	$7.5 \cdot 10^3$	-	-
Pb	-	-	-	-	-	-	$4 \cdot 10^3$	$4 \cdot 10^3$
K	-	-	-	$5 \cdot 10^3$	$2 \cdot 10^5$	-	-	-

#### Sodium metaborate deposition

Exhaust gas number I in table 4.1 simulates the flue gas to be found in regenerators or recuperators of sodium-borosilicate glass furnaces. From our experimental studies and calculations it is concluded that at surface temperatures above 1000 K only sodium metaborate ( $\text{NaBO}_2$ ) condenses.

The deposition rate (in  $\text{mg NaBO}_2/\text{cm}^2\cdot\text{hr}$ ) determined at different cylinder temperatures is presented in figure 4.2, curve I. Experimental results (not presented in this figure) show that the deposition rate is independent of the duration of the experiment. The deposition rates are approximately proportional to the concentration of the dopants (sodium and boron) below 1100 K. Curve II presents the deposition rates calculated with the CFBL-model for the same flue gas composition as for the experimental case.

Appendix C shows the calculation procedure for this deposition process. The experimentally derived dew point is approximately 40 K lower than the theoretically calculated dew point. The maximum deposition rate is experimentally measured at a surface temperature of 950 K, at lower temperatures this rate (curve I) decreases slightly. The theoretically determined rates for sodium metaborate deposition increase at temperatures decreasing from the dew point temperature till 1050 K. Below 1050 K these deposition rates remain constant according to the CFBL-approach.

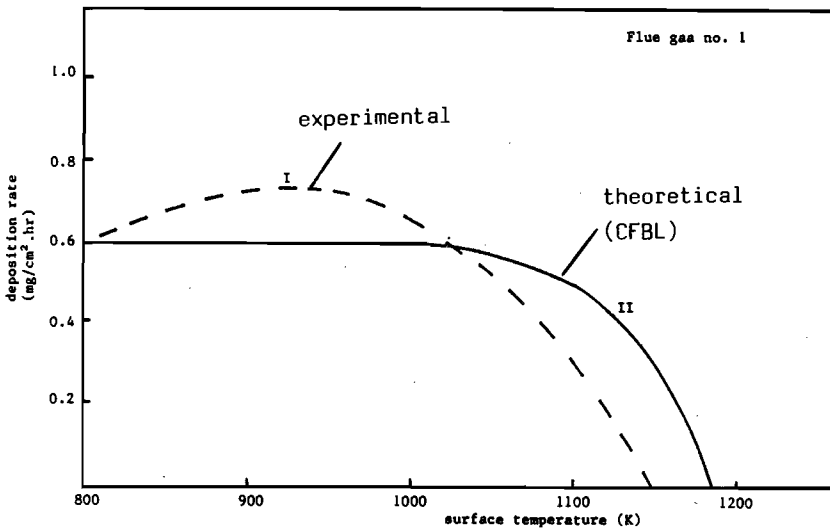


Figure 4.2: Deposition behaviour of sodium metaborate from a flame doped with boron and sodium on a cylindrical surface in cross flow configuration.

From the comparison between theory and experimental results it is concluded that the absolute values for the deposition rates below 1100 K are fairly predictable with the CFBL calculations.

The change in deposition behaviour is determined by the theoretical model for an exhaust gas with a dopant enrichment of 50%.

The dew point shifts to a 15 K higher temperature and the maximum deposition rate increases nearly 50%. The main species transported in the boundary layer towards the surface are NaOH, NaBO<sub>2</sub> and HBO<sub>2</sub> (below 1100 K) and from the surface, H<sub>3</sub>BO<sub>3</sub>.

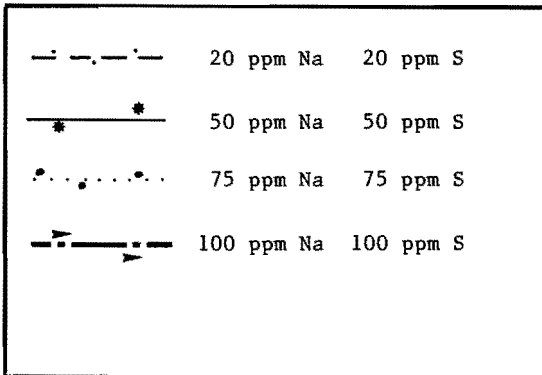
The reaction preceding sodium metaborate deposition is:



### Sodium sulphate deposition

Deposition of sodium sulphate is the most important process for the pollution of regenerators of soda lime glass furnaces. Chemical analysis of deposition products in a container glass furnace was carried out. For checker temperatures below 1300 K, the deposit consists at least for 80% of Na<sub>2</sub>SO<sub>4</sub>.

The experimentally derived deposition behaviour of sodium sulphate from flue gas number 2 is presented by figure 4.3a with the dopant concentration as a parameter. CFBL-calculations have been carried out for the same situation.



Various types of lines indicating different situations in figure 4.3

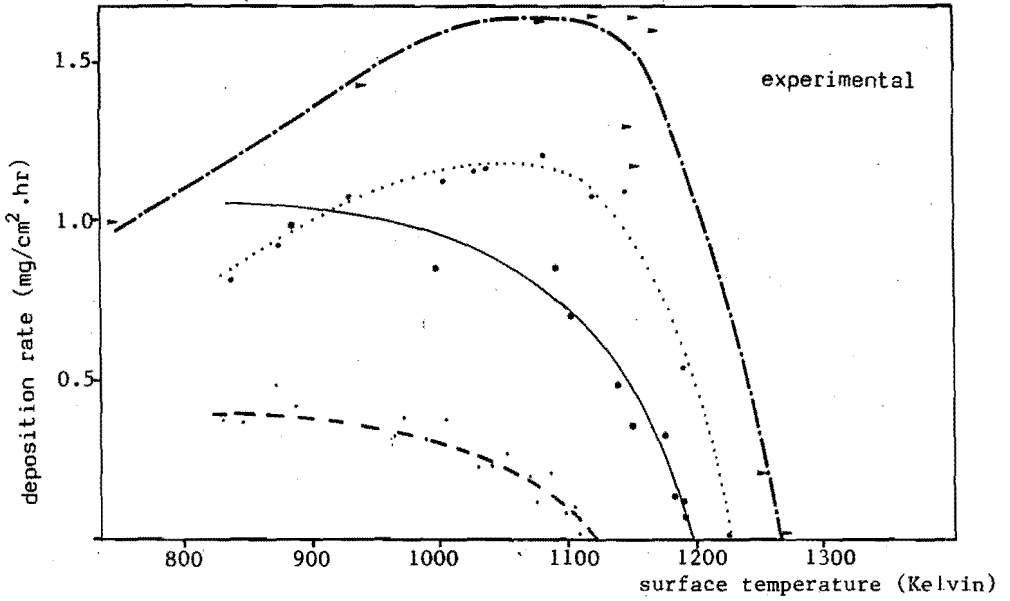


Figure 4.3a: Experimentally derived deposition rates for sodium sulphate on the cylinder in cross flow configuration.

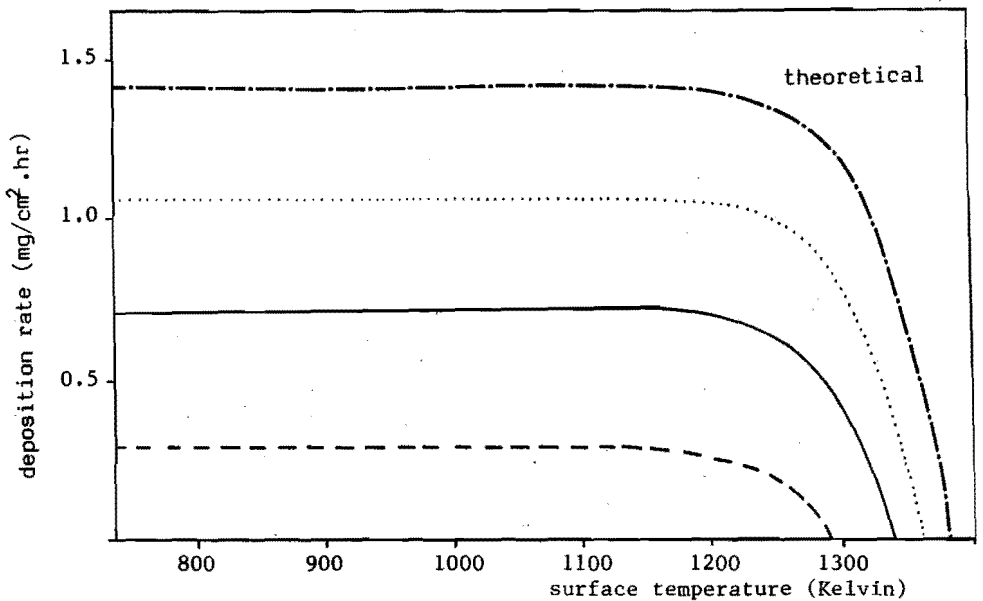


Figure 4.3b: Deposition of sodium sulphate at cylindrical surface in cross flow configuration according to the CFBL-theory.

According to the CFBL-theory the transported species are mainly NaOH, Na, SO<sub>2</sub> and SO<sub>3</sub>. For the formation of sodium sulphate at least three or four reaction steps are required see section 2.2.1. As mentioned earlier the CFBL-model assumes chemical equilibrium in the gas phase near the deposition surface. However, it is questionable whether this assumption is realistic for the complex situation of Na<sub>2</sub>SO<sub>4</sub>-formation. Figure 4.3b represents the deposition rates calculated with the CFBL model for the same situations as the experimental cases.

The magnitude of the values for deposition rates calculated by the theoretical model are in good agreement with the experimental values. The experimentally derived deposition rates for sodium sulphate decreased below 1050 K for high dopant concentrations. The CFBL-theory however, predicts a constant deposition rate at temperatures below 1150 K. The difference may be due to homogeneous nucleation within the boundary layer (section 4.3.2), which may take place especially at high dopant concentrations and at high supersaturations for temperatures far below the dew point.

Deposition rates are expected to decrease as a result of these nucleation processes at temperatures below 1100 K. The maximum deposition rates derived from experimental results and the CFBL calculations are listed in table 4.2.

Table 4.2: Maximum deposition rates for sodium sulphate at a cylindrical surface in cross flow configuration.

dopant concentrations volume-ppm				maximum deposition rate (experimentally) (mg/cm <sup>2</sup> .hr)	maximum deposition rate (CFBL) (mg/cm <sup>2</sup> .hr)
Na	20	S	20	0.38	0.28
	50		50	1.04	0.70
	75		75	1.17	1.04
	100		100	1.60	1.40

The rather small deviations between the experimentally derived maximum rates and the CFBL-predictions are 25-30% for low dopant concentrations and approximately 15% for the high dopant laden flue gases. CFBL-calculations slightly overestimate the maximum deposition rates in these cases. However, the high degree of uncertainties in the determination of the transport parameters (diffusion constant, Sherwood relation) might explain this difference.

Large discrepancies between the experiments and the theoretical calculations have been found for the dew points of sodium sulphate. For the flue gases doped with 20 volume-ppm sodium and sulphur this difference is 160 K and for the flue gases with 100 volume-ppm dopants this deviation amounts to 120 K.

With the cylindrical surface in cross flow configuration and flue gas velocities of approximately  $4 \text{ m}_n/\text{s}$ , the boundary layer thickness is a few millimetres. For the high mass transfer rates in these situations the deposition rate may also depend on condensation kinetic limitations at the deposition surface. To study this effect we calculated the deposition of sodium sulphate in the case that the supersaturation value for the onset of sodium sulphate condensation amounts to 10. The deposition rates for sodium sulphate for this case have been presented in figure 4.4. The value 10 for the supersaturation factor is chosen arbitrarily, but from the results it is clear that condensation kinetic limitations have a considerable influence on the dew point value for sodium sulphate deposition.

The dew points for the experimental and theoretical results are summarized in table 4.3.

To explain the experimentally derived dew point we would have to assume supersaturation factors larger than 100. Besides condensation kinetic limitations however, reaction kinetic limitations may cause a delay in the condensation of sodium sulphate.

The lack of data for the reaction kinetic parameters for sodium sulphate formation from sodium hydroxide and sulphur oxides makes it difficult to determine the importance of the reaction kinetic limitations.

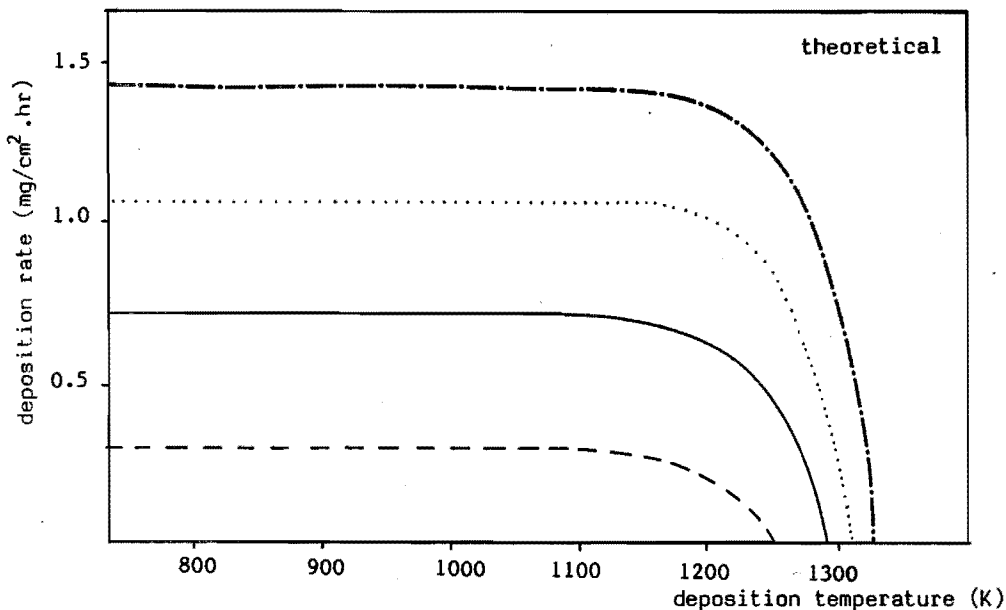
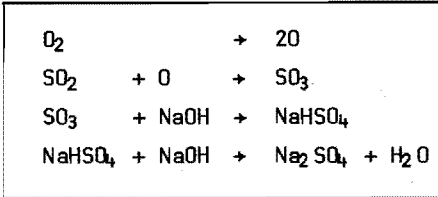


Figure 4.4: Deposition rates for sodium sulphate on a cylindrical surface in cross flow configuration in the flame, according to CFBL calculations assuming supersaturation values of 10.

Table 4.3: Dew point values for sodium sulphate at a cylindrical surface in cross flow.

dopant concentrations		dew point (K)	dew point (K)	dew point (K)
volume ppm		experimental	CFBL super-saturation=1	CFBL super-saturation=10
Na 20	S 20	1120	1290	1252
50	50	1190	1338	1290
75	75	1237	1362	1310
100	100	1263	1377	1328

A reaction mechanism for sodium sulphate formation might be:



The first two steps, involved in the formation of sulphur trioxide are known to be slowly proceeding conversions, when no catalysing agents are present.

The sulphur trioxide concentration near the deposition surface is negligible as the two following reaction steps are relatively fast. From these considerations we believe that the CFBL-theory provides a calculation method to determine  $Na_2SO_4$  deposition rates for these cases at lower temperatures than 150 K below the theoretical dew point.

#### Deposition of sodium sulphate from flue gases with chloride additions

The deposition rate of a condensing component can be altered by the presence of other impurities in the flue gases. These impurities do not necessarily participate in the deposition product but they can change the nature of for instance the sodium compounds in flue gases from glass furnaces.

Exhaust gases from glass furnaces using synthetic soda ash, contain  $2 \cdot 10^{-2}$  till  $5 \cdot 10^{-2}$  volume-% chlorides. Although, no or almost negligible amounts of chlorides deposit in regenerators of soda-lime glass furnaces, the deposition of sodium sulphate sets on at lower temperatures for increasing chloride amounts.

The deposition of a flue gas with  $3.75 \cdot 10^{-2}$  volume-% Cl, has been studied in our laboratory in the same set-up as mentioned previously. The experimentally derived deposition rates for flue gas number 3 from table 4.1 is presented by figure 4.5 and compared with the calculations of the CFBL-approach. The deposition rates for the same flue gas without chlorides are also presented in this figure. From the theoretical results as well as from the experimental results it may be concluded that the presence of sodium chloride in the flue gas causes a decrease in the dew point temperature.

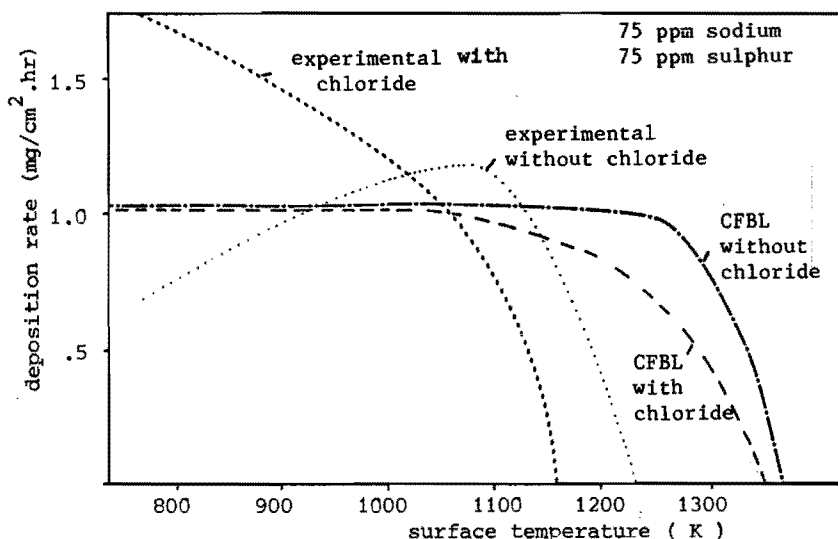


**Figure 4.5:** Sodium sulphate deposition on a cylindrical surface in the flame with and without chloride additions.

Chlorides tend to keep the sodium in the gaseous phase. This process interferes with the sodium sulphate deposition. Remarkable is the increasing deposition rate at temperatures below 1100 K in case of chloride addition to the flue gas.

The reason for this behaviour is not known and cannot be explained by the CFBL-theory; to which extent chemical reactions in the boundary layer accelerate the mass transport process in this case is not clear.

It can be seen that the temperature region, where the deposition increases from zero to a maximum rate, is much larger for the chloride-doped flue gases. The same behaviour is expected for condensation processes in the main flue gas flow resulting in sodium sulphate dust.

For chloride lean gases condensation takes place till temperature 150 K below the dew point. But for exhaust gases with chloride additions the condensation process exceeds a temperature region of 250 K. In practice this may have an influence on the particle sizes of the dust formed by these condensation processes. The rates of nucleation and nucleus growth of the saturated vapors is different for a chloride lean and a chloride rich flue gas. It is expected that chloride free flue gases produce particles with smaller sizes than the chloride rich ones.

## Deposition of potassium sulphate from simulated flue gas

Another case, where chemical conversions at the deposition surface may influence the deposition rate, is the condensation of potassium sulphate ( $K_2SO_4$ ). Formation of potassium sulphate is expected to be similar to the conversion of flue gas constituents into sodium sulphate.

If the conversion of  $SO_2$  into  $SO_3$  is the reaction limiting step in both the deposition of  $Na_2SO_4$  and  $K_2SO_4$ , this will influence the deposition rate in a similar way.

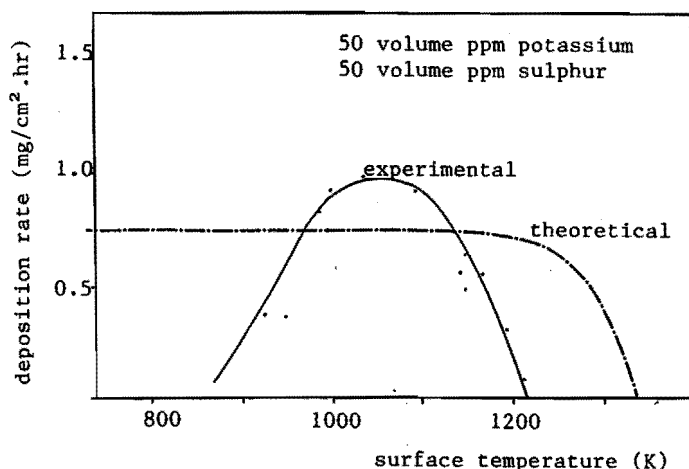


Figure 4.6: Experimentally and theoretically (CFBL) derived rates for potassium sulphate deposition on a cylindrical surface in cross flow configuration.

Figure 4.6 represents the dependence of the potassium sulphate deposition rates for flue gas number 4 on surface temperature. Indeed the theoretically determined deposition curve also indicates a large difference between the experiments and the CFBL-predictions for the potassium sulphate dew point. This difference of approximately 120 K is comparable with the differences for the similar cases for sodium sulphate deposition. Deposition of potassium sulphate decreases rapidly at temperatures below 1000 K. In this case the effect is even stronger than for sodium sulphate.

From the similarity between the deposition of both alkali sulphates it seems that the same phenomena take place:

- At high temperatures condensation or reaction kinetic limitations prevent deposition at the theoretically determined dew point.
- For temperatures lower than 1000 K, homogeneous condensation within the boundary layer causes a diminishing mass transfer towards the deposition surface.

For the case of a flue gas with only sulphur and potassium only potassium sulphate has been determined by means of X-ray diffraction in the whole temperature range under investigation.

#### Simultaneous sodium sulphate and potassium sulphate deposition

From furnaces producing glasses with potassium and sodium, exhaust gases are obtained with dust existing of combinations of sodium and potassium sulphate. From flue gases with equal amounts of sodium and potassium, sodium sulphate condenses first. At a somewhat lower temperature potassium sulphate deposition or condensation sets on.

The total amount of deposited material ( $K_2SO_4 + Na_2SO_4$ ) at the cylindrical surface is presented by figure 4.7 for flue gas 5. The molar ratios of potassium and sodium are presented in the same figure. These ratios have been determined by means of chemical analysis with an atomic emission spectrometer.

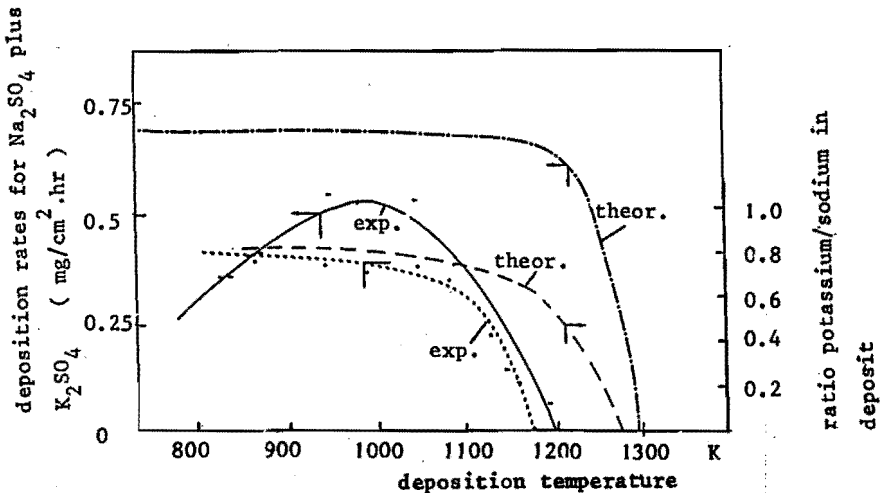


Figure 4.7: Deposition behaviour of sodium and potassium sulphate on a cylindrical surface in the flame.

First sodium sulphate is formed at 1210 K without potassium sulphate deposition. The potassium sulphate/sodium sulphate ratio increases from zero at 1180 K to 0.8 at 800 K. The total rate of deposition reaches a maximum at 980 K, below this temperature the total deposition rates decrease at 800 K to 50% of the maximum rate.

The calculations based on the CFBL-model also predict increasing potassium/sodium ratios from 0 to approximately 0.85. Although the CFBL-model underestimates the maximum deposition rates for the one-component deposition experiments, the model overestimates the maximum deposition rate for this case with a maximum of 20%. The dew point determined by means of the CFBL model differs only 80 K with respect to the experimental value. From both the experimental results and the theoretical results it may be concluded that the deposition of potassium sulphate sets on at a 30 K lower temperature than the sodium sulphate deposition. This difference is mainly due to the difference in thermodynamic properties of these components. The calculations do not take into account the formation of a liquid or solid mixed alkali sulphate phase. The assumption is made that  $K_2SO_4$  and  $Na_2SO_4$  condense as pure phases.

However, X-ray analysis of the deposition products shows the presence of 10%-15%  $KNaSO_4$  and  $K_3Na(SO_4)_2$  together with sodium sulphate V. According to preliminary thermodynamic calculations, only a slight change in the theoretically determined deposition rates may be expected from the formation of mixed alkali sulphates.

### **Deposition of sodium chloride**

From sulphur lean flue gases of glass furnaces, deposition of NaCl might take place, but the conditions for this phenomenon will hardly be met in real furnaces.

Mainly the deposition of sodium chloride was studied since in this case but one or two reactions precede the condensation at the surface. Sodium chloride has a rather simple deposition mechanism in which reaction kinetic limitations hardly influence the deposition rate and is therefore interesting to prove the CFBL-theory. The experimental deposition curve and the CFBL-derived deposition dependence on the surface temperature are given in figure 4.8 for flue gas number 6.

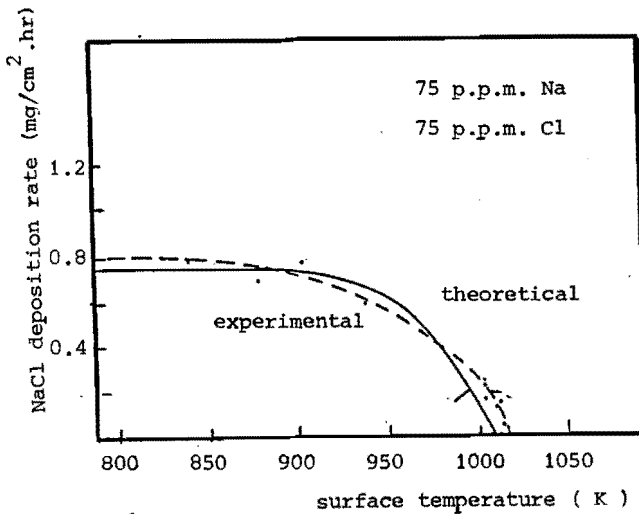


Figure 4.8: Experimental and CFBL predicted deposition rates for sodium chloride on a cylindrical surface in cross flow configuration.

The CFBL-curve deviates only slightly from the experimentally determined deposition rates. From these observations it may be concluded that for the rather simple deposition mechanism of NaCl-condensation on the cylindrical surface, the CFBL-theory gives accurate results. Of course, if condensation kinetics limit the deposition of salts near the theoretically calculated dew point, this would also limit NaCl deposition. This, however, has not been observed, and so it is assumed that deposition of salts is primarily limited by reaction kinetics.

#### Lead oxide and lead sulphate deposition

So far only deposition products and rates from exhaust gases of borosilicate and soda-lime glass furnaces have been investigated. Lead oxides are rather volatile components in lead glass melts and lead components are generally the main impurities in exhaust gases from lead glass furnaces.

Deposition rates for lead compounds from simulated flue gases with and without sulphur have been determined with the cylinder in cross flow configuration. Figure 4.9 represents the results for lead oxide deposition from a sulphur free exhaust gas like flue gas number 7. The CFBL theory predicts a 45 K lower dew point than experimentally determined for the deposition of lead oxide in this case.

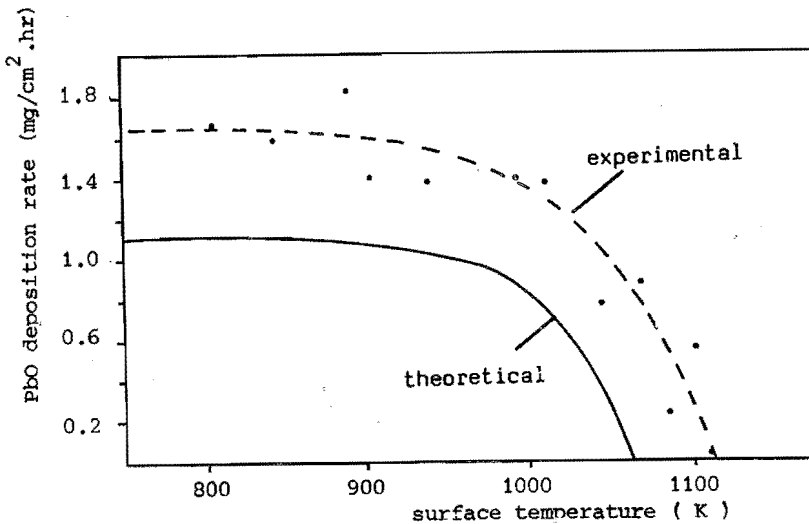


**Figure 4.9:** Deposition of lead oxide from flue gases doped with 40 volume-ppm lead (Pb) on a cylindrical surface in cross flow configuration.

In the calculations based on the CFBL theory account is taken for the formation of oligomers of lead oxide. The calculated dew point shifts to a 100 K higher value, if the presence of  $Pb_nO_n$ -molecules ( $n=2$  till 6) is neglected.

The presence of oligomer molecules may be overpredicted by the applied thermodynamic values for these components. The diffusion constants for gaseous lead components are rough estimates and explain the difference of the maximum deposition rate for lead oxide, comparing the theoretical results with the experimental determinations. The deposition behaviour of lead sulphate is shown in figure 4.10, for a flue gas with sulphur. The theoretical maximum deposition rates for lead sulphate are approximately 20% lower than the experimentally derived values. A discrepancy of only 40 K for the dew points is quite reasonable. It is remarkable that the dew point values of these experiments are higher than the dew point calculated with the CFBL model. This is in contrast with the other cases.

This could only be explained by the uncertainties in the thermodynamic data for the polymerization reactions, since the dew point temperature is very sensitive to these thermodynamic values.

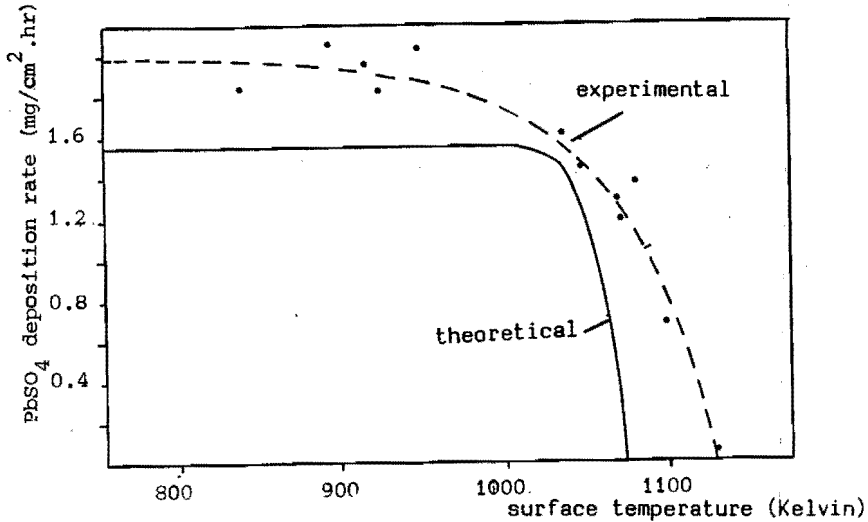
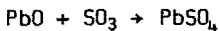


**Figure 4.10:** Deposition of lead sulphate from a flame doped with 80 volume-ppm sulphur and 40 volume-ppm lead on the cylindrical surface in cross flow configuration.

For the sulphate experiments the delay in deposition below the theoretical dew point has not been observed. The experimental dew points for the alkali sulphates however, are more than 100 K below the theoretical value, probably due to reaction kinetic limitations. According to the calculations deposition of alkali sulphate sets on at 1250 K - 1350 K, at these temperatures the concentrations of SO<sub>3</sub> in the gas phase are very low. The conversion of SO<sub>2</sub> into SO<sub>3</sub> as the first step in the alkali sulphate formation is probably the limiting step. At lower temperatures the formation of SO<sub>3</sub> is favoured and the reaction:



takes place. It is clear that the deposition of lead sulphate at temperatures below 1100 K is only slightly limited by reaction kinetics.

#### **4.4 Application of the CFBL model to describe deposition in glass furnace regenerators and recuperators**

Before using a model based on the Chemically Frozen Boundary Layer theory to describe the deposition of for example  $\text{Na}_2\text{SO}_4$ ,  $\text{K}_2\text{SO}_4$ ,  $\text{NaBO}_2$  or  $\text{Na}_2\text{B}_4\text{O}_7$ ,  $\text{PbO}$  and  $\text{PbSO}_4$  from flue gases in exhaust channels, regenerators or recuperators, it is necessary to consider the restrictions of this theory. Later (section 4.5) in this chapter the deposition in an exhaust channel on laboratory scale is experimentally and theoretically investigated for different situations.

##### **4.4.1 Influence of chemical conversion in the boundary layer on transport rates.**

The values for the Sherwood numbers derived from semi-empirical treatments do not account for chemical reactions that may take place in the boundary layer. For instance, consider the transport of sodium hydroxide from the main gas stream through the layer towards the deposition surface.

Inside the layer sodium hydroxide may be consumed by reactions with  $\text{SO}_2$  or  $\text{SO}_3$  forming sodium sulphate. This causes a sink term in the differential equation of formula 4.2 for sodium hydroxide transport. This results in an increasing mass transport rate for sodium hydroxide species towards the deposition surface.

From this point of view it is expected that chemical reactions in a boundary layer near a relatively cool surface enhance deposition of sodium sulphate.

There is little knowledge about the kinetic parameters for these systems and the information available is insufficient to calculate the increase of the deposition rate as a result of the chemical conversion in the boundary layer, nor is it possible to obtain values for the Damköhler ratios.

Rosner [2] considered the opposite case of a chemically frozen boundary layer namely the case of a local thermochemical equilibrium in the entire boundary layer.

From this consideration Rosner concluded that the dependence of the deposition rate on temperature will indeed change if reactions take place in the boundary layer itself. A very rough estimate for the molecular diffusion time in the boundary layer is given by:

$$\tau_{\text{dif},i} = \delta^2/D_i \quad (4.10)$$

where:

$\delta$  is the thickness of the boundary layer (m)

$\tau_{\text{dif},i}$  is the transport time of component  $i$  through this layer (s)

An estimate for  $\delta$  using the value for the Sherwood number is:

$$\delta \approx L/Sh \quad (4.11)$$

where:

$L$  is characteristic length of the surmerged obstacle, or the diameter of the tube on which deposition take place (m).

For regenerators  $\delta \approx 0.01$  m.  $D_i$  as a function of temperature is presented for different species in Appendix A. Take  $D_i = 10^{-4}$  m<sup>2</sup>/s then  $\tau_{\text{dif},i} \approx 1$  second.

Especially for temperatures above 1000 K, the relevant reaction times as defined in section 3.2.3.1 of this dissertation are lower than this value for  $\tau_{\text{dif},i}$ .

For these temperatures it is expected that chemical conversion take place in the boundary layer. However, for high temperatures inside the entire boundary layer the vapor pressures of SO<sub>2</sub> and NaOH differ only slightly when regarding a chemically frozen boundary layer instead of a boundary layer with equilibrium for every location.

For most situations the assumption of a chemically frozen boundary layer results in a solution adequate for our purposes.

#### 4.4.2 Homogeneous nucleation in boundary layers

From earlier works of Epstein [8] it is known that nucleation of supersaturated vapors may enhance or reduce mass transport rates through boundary layers. Brown [4] suggested that the deposition rates for sodium sulphate from combustion gases on relatively cold surfaces is reduced by homogeneous condensation processes in the boundary layer, as indicated by figure 4.11.

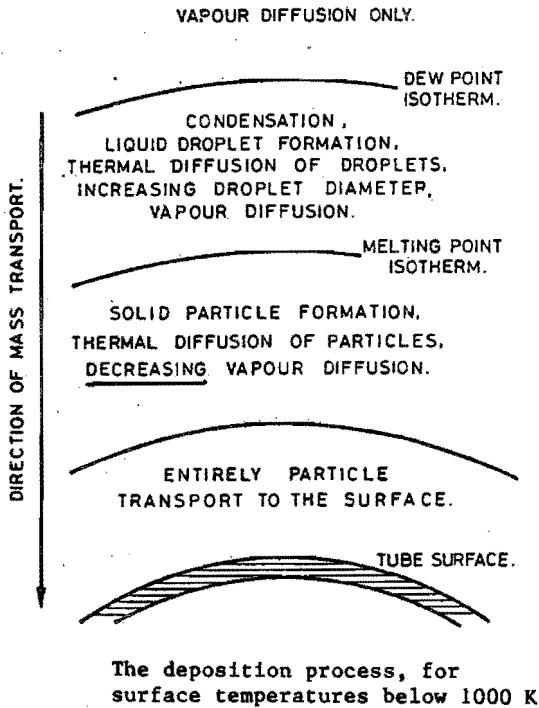


Figure 4.11: The deposition process according to Brown [4].

The effect of homogeneous nucleation on transfer rates is only measurable for nucleation rates above  $10^{18}$  nuclei /  $m^3$  sec. according to Epstein.

The nucleation rate  $J$  is given by relation 4.12:

$$J = \alpha_m \left( \frac{P_i^*}{kT} \right)^2 \left( \frac{2 \sigma M_i}{\pi N a} \right) \cdot \frac{S_i^2}{\rho} \exp \left[ - \frac{4 \pi \sigma}{3 k T} \cdot r^{*2} \right] \quad (4.12)$$

where:

$S_i$  is the supersaturation ratio component  $i$  ( $p_i/p_{i*}$ )

$p_{i*}$  is the vapor pressure at saturation conditions (Pascal)

$\sigma$  is the surface tension (in case of liquid phases) (N/m)

$M_i$  is the molecular weight of component  $i$  (kg/mol)

$N_A$  is the Avogadro number

$k$  is the Boltzmann's constant ( $1.38 \cdot 10^{-23}$  J/K)

$\alpha_m$  mass accommodation coefficient

$r^*$  is critical size of nucleus (m)

$\rho$  is the density of the flue gas ( $\text{kg/m}^3$ ).

Only nuclei with a radius  $r > r^*$  can grow infinitely, nuclei with a radius  $r < r^*$  tend to decrease in size. The supersaturation factor that may occur in the boundary layer depends on the ratio of  $p_i$  and  $p_{i*}$  in the main gas flow. Two examples are given in this discussion:

#### Example 1:

Deposition from an exhaust gas flow where the actual sodium sulphate vapor pressure is 0.1 times the saturation pressure ( $S_i = 0.1$ ). The exhaust gas temperature is 1600 K and the surface temperature is chosen to be 1200 K. The saturation pressure for sodium sulphate as a function of the absolute temperature is given by relation (4.13):

$$p^*_{\text{Na}_2\text{SO}_4} = \text{EXP} (-0.00494 * T + 26.33 - 44100/T) \quad (4.13)$$

The maximum value for  $J/\alpha_m$  may be obtained from equation (4.12) and (4.13) for  $\rho_T = 0.1$  and  $S_i = 1200$  K.

This value is approximately  $10^{10}$ , the critical value for  $J/\alpha_m$  at which the effects of condensation in the layer are measurable is approximately  $10^{12}$  or higher. Thus no influence of homogeneous nucleation is expected for this case.

#### Example 2:

Deposition from an exhaust of 1600 K (with an  $S_i$  value for sodium sulphate of 0.1) and surface temperature  $T_w = 1000$  K, results in a maximum value for  $J/\alpha_m$  of  $10^{14}$ . At this surface temperature the deposition rates are decreased by diffusional transport (directed from the wall) of the small particles formed near the cold surface.

For our purpose the CFBL-theory may be applied for surface temperatures above 1000 K in regenerators or recuperators. the CFBL-theory fails to describe deposition for exhaust gas temperatures below 1100 K because at these temperatures condensation in the main gas flow causes deposition of formed dust or particles present in the gas flow.

#### 4.4.3 Heterogeneous nucleation

The growth of already present dust particles in exhaust gases, by salt condensation may change the deposition behaviour.

According to calculations for the  $\text{Na}_2\text{SO}_4$  vapor pressures Rosner concluded that heterogeneous nucleation may be neglected at surface temperatures above 1200 K for low concentration gradients and high temperature gradients in the boundary layer:  $Le > 0.4$ .

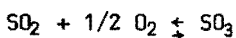
( $Le = k_h / (\rho c_p D)$ , number of Lewis where  $k_h$  is the heat transfer coefficient). So far heterogeneous nucleation can only be treated in a qualitative way because no information is available of the presence of particles in the combustion gases and the condensation coefficients for sodium sulphate on these particulates.

#### 4.4.4 Reaction kinetic limitations at the deposition surface

Kinetic limitations at the deposition surface may influence deposition rates.

Especially at low temperatures, kinetic limitations as for example the conversion of the sodium hydroxide molecules and sulphur oxide molecules into sodium sulphate, reduces the deposition rate.

The conversion of  $\text{SO}_2$  to  $\text{SO}_3$  for instance is a very slowly proceeding reaction as is shown in chapter 1 section 1.1.1.5. Making the assumption that the reaction:



can be neglected and that the ratio of  $\text{SO}_2/\text{SO}_3$  at the deposition surface equals the  $\text{SO}_2/\text{SO}_3$  ratio in the bulk gas stream, this considerably reduces the rates of deposition of sulphate at these high temperatures.

#### 4.4.5 Transport of condensed material from the exhaust gas to the deposition surface

At temperatures below 1250 - 1300 K condensation takes place in the main gas flow. Below 1000 K nearly all of the available sodium containing components have been converted into solid particulates like sodium sulphate, sodium metaborate or sodium chloride. Transport of particles instead of vapor molecules, plays a part in the deposition processes at these temperatures.

For smooth surfaces, where interception of particles is not likely to occur and therefore the transport processes of particulate matter through boundary layers is small compared to the deposition of vapor molecules. The transport process for very small particles, is similar to the diffusion of gaseous molecules and may take part in the deposition processes in the exhaust gas channels.

However, deposition of particulate matter from exhaust gases, laden with dust, is enhanced by an increasing surface roughness, Fernandez de la Mora et al [9], because of the increasing interceptional deposition processes. Below main stream temperatures of 1000 K the 'vapor deposition' may be neglected and only deposition of dust from the exhaust gases takes place.

#### 4.4.6 Conclusions

The deposition of salt components from simulated flue gases or flames on small cylinders is investigated. The experimental results have been compared to study the applicability and restrictions of the CFBL-theory for this kind of process.

The difference between the exhaust gas temperature and the surface temperature in the cases studied was very large. Besides this, the thickness of the boundary layer around the cylinders was very small. However the CFBL-theory gave quite accurate predictions for the deposition rates of sodium chloride, lead oxide, lead sulphate and to a somewhat lesser degree for deposition of sodium borates.

For all cases, inclusively the deposition of alkali sulphate, the experimental deposition rates are of the same magnitude as the theoretically calculated rates.

However, the deposition of alkali sulphates sets on at temperatures 100 K to 150 K lower than expected from theory. Reaction kinetic limitations are possibly the main reason for this delay in deposition of the alkali sulphates formed from alkali hydroxide and sulphur dioxide.

Taking the severe conditions of the experimental situations into account (high temperature gradients, small boundary layer thicknesses), it can be concluded that the CFBL-theory provides a basis for calculating deposition rates in exhaust gas channels or regenerators.

#### **4.5 Deposition processes in cylindrical tubes: A laboratory study.**

The deposition of salt components from simulated flue gases at small cylinders has only been carried out to investigate the applicability and restrictions of the CFBL-theory for processes of this kind.

Practical difficulties inhibit the comparison between theoretical calculations and real deposition rates for the situation of industrial regenerators or recuperators. Therefore, we studied the deposition behaviour of alkali sulphate, alkali borates and lead oxide in simulated flue gas channels on laboratory scale.

For these cases the reaction kinetic limitations are less important than for a cooled cylinder in cross flow configuration in the propane-air flame.

The investigations with the exhaust gas channel are presented in this section and the experimental deposition rates are compared with the theoretical results for the same situations.

##### **4.5.1 Equipment to study deposition processes at the inner wall of cylindrical exhaust gas channels**

Sodium, chlorine, sulphur and/or boron containing solutions have been atomized into the combustion air of small propane burners. The burners are cooled with air to prevent over-heating. The flue gases from these burners have been conducted through a cylindrical channel, presented in figure 4.12. Deposition products and rates have been determined at several positions of the inner wall of the channel.

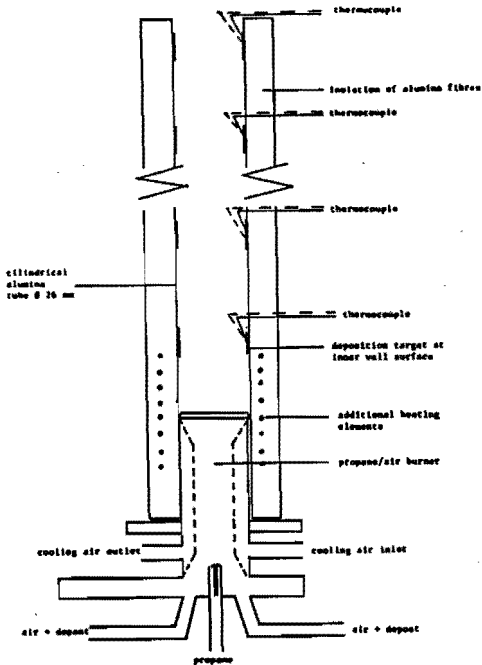


**Figure 4.12:** Schematic presentation of laboratory equipment to determine deposition rates from simulated flue gases.

**Table 4.4:** Experimental standard conditions for the laboratory studies with the cylindrical exhaust gas channel.

Flue gas temperature	: 1700 - 700 Kelvin
Flue gas velocity	: 4.5 m <sub>n</sub> /s
Flue gas Reynolds* number	: 2200 (1700 K) 4900 ( 600 K)
Deposition surface temperatures	: 1380 - 550 K
Inner diameter cylindrical channel	: 0.026 m
Channel height	: 1.0 m
Flue gas volume	: 1.44 m <sup>3</sup> <sub>n</sub> /min
Range of Sherwood* numbers	: ± 3.65 (600 K) ± 12.00 (1700 K)
Temperature difference central gas flow inner wall surface	: 400 ± 25 Kelvin
Duration of experiment	: 16 - 24 hours

\* Sherwood and Reynolds numbers are based on the channel diameter.



The mass conservation equation, governing the mass transport of an element component  $i$  is given by (4.16) for the stationary situation:

$$\frac{d(\phi \cdot \rho_m \cdot w_{mj})}{dz} = A_s \cdot \sum_{i=1}^n \left\{ a_{i,j} \cdot \frac{Sh_i \rho_m}{L} \cdot D_{i,m} \cdot F_i(\text{soret}) \cdot \left( (w_{m_i} - w_{w_i}) + \frac{\tau_i}{F_i(\text{soret})} \cdot w_{w_i} \right) \right\} \quad (4.14)$$

where:

- $\phi$  volume flow of the exhaust gas ( $\text{m}^3/\text{s}$ )
- $\rho$  density of the exhaust gas ( $\text{kg}/\text{m}^3$ )
- $w_{mj}$  weight fraction of element  $j$  in main flow
- $z$  position in the direction of the channel axis
- $Sh_i$  Sherwood number for component  $i$
- $\lambda$  equivalent channel diameter (m)
- $D_{i,m}$  diffusion coefficient component  $i$  ( $\text{m}^2/\text{s}$ )
- $a_{i,j}$  weight fraction of element  $j$  in component  $i$ .
- $A_s$  specific surface area per unit of channel length ( $\text{m}^2/\text{m}$ )

subscripts:

- $i$  component  $i$
- $j$  element  $j$
- $m$  main gas flow
- $w$  wall positions

For the case of sodium sulphate deposition, for example, the following constraint has to be taken into account:

$$\sum_{i=1}^n \left[ a_{i,Na} \cdot \frac{Sh_i \cdot \rho_m}{L} \cdot D_{i,m} \cdot F_i(\text{soret}) \cdot \left( (w_{m_i} - w_{w_i}) + \frac{\tau_i}{F_i(\text{soret})} \cdot w_{w_i} \right) \right]$$

$$= 2 * \left[ \sum_{i=1}^n a_{i,S} \frac{Sh_i \cdot \rho_m}{L} \cdot D_{i,m} \cdot F_i(\text{soret}) \cdot \left( (w_{m_i} - w_{w_i}) + \frac{\tau_i}{F_i(\text{soret})} \cdot w_{w_i} \right) \right] \quad (4.15)$$

with  $i = \text{SO}_2, \text{SO}_3, \text{NaOH}, \text{Na}, \text{NaCl}$  and  $\text{Na}_2\text{SO}_4$ .

The Sherwood relation is approximated by formula:

$$\left. \begin{aligned} \text{Sh}_i &= 1.08 * (\text{Re} * \text{Sc}_i)^{1/3} * \left(\frac{D}{Z}\right)^{1/3} \text{Re.Sc}_i \frac{D}{Z} > 5 \\ &= 3.65 \text{Re.Sc}_i \frac{D}{Z} < 5 \end{aligned} \right\} \quad (4.16)$$

$Z$  is distance between deposition location and flue gas entrance (m).

Relation (4.15) is valid for sodium sulphate deposition, since the net transport rates of sodium (transported as  $\text{Na}, \text{NaOH}, \text{NaCl}$  and  $\text{Na}_2\text{SO}_4$ ) has to be twice the net transport of sulphur (transported as  $\text{SO}_2, \text{SO}_3$  and  $\text{NaSO}_4$ ). The theoretical model for the simulation of the experimental situation has been extended for the simultaneous deposition of more than one component.

In our calculations the simplification has been made that the different deposition products (like  $\text{Na}_2\text{SO}_4$  and  $\text{K}_2\text{SO}_4$ ) do not interact. The mixing enthalpy is assumed to be zero, however, in the real situation solid or liquid solutions may be formed with negative values for the mixing enthalpy. X-ray diffraction analysis has shown no reaction or mixing between sodium sulphates and sodium borates. Mixtures of sodium sulphates and potassium sulphates have been found in the deposition products obtained from our experiments. Preliminary investigations have shown only a minor influence on the results when this mixing enthalpy is taken into account in the thermodynamic part of the model.

In this model the transport of condensed material from the flue gas flow through the boundary layer has not been accounted for. Only transport of gaseous species through the boundary layer has been considered in this model.

At low flue gas temperatures, below 1000 K, nearly all alkali or lead compounds have been condensed. This condensation leads to decreasing transfer rates of gaseous components through the boundary layer causing decreasing deposition rates.

### 4.5.3 Deposition rates of sodium sulphate for various flue gas compositions

Experiments have been carried out with flue gases doped with sulphur, sodium and occasionally chlorides. Table 4.5 represents the used flue gas compositions and exhaust gas flows.

Table 4.5: Flue gas simulations for deposition experiments in the exhaust gas channel.

Experiment number	A1	A2	A3	A4
Total exhaust gas flow $m^3/s$	$4.0 \cdot 10^{-4}$	$4.0 \cdot 10^{-4}$	$4.0 \cdot 10^{-4}$	$4.0 \cdot 10^{-4}$
sodium volume-%	$1.4 \cdot 10^{-2}$	$1.0 \cdot 10^{-2}$	$8 \cdot 10^{-3}$	$1.6 \cdot 10^{-3}$
sulphur volume-%	$1.4 \cdot 10^{-2}$	$1.0 \cdot 10^{-2}$	$8 \cdot 10^{-3}$	$8 \cdot 10^{-3}$
chloride volume-%	$7.0 \cdot 10^{-2}$	$5 \cdot 10^{-3}$	-	-
carbon dioxide (CO <sub>2</sub> ) volume-%	10.3	10.3	10.3	10.3
water vapor (H <sub>2</sub> O) volume-%	13.8	13.8	13.8	13.8
oxygen (O <sub>2</sub> ) volume-%	2.2	2.2	2.2	2.2

The experiments, as well as the calculations show that below a certain temperature ( $T_d$ ) deposition rates increase very rapidly. Maximum deposition rates have been determined at a temperature defined as  $T_{max}$ . The experimental results are presented and compared with theoretical determinations for flue gas number A1 in figure 4.14.

Reaction kinetic limitations for conversion to the deposition products (like alkali sulphate deposition) are less important in these experimental cases with less large temperature differences within the boundary layers as for the cylinder in the flame. Therefore, the discrepancies between the theoretically determined dew points and the experimental values is smaller than those discussed in section (4.3). The theoretically calculated dew point value is only 60 K higher than the experimental one. The experimental curve resembles the theoretical curve but has shifted to temperatures 60 - 100 K lower.

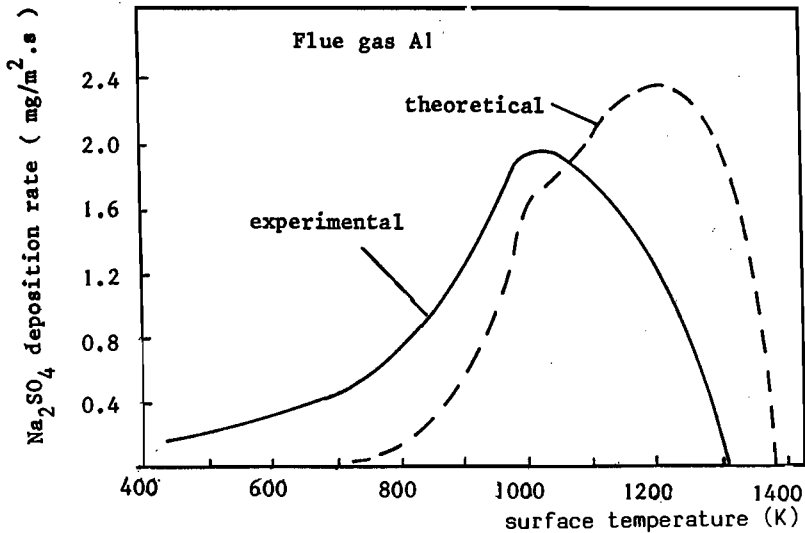


Figure 4.14: Deposition rates of sodium sulphate from simulated flue gases in a cylindrical tube.

The theoretically calculated maximum deposition rate at 1200 K is 2.3 mg/m<sup>2</sup>.s, for the experimental case this value is approximately 20% lower. The discrepancy between this experimental result and the calculation is surprisingly low, taking the uncertainties for the values of the transport and thermodynamic parameters into account.

The theoretical deposition rates are very low at surface temperatures lower than 800 K. In these sections of the tube nearly all the sodium components have been converted into condensed sodium sulphate according to the calculations. The nod in the theoretical curve at approximately 1000 K indicates the onset of condensation in the main flue gas flow. The model assumes only diffusional transport of gaseous species across the boundary layers, resulting in a nearly zero deposition rate below 800 K. Obviously, this assumption is not fully correct regarding the experimentally derived deposition rates till temperatures of 400 K. The results for example number A2 are presented by figure 4.15.

Again according to the mathematical simulation model the deposition sets on at a higher temperature than observed experimentally. The differences between the theoretical approach and the experimental results are similar to those of example A1.

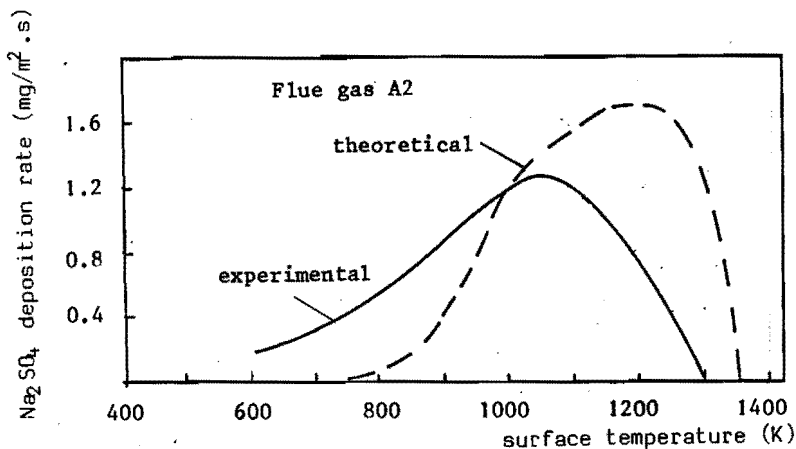


Figure 4.15: Deposition rates of sodium sulphate at the inner surface of a cylindrical tube.

Comparing example A2 (with 100 ppm sodium) with A1 (with 140 ppm) sodium, it appears that the theoretically and experimentally derived dew point for A2 is lower, due to the lower sodium concentration in the flue gas. The maximum theoretically derived deposition rate is 27% lower for A2 than for A1; in the experiments this difference is 30% reflecting also the deposition rate to be decreasing nearly proportionally to the decreasing sodium concentration.

For flue gases only doped with sulphur and sodium the deposition rate appears to be higher above 1100 K compared to chlorine rich flue gases. Figure 4.16 shows the deposition rates for flue gas number A3. Although the sodium and sulphur concentrations are lower than for case A2, the deposition of sodium sulphate at 1100 - 1200 K is nearly the same for the theoretical case and even higher for A3 relative to A2 according to the experimental determinations. The addition of chlorides causes reduction of the maximum deposition rates and a decrease of the dew point temperature.

Finally the case of decreased sulphur concentrations relative to the sodium concentration has been studied by flue gas A4 with a sodium/sulphur ratio of 2.0. The theoretical approach overestimates the maximum deposition rate as in the previous cases. The calculated and experimentally derived deposition rates for case A4 are represented in figure 4.17.

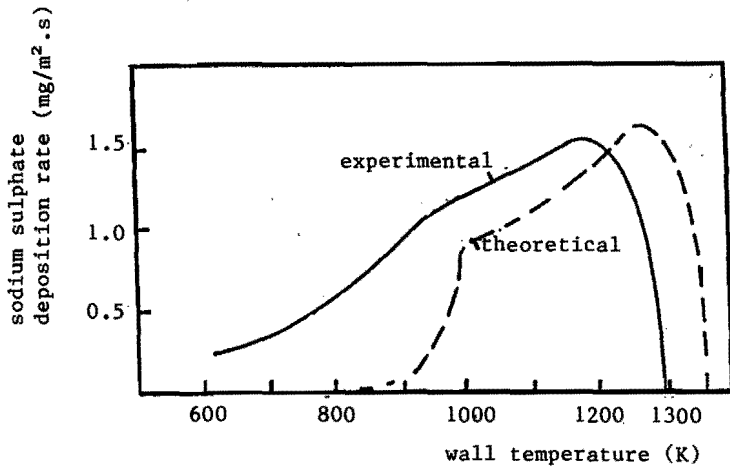


Figure 4.16: Experimental and theoretically determined deposition rates for sodium sulphate from simulated flue gas in a cylindrical tube for composition A3.

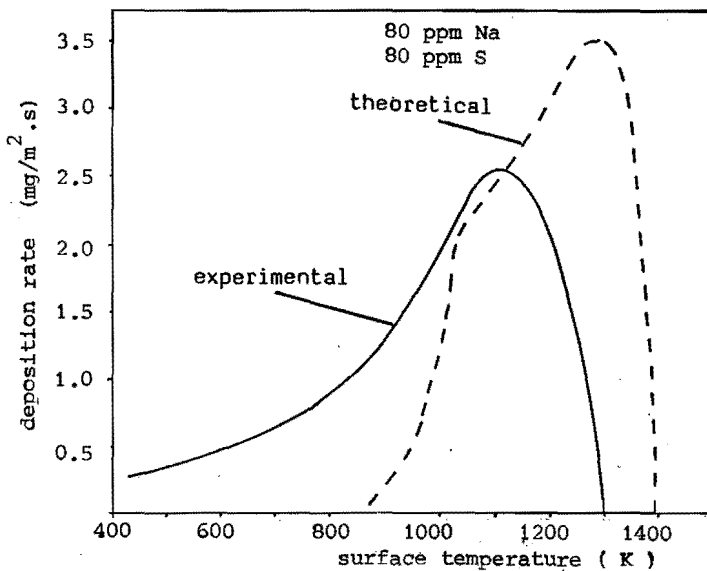


Figure 4.17: Deposition rates of sodium sulphate at inner the surface of cylindrical tube, for simulated flue gas A4.

Comparing this case (A4) with flue gas number (A3) it may be concluded that high chlorine concentrations (as for A1) result in decreases in the deposition rates larger than the increases in deposition rates caused by higher sulphur concentrations.

A change in the fuel/air ratio hardly influenced the deposition rate in oxidizing flue gases. The deposition behaviour strongly depends on the sodium and chloride concentration of the flue gas. From these three examples it may be concluded that the theoretical model predicts the deposition behaviour of sodium sulphate from flue gases rather accurately.

#### 4.5.4 Deposition rates of sodium metaborate for various flue gas compositions

Regenerators or recuperators of natural gas fired sodium-borosilicate furnaces are often fouled by sodium borates. Deposition rates of sodium metaborate in the laboratory equipments have been determined for two flue gas compositions, given in table 4.6.

Table 4.6: Flue gas compositions for deposition experiments in a channel for sodium and boron containing exhaust gases.

Experiment number	B1	B2
Exhaust gas flow $m^3_n/s$	$5 \cdot 10^{-4}$	$3.0 \cdot 10^{-4}$
Sodium volume-ppm	36	60
Boron volume-ppm	36	120
Carbon dioxide volume-%	10.0	10.0
Water vapor volume-%	15.0	15.0
Oxygen volume-%	4.4	4.4
Nitrogen volume-%	70.6	70.6

Figure 4.18 represents the deposition behaviour for case B1. The deposition rate of sodium metaborate at the surface of the inner wall of the tube reaches its maximum at 1080 K in the experimental curve. The deposition of sodium metaborate sets on below 1260 K according to the experimental observations. From the theoretical simulation model no deposition is expected above 1200 K. The theory predicts higher deposition rates between 800 and 1100 K than the experimental studies. The thermodynamic parameters for these systems are rough estimates especially for gaseous sodium metaborate ( $\text{NaBO}_2$ ) its dimer ( $\text{NaBO}_2$ )<sub>2</sub> and gaseous sodium tetraborate ( $\text{Na}_2\text{B}_4\text{O}_7$ ). A more precise theoretical approach is only possible if the relevant thermodynamic values for the Gibbs' Free Enthalpies of these components are determined more accurately. The absolute values for the deposition rates of this system as determined by the model deviate in most cases not more than 35% from the experimental results.

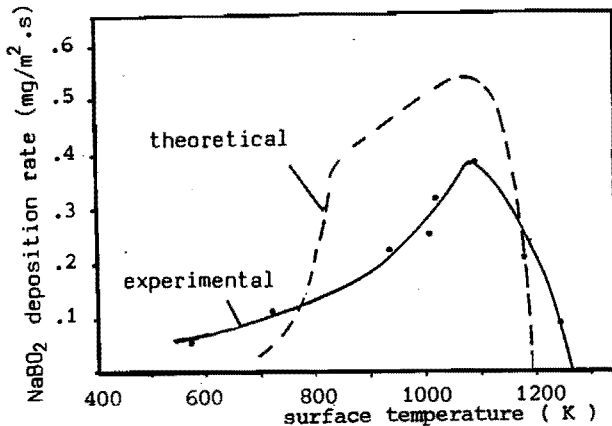


Figure 4.18: Deposition of sodium metaborate from simulated flue gas doped with 45 volume ppm Na and 45 volume ppm B in a cylindrical channel.

Figure 4.19 shows the deposition rates at different surface temperatures for a simulated flue gas with a boron concentration twice as high as the sodium concentration. Above 900 K the theoretical curve differs only slightly from the experimentally derived rates for sodium metaborate. Again the measured deposition rates at temperatures lower than 700 K differ significantly from the theoretical results.

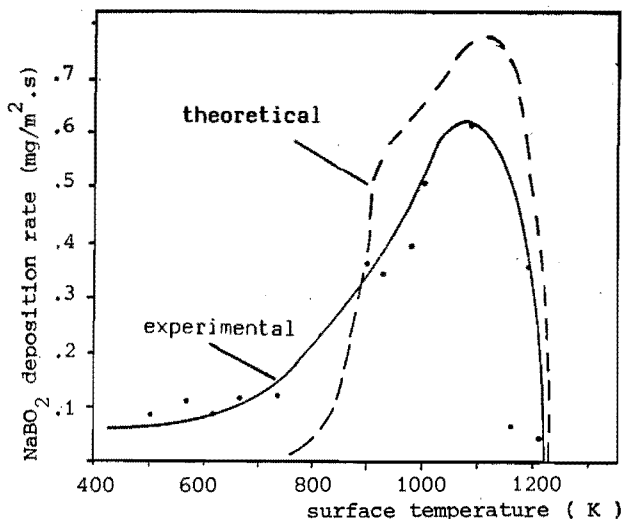


Figure 4.19: Deposition rates of sodium metaborate from simulated flue gas in a cylindrical channel.

The sodium and boron concentrations in these two examples of simulated flue gases are rather low, so that no sodium tetraborate is formed in the deposits. The deposition products have been analysed by means of X-ray diffraction. At temperatures above 600 K the deposits consist mainly of  $\text{NaBO}_2$ , some sodium tetraborate ( $\text{Na}_2\text{B}_4\text{O}_7$ ) may be formed below 600 K. From the comparison between the experimental studies and the theoretical results it may be concluded that the deposition rates for the system sodium-boron are derived rather accurately by the model for temperatures above 850 K.

The examples in this section show the importance of the diffusion of particulate matter through the boundary layer, causing deposition below temperatures of 700 K - 800 K.

#### 4.5.5 Deposition rates of potassium sulphate

Exhaust gases of glass furnaces producing glasses that contain potassium oxide, consist of gaseous potassium components above 1350 K like KOH, K, KCl or potassium borates for example. In case of oil-firing or sulphate refining these components are converted mainly into potassium sulphate, condensing or depositing during the cooling period.

Deposition of potassium sulphate is usually less important than that of sodium sulphate in furnaces producing container or flat glass.

To illustrate the application of the theoretical model for this case, experiments have been carried out on the basis of the flue gas composition presented by table 4.7.

**Table 4.7:** Flue gas compositions for deposition experiments of potassium sulphate in a cylindrical channel.

Exhaust gas flow $m^3/s$	$3.75 \cdot 10^{-4}$
Potassium concentration volume-ppm	160
Sulphur concentration volume-ppm	160
Oxygen concentration volume-%	4.4
Carbon dioxide concentration volume-%	10.0
Water vapor concentration volume-%	15.0
Nitrogen concentration volume-%	70.6

The comparison between the theoretical results and the experimentally measured deposition rates is presented in figure 4.20.

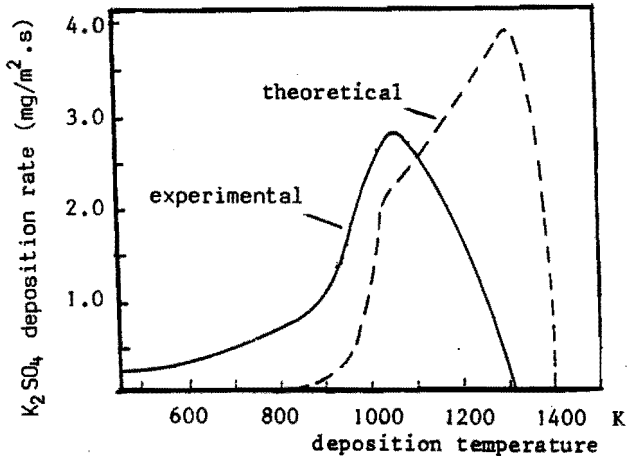


**Figure 4.20:** Deposition rates for potassium sulphate at the inner wall of a cylindrical channel.

The deviations between the theoretical and experimental approach are similar to those of sodium sulphate deposition. The deviations are:

1. The theoretical dew point is higher (in this case 80 K) than the experimental dew point of potassium sulphate.
2. The maximum deposition rate at approximately 1280 K for the theoretical case is 30% higher than the measured maximum rate at 1100 K.
3. At temperatures below 800 K the theory predicts zero deposition rates but the experimental results show that deposition takes place till at least 450 K.

The experimental curve coincides with the larger part of the theoretical curve when it is shifted to a 100 - 150 K higher temperature. Again this delay of the deposition process is probably partly due to kinetic limitations for the conversion of gaseous potassium compounds and sulphur oxides to condensed potassium sulphate.

The melting point of potassium sulphate is 1342 K so that deposition of mainly solid  $K_2SO_4$  takes place. The maximum deposition rate of potassium sulphate,  $2.9 \text{ mg/m}^2 \cdot \text{s}$  according to the experiments is somewhat higher than the maximum rate of sodium sulphate deposition for the same concentrations (in volume ppm)  $2.3 \text{ mg/m}^2 \cdot \text{s}$ . This is partly due to the higher molar weight of  $K_2SO_4$  (174.3 g/mol) relative to the molar weight of  $Na_2SO_4$  (142 g/mol). Besides this, the diffusion of gaseous potassium compounds through the boundary layer appears to be slightly faster than the diffusion of sodium components.

At low temperatures diffusion of particulate matter through the gaseous boundary layers causes the deposition of potassium sulphate at the tube.

#### **4.5.6 Deposition rates of lead oxide**

Natural gas fired lead glass furnaces emit flue gases loaded with lead oxide dust. Lead oxide condenses and deposits from these exhaust gases at temperatures below approximately 1100 K. As described in section 3.2.2.3 of this thesis, lead sulphate condenses primarily from flue gases of lead glass furnaces in case of heavy oil firing as shown in section 4.4.

The deposition rates of lead sulphate are quite similar to those of lead oxide at the same temperatures. Therefore, only the deposition of lead oxide has been studied in the cylindrical channel by means of the simulated flue gas given by table 4.8.

Table 4.8: Flue gas composition for deposition experiments of lead oxide with the equipment of figure 4.12.

Exhaust gas flow $m_n^3/s$	$3.75 \cdot 10^{-4}$
Lead concentration volume-ppm	100
Oxygen concentration volume-%	4.4
Carbon dioxide concentration volume-%	15.0
Water vapor concentration volume-%	10.0
Nitrogen concentration volume-%	70.6

Deposition of lead oxide mainly takes place at surface temperatures between 750 and 1100 K as shown in figure 4.21.

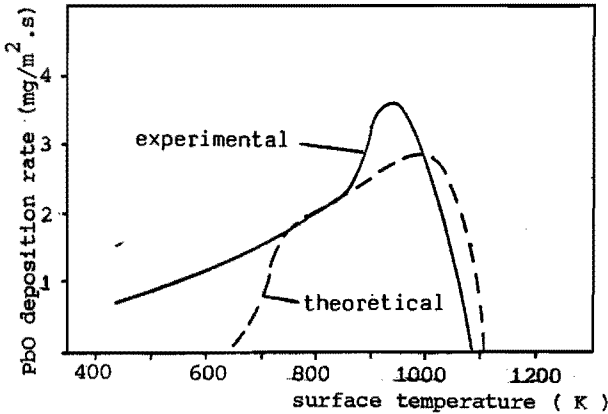


Figure 4.21: Deposition rates for lead oxide at inner wall of cylindrical tube.

According to the experimental measurements the deposition of PbO sets on at 1090 K. The theoretical model slightly overestimates the dew point with 20 K.

Contrary to the deposition behaviour of sodium or potassium sulphate, the maximum experimentally derived deposition rate as for lead oxide is higher (15%) than theoretically expected. The deposition rate reaches its maximum at approximately 1000 K and reaches values of  $3.0 \text{ mg/m}^2 \cdot \text{s}$ . The curvature of the experimentally derived graph deviates remarkably from the theoretical curve at this temperature. According to the experiments the deposition rates are quite high in a very narrow temperature range between 900 and 1050 K. Lead oxide deposits only as a solid component. Corrosion due to liquid phases condensed from exhaust gases doped with lead is not expected.

Below 700 K deposition still takes place probably due to diffusion of dust particles towards the surface of the inner wall of the tube.

#### 4.6 Summary and conclusions

The deposition processes that take place in channels of exhaust gas systems have been described by a theoretical model based on thermodynamics and mass transfer laws. The deposition is caused by condensation of exhaust gas components at the relatively cold surfaces in the exhaust gas channels. In the model the assumption has been made that chemical equilibrium conditions are met in the main exhaust gas flow and at the deposition surface.

The applicability of the model has been studied for two experimental situations:

1. Deposition of salt components from a flame doped with various types of inorganic substances (sodium, sulphur, chlorine, boron, potassium, lead) on a cylindrical surface at a homogeneous temperature.
2. Deposition of salts from simulated exhaust gases in a cylindrical channel with an inlet temperature of 1750 K and an flue gas outlet temperature of 800 K - 900 K.

In both experimental cases the deposition rates are measured and compared with the theoretical calculations for these situations. The temperature gradients across the boundary layer at the cylindrical surface in cross flow configuration in the flame are very large (200 to 500 K per mm). In this case reaction kinetic limitations are likely to influence the deposition as it is indeed observed by comparing the experimental results with the theoretically derived  $\text{Na}_2\text{SO}_4$  and  $\text{K}_2\text{SO}_4$  deposition rates.

The discrepancy between the experimental results and the theoretical calculations is considerably smaller in the second experiment where the temperature gradients in the boundary layers are more in agreement with practical situations gradients. Deposition of sodium metaborate, sodium sulphate, potassium sulphate, sodium chloride, lead oxide and lead sulphate have been studied with one or both methods.

#### **Sodium metaborate deposition**

From exhaust gases only doped with sodium and boron components, sodium metaborate and sometimes sodium tetraborate condenses. The dew point temperature increases with higher sodium and boron concentrations. The deposition rates measured on a cylinder in the flame deviate from the calculated rates in mainly three ways:

- the measured dew point is approximately 40 K lower than the theoretical dew point
- the experimentally derived maximum deposition rates are 10 to 20% lower than theoretically expected
- at temperatures below 900 K deposition rates decrease with further cooling, the model predicts a constant deposition rate below 1000 K.

These deviations can be explained by reaction or condensation kinetic limitations. The deposition rates of sodium metaborate in the simulated flue gas channel agree quite well with the results of the theoretical model. The maximum deposition rate measured at the surface of the cylindrical channel is 10-20% lower than theoretically determined.

The theory, based on transport of only gaseous molecules towards the deposition surface, of course predicts zero deposition rates as soon as all the sodium metaborate has already been condensed in the gas flow, i.e. for exhaust gas temperatures below 1050 K when surface temperatures are below 700 K. Below these surface temperatures however, experiments show that deposition still takes place probably caused by transport of already condensed material towards the deposition surface.

#### **Sodium sulphate deposition**

The maximum deposition rate measured on the cylinder in cross flow configuration in the flame, is proportional to the sodium concentration in the flame.

For this case the experimentally determined dew points are 120-160 K lower than derived theoretically. This delay in deposition is probably due to the limited rates of the reactions between  $\text{SO}_2$  and  $\text{NaOH}$  in these gases resulting in formation of condensed  $\text{Na}_2\text{SO}_4$ . Addition of chlorides to the flame reduces the dew points for sodium sulphate condensation on the cylindrical surface, although no chloride components condense. According to these experiments deposition of sodium sulphate increases steadily for decreasing surfaces temperatures in chloride rich flames. For the chloride free case deposition of sodium sulphate decreases below 1050 K. The calculations show a constant deposition rate for both cases below 1100 K.

The similarity between the theoretical approach and the experimentally derived deposition rates in the cylindrical channel is quite satisfactory. The experimental dew points are only 50 K lower than expected from the theoretical model. Deposition of sodium sulphate mainly takes place at wall temperatures between 800 and 1300 K. At temperatures above 1000 K the theory slightly overestimates deposition rates. Below 750 K, deposition of already condensed material takes place in the flue gas channel. The theory predicts no condensation at the deposition surface below this temperature.

From both theoretical and experimental results it is concluded that the increase in the sulphur concentration has only a slight effect on the deposition behaviour of simulated flue gases of glass furnaces.

#### **Deposition of potassium sulphate**

The actual deposition behaviour on the cylindrical surface in cross flow configuration of potassium sulphate from a flame doped with potassium and sulphur deviates considerably from the results of the theoretical calculations. However, the deposition rates in the simulated flue gas channel can be calculated rather accurately by the theoretical model for surface temperatures between 800 and 1250 K.

The similarity between the deposition behaviour of sodium sulphate and potassium sulphate has been illustrated by experiments with a flame doped with sodium, potassium and sulphur.

### **Sodium chloride deposition**

Sodium chlorides condense from sulphur lean flue gases of soda-lime glass furnaces below 1025 K. The theory gives a nearly 100% accurate description of the deposition process. Both deposition rates and dew point values are nearly the same for the experimental approach as for the theoretical predictions in case of the situation of the cylinder in cross flow configuration in the flame.

### **Lead oxide deposition**

The deposition product from flue gases only doped with lead is mainly lead monoxide (PbO) which is converted below 700 K into  $Pb_3O_4$ . The theoretical model slightly underestimates the dew point temperature for the case of deposition at the cylindrical surface positioned in the doped flame.

The experimentally derived deposition rates of lead oxide at the inner wall surface of the simulated flue gas channel can be explained accurately by the model above surface temperatures of 700 K.

### **Lead sulphate deposition**

Lead sulphate deposition is only studied experimentally on the surface of the cylinder positioned in a flame doped with sulphur and lead. The comparison between the theoretical model and the experimentally derived deposition behaviour is similar as for lead oxide.

In sulphur rich flue gases lead sulphate deposits are formed at surface temperatures below 1125 K. The theoretical calculations slightly underestimate the dew point temperature.

Finally, it can be concluded that for the most important exhaust gases of glass furnaces, the model presented here gives quite accurate predictions for deposition rates and the nature of the deposition products above 750 K. At lower temperatures deposition may be reduced by reaction and/or condensation kinetic limitations. Besides these limitations, deposition at gas temperatures below 1000 K is mainly caused by transport of condensed material (dust or particulates) from the flue gas to the deposition surface. Deposition caused by condensation of gaseous components at the surface is of minor importance below flue gas temperatures of 1000 K.

#### Literature references chapter 4

- [ 1 ] Rosner D.E., Seshadri K.;  
'Experimental and theoretical studies of the laws governing condensate deposition from combustion gases'.  
Eighteen Sym. on Combustion (1981) 1385-1394.
- [ 2 ] Rosner D.E., Chen B-K., Fryburg G.C., Kohl F.J.;  
'Chemically frozen multicomponent boundary layer theory of salt and/or ash deposition rates from combustion gases'.  
Combustion Science and Technology 20 (1979) 87-106.
- [ 3 ] Rosner D.E., Seshadri K., Fernandez de la Mora J., Fryburg G.C., Kohl F.J., Stearns C.A., Santoro G.J.;  
'Transport, thermodynamic and kinetic aspects of salt/ash deposition rates from combustion gases'.  
Proc. 10<sup>th</sup> Materials Research Symposium, NBS Spec. Publication 561 (1979) 1451 - 1474.
- [ 4 ] Brown T.D.;  
'The deposition of sodium sulphate from combustion gases'.  
J. Inst. Fuel, 39 (1966) 378-385.
- [ 5 ] Srivastava R., Rosner D.E.;  
'A new approach to the correlation of boundary layer mass transfer rates with thermal diffusion and/or variable properties'.  
Int. J. Heat Mass Transfer 22 (1979) 1281-1294.
- [ 6 ] Bird R.B., Stewart W.E., Lightfoot E.N.;  
'Transport Phenomena'.  
John Wiley, New York (1960).
- [ 7 ] Rosner D.E.;  
'Thermal (Soret) Diffusion Effects on Interfacial Mass Transport rates'.  
Physicochemical Hydrodynamics, 1 (1980) 159-185.
- [ 8 ] Epstein M., Rosner D.E.;  
'Enhancement of diffusion-limited vaporization rates by condensation within the thermal boundary layer: 2 comparison of homogeneous nucleation theory with the critical supersaturation model'.  
Int. J. Heat Mass Transfer 13 (1970) 1393-1414.

- [ 9] Fernandez de la Mora J., Friedlander S.K.;  
'Aerosol and gas deposition to fully rough surfaces: filtration  
model for blade-shaped elements'.  
Int. J. Heat Mass Transfer, 25 (1982) 1725-1735.

## NOMENCLATURE CHAPTER 4

$A_s$	specific surface area per unit of length ( $m^2/m$ )
$a_{i,j}$	weight fraction of component $j$ in component $i$
$B$	driving force equation 4.1, concentration difference $Na_2SO_4$ ( $kg/m^3$ )
$cb_i$	weight-fraction component $i$ in main stream
$c_{wi}$	weight-fraction component $i$ in gas phase at surface position
$c_p$	heat capacity ( $J.kg^{-1}.K^{-1}$ )
CFBL	Chemically Frozen Boundary Layer
$D$	diffusion coefficient ( $m^2/s$ ) in equations 4.2, 4.3 en 4.4
$D$	characteristic diameter (m) in equation 4.1
$D_{i,b}$	diffusion coefficient for component $i$ in main stream ( $m^2/s$ )
$D_{i,g}$	diffusion coefficient component $i$ ( $m^2/s$ )
$D_{i,m}$	diffusion coefficient component $i$ in main stream ( $m^2/s$ )
$F_i(\text{soret})$	correction term for thermodiffusion
$F(\text{ncp})$	correction term for non-constant properties in boundary layer
$J$	nucleation rate ( $m^{-3}.s^{-1}$ )
$k$	Boltzmann's constant ( $1.38 \cdot 10^{-16} J/molecule.K$ )
$L$	characteristic length (m)
$Le_{i,w}$	Lewis number ( $D.p.c_p/\lambda$ ) at wall positions ( $D.p.c_p/\lambda$ )
$M_i$	mass of one mole molecules $i$ (g/mol)
$M_g$	mass of one mole gas molecules (g/mol)
$N_a$	Avogadro number
$p_i^*$	saturation pressure component $i$ (Pascal)
$P$	absolute pressure (Pascal)
$Pr$	Prandtl number ( $c_p.\mu/\lambda$ )
$Re$	Reynolds number ( $\rho.v.D/\mu$ )
$r^*$	critical nucleus size (m)
$r_{i,eff}'''$	source term defined by (4.4)
$S_i$	supersaturation factor
$Sc_i$	Schmidt number ( $\mu/\rho.D_{i,g}$ )
$Sh_i$	Sherwood number
$T$	absolute temperature (K)

$u$	gas velocity in x-direction
$v$	gas velocity in y-direction (m/s)
$V$	flue gas velocity (m/s)
$v_s$	suction-like term defined by equation 4.3 (m/s)
$y_i$	mass fraction of species $i$
$w_{ni}$	weight fraction component $i$ in main stream
$w_{wi}$	weight fraction component $i$ in gas phase near deposition surface
$z$	distance along axis of cylinder or channel from the entrance (m)

### Greek symbols

$\alpha_m$	mass accommodation coefficient
$\alpha_{-1}$	parameter for estimation of $\alpha$ , equation 4.7b (K)
$\alpha$	parameter for estimation of $\alpha$ , equation 4.7b
$\alpha_{i,w}$	thermodiffusion coefficient component $i$ at wall position
$\alpha$	thermodiffusion coefficient
$\tau_i$	thermophoretic parameter defined by (4.7)
$\rho_b$	density of gas phase in main stream ( $\text{kg}/\text{m}^3$ )
$\rho_m$	density of gas phase in main stream ( $\text{kg}/\text{m}^3$ )
$\rho$	density ( $\text{kg}/\text{m}^3$ )
$\sigma_{i,g}$	Lennard-Jones diameter component $i$ in gas $g$ (m)
$\Omega_{i,g}$	intermolecular potential field parameter
$\delta$	boundary layer thickness (m)
$\sigma$	surface tension in equation 4.18, (N/m)
$\phi$	volume flow ( $\text{m}^3/\text{s}$ )
$\mu$	dynamic viscosity ( $\text{kg}\cdot\text{m}^{-1}\cdot\text{s}^{-1}$ )
$\lambda$	thermal conductivity ( $\text{W}\cdot\text{m}^{-1}\cdot\text{K}^{-1}$ )

## 5. APPLICATION OF THEORETICAL SIMULATION MODEL TO INVESTIGATE DEPOSITION FROM AND CONDENSATION IN EXHAUST GASES FROM INDUSTRIAL GLASS FURNACES

### 5.1 Introduction

In the previous chapters the most essential processes that determine the deposition of components from the flue gas phase to obstacles or surfaces in exhaust gas channels have been discussed. Besides deposition, also condensation and dust formation in flue gases has been considered. It has been shown that lack of fundamental data, especially with respect to kinetic parameters, inhibits a full and detailed description of the chemical processes occurring in the relevant temperature range.

However, combination of a simplified boundary layer transport model with a thermodynamic equilibrium model supplied us with a tool to analyse the main characteristics of deposition and condensation processes as shown in chapter 4. First, this model gives a prediction of the transport rates of gaseous components through boundary layers towards relatively cool surfaces where condensation takes place.

Secondly the model predicts the chemical composition of the main flue gas flow including the composition of the formed dust. These compositions are calculated by means of the methods described in chapter 3.

In the previous chapter it was shown that this model rather accurately predicts the nature of deposition products and the rates of deposition in a simple laboratory flue gas channel. This chapter deals with the application of this model to predict deposition and condensation in industrial regenerators or recuperators. The deposition and condensation processes in regenerators are presented in section 5.2. The influence of the regenerator construction, temperature distribution and flue gas velocities on deposition behaviour is also described. Results of calculations with the model for different regenerative furnaces producing soda-lime glass, borosilicate glass or lead glass are presented in this section. A similar investigation has been conducted for recuperative devices in section 5.3.

As shown in section 4, the simulation model is not suitable for deposition processes at flue gas temperatures below 1000 K, since reaction kinetic limitations and deposition of dust from the flue gases have to be considered. Below these temperatures all alkali or lead compounds are already condensed in these flue gases; transport of gaseous species towards deposition surfaces where condensation takes place is in most cases negligible below 1000 K.

Therefore, at low temperatures we may still encounter deposition, but this will be due to dust particles formed in the gas stream. A complication in the dealing with this process is the possibility that these dust particles react with gaseous components below 800 K thereby altering their nature and physical behaviour.

In section 5.4 a short qualitative description is given of the chemical reactions and processes that may take place below 800 K in flue gases of soda-lime glass furnaces. These processes are of primary importance for heat exchangers in the low temperature region.

Finally, in section 5.5 the thermodynamic equilibrium model of chapter 3 is used to predict particulate and gaseous emissions from industrial glass furnaces.

## **5.2 Deposition processes in the checkers of glass furnace regenerators**

The model presented in chapter 4 has been applied for the regenerator situation in industrial glass furnaces. The deposition rate is calculated by means of formula 4.9 for the relevant deposition products. The construction and processing of regenerators is described in the next section.

### **5.2.1 Heat and mass transfer in different regenerator construction**

Before applying the simulation model of chapter 4, the diversifications of regenerator constructions will be outlined. Several types of checker constructions are being applied in regenerators. The bricks may be piled up in different ways or the form of these bricks may be different. In figure 5.1 some checker constructions are shown.

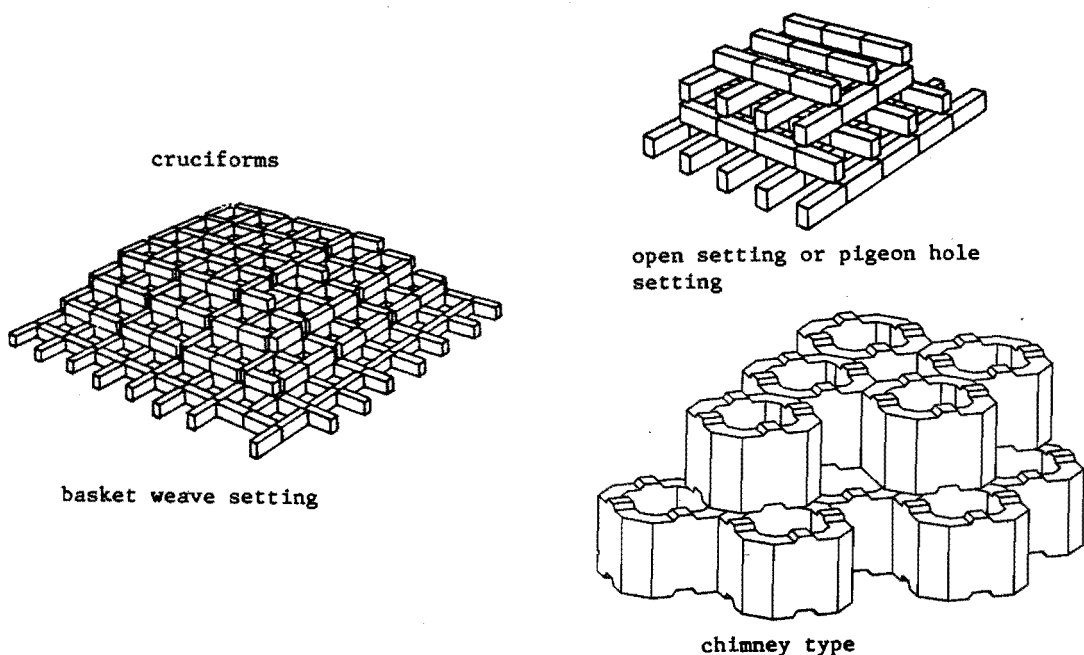


Figure 5.1: Three types of checker packing.

The flue gases from the glass furnace pass the checker work through mostly rectangular channels. The gas flow is periodically disturbed by the openings in the checker work perpendicular to the main stream direction. These disturbances result in increasing mass and heat transfer rates. The gas velocities in the channels (calculated for normalized conditions at 1013 mbar and 295 K) range between 0.25 and 1.0  $m_n/s$  in industrial regenerators.

The specific heat or mass transferring area per cubic metre checker volume ranges between 12 and 18  $m^2/m^3$ . Practical values for the Sherwood number to calculate mass transport rates are not given in the literature. However, from the analogy of heat and mass transfer, Sherwood numbers can be calculated in a way similar to Nusselt numbers from the well known relations between Nu and Re (Reynolds number) for heat transfer in regenerators. For most situations the analogy between mass and heat transfer correlations is presented by:

$$Sh = (Nu - A) * Sc^n / Pr^n \quad (5.1)$$

with Nusselt related to Reynolds as in equation 5.2:

$$Nu = A' + B' \cdot Re^m \cdot Pr^n \tag{5.2}$$

and

$$Sc = \mu / \rho \cdot D \tag{5.3}$$

$$Pr = c_p - \mu / \lambda \tag{5.4}$$

where:

- Sh = Sherwood number
- Nu = Nusselt number
- Re = Reynolds number ( $\rho \cdot v \cdot d / \mu$ )
- Pr = Prandtl number
- Sc = Schmidt number
- B', A', m, n = constants depending on construction geometry
- D = diffusivity ( $m^2 s^{-1}$ )
- $\rho$  = gas density ( $kg \cdot m^{-3}$ )
- $\mu$  = dynamic viscosity ( $kg \cdot m^{-1} s^{-1}$ )
- d = characteristic diameter (m)

Our approach made use of the simple but very practical relation given by Schmalenbach [1]:

$$Nu = A + B \cdot Re \tag{5.5}$$

The values for A and B are given in table 5.1 for different checker constructions.

checker work:	A	B
basket weave setting	10	0.00691
cruciform stones	10	0.00691
chimney type	11	0.00682
pigeon hole setting	13	0.0067
staggered packing	14.2	0.0074

from reference [1]

With these correlations it is possible to derive Sherwood numbers in the different sections in the regenerator and as a function of gas velocity.

### 5.2.2 Temperature distribution in regenerators

The temperature of a certain location in a regenerator is time dependent due to the cyclic operation of this type of heat exchanger. The temperature of the combustion air at a certain location during the air-preheat period is approximately 200 K lower than the exhaust gas temperature during the regenerator heating period at the same location. The combustion air temperature is generally too low to evaporate the deposited material at the regenerator bricks during the air-preheat period.

The difference between the exhaust gas temperature at the beginning and at the end of the regenerator heating period is 30 to 40 K at a certain location. The difference between the exhaust gas temperature and the surface temperature of the adjacent checker bricks is 50 to 100 K, Trier [2]. Barklage-Hilgefort [3]. The temperature of the flue gases decreases from 1600-1700 K to 700-850 K in the regenerators.

### 5.2.3 Deposition of salt components in regenerators of soda-lime glass furnaces

In regenerators of flat glass and container glass furnaces deposition of sulphates in the middle sections may result in blockage of the channels and lower the thermal efficiency of these heat exchangers.

Sodium sulphate is the most important constituent of the material deposited from the exhaust gases of these furnaces.

From the melts, (section 1.1.3.1) sodium and sulphur components volatilize in these kinds of furnaces.

The sodium concentrations in the flue gases leaving the furnace vary from 30 to 100  $\text{mg}/\text{m}_n^3$ , the sulphur concentrations in natural gas fired furnaces vary from 40 till 150  $\text{mg}/\text{m}_n^3$ . In case of oil-firing the sulphur concentrations may exceed 600  $\text{mg}/\text{m}_n^3$ .

Sodium chloride may vaporize from the batch due to impurities in the synthetic soda. Chloride concentrations in the flue gas range from 40 to 80 mg/m<sup>3</sup>. In this section the influence of the exhaust gas composition, the temperature distribution in the regenerator and the regenerator dimensions, on the deposition behaviour is discussed in terms of calculations based on the simulation model. The basic situation is presented in table 5.2 for a regenerative soda-lime glass furnace.

Table 5.2: Process parameters for exhaust gas and regenerator of a soda-lime glass furnace (basic situation).

type of checker work	pigeon hole
channel dimension between bricks	0.16 * 0.16 m
brick height	0.12 m
temperature difference brick surface - flue gas	100 K
flue gas velocity	0.6 m <sub>n</sub> /s
temperature flue gas at top	1700 K
temperature flue gas at bottom	800 K
oxygen concentration flue gas	4.4 volume-%
water vapor concentration flue gas	15.5 volume-%
carbon dioxide concentration	10 volume-%
sodium concentration	125 volume-ppm*
sulphur concentration	250 volume-ppm
chloride concentration	62.5 volume-ppm

\* volume-ppm = parts per million molecules in gas, assuming the elements mentioned to be gaseous atoms irrespective of the molecular composition.

The method of calculation is similar to the procedure presented in chapter 4 and outlined in appendix C. The model gives predictions for the deposition rate of components condensing at the brick surfaces in the regenerator, by means of the boundary layer mass transfer theory. The flue gas compositions are calculated in this model by means of the chemical equilibrium theory. For this situation the deposition product is only sodium sulphate (Na<sub>2</sub>SO<sub>4</sub>).

The calculated deposition rate of  $\text{Na}_2\text{SO}_4$  in the regenerator, as a function of the deposition temperature (temperature of the deposition layer) is given in figure 5.2 curve A1. The melting temperature of sodium sulphate is 1157 K and from curve A1 it can be concluded that  $\text{Na}_2\text{SO}_4$  condenses mainly as a liquid phase at the regenerator bricks. Deposition sets on below 1370 K (dew point temperature) and the deposition rate rises rapidly at decreasing brick temperatures.

The maximum deposition rate for this case is  $2.5 \text{ mg/m}^2 \cdot \text{s}$  (or a deposition layer of 5 cm/year) at 1275 K. Condensation of sodium sulphate at the surface of regenerator bricks hardly takes place at temperatures below 1000 K. According to equilibrium calculations the exhaust gases leaving the regenerator contain  $220 \text{ mg/m}^3$  sodium sulphate dust.

Approximately 12.5% of the sodium sulphate is deposited on the regenerator bricks. This finding is in good agreement with practical values; between 10% and 20% for sodium sulphate retention in the regenerators of soda-lime glass furnaces.

#### **5.2.3.1 Influence of changing flue gas compositions on deposition behaviour in regenerators of soda-lime glass furnaces**

According to the calculations with the simulation model, the concentrations of oxygen, water vapor and carbon dioxide in the exhaust gases hardly influence the deposition and condensation rates in the regenerator.

However, a change in the concentrations of sodium, chlorine and sulphur alter the shape of the presented curve A1 of figure 5.2. To illustrate this, we calculated the deposition rates of 4 different flue gases and compared the results with those presented in the previous section (basic situation A1). These flue gas compositions are listed in table 5.3 and the results are presented in figure 5.2 and figure 5.3.

In chapter 1 it was shown that the volatilization rates for sodium components may be changed by alterations in the combustion processes in the melting furnace. Curve A2 presents the deposition behaviour of a flue gas with a 50% reduced sodium concentration. Comparing situation A1 with example A2 shows that the maximum sodium sulphate deposition rate is almost proportional to the sodium concentration or the sodium volatilization rate from the melts.

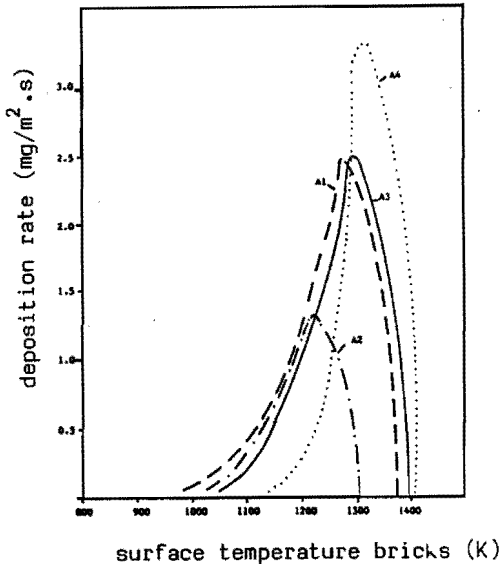


Figure 5.2: Deposition rates for sodium sulphate in the regenerator of soda-lime glass furnaces.

This was verified by more extensive calculations for flue gases with an excess of sulphur for sodium sulphate formation. From figure 5.2 it is clear that deposition rates decrease considerably at diminishing sodium vaporization rates from the glass melt. Deposition in case A2 sets on at a 55 K lower temperature and reaches a rate of only  $1.3 \text{ mg/m}^2.\text{s}$  at 1220 K for this situation.

Only 11% of the sodium sulphate deposits in the regenerator, 89% is entrained in the flue gases as condensed material and will leave the regenerator. The chance of blockage of the regenerator channels is very small. The maximum rate of material deposited is only  $2 \text{ g/cm}^2.\text{year}$  for case A2.

A change from natural gas-firing to combustion of oil in the glass melting furnaces causes an increase in the sulphur oxide concentrations in the exhaust gases.

Curve A3 represents the dependence of the deposition rate on the brick temperature for a flue gas with a concentration of 500 ppm sulphur instead of 250 ppm for case A1. The curves A1 and A3 are quite similar although the A3-curve has shifted to a somewhat (20 K) higher temperature.

It appears that the sulphur concentration has only a slight effect on the deposition behaviour of sodium sulphate in regenerators of soda-lime glass furnaces. However, at much lower temperatures, the nature of the deposition and condensation products may be influenced by the sulphur content of the applied fuels as will be discussed in section 5.5. The use of natural soda reduces the chlorine concentrations in the exhaust gases to a very low level in soda-lime glass furnaces.

The deposition behaviour of sodium sulphate for a chlorine free exhaust gas is represented by curve A4. Deposition sets on at a temperature slightly higher than for the basic situation (A1). The most important feature is the high rate for sodium sulphate fouling at 1320 K. In case A4 nearly 100% of the deposited  $\text{Na}_2\text{SO}_4$  in the regenerators is in the liquid phase. The deposition of large amounts of liquid sodium sulphate from chlorine free gases accelerates corrosion of the checker bricks above the  $\text{Na}_2\text{SO}_4$ -melting point of 1157 K.

So far only the deposition of sodium sulphate has been considered. From melts with no or little addition of sulphates as refining agents (as in case of sodium chloride refining), sodium carbonate and sodium chloride may condense from natural gas-fired furnaces. The deposition behaviour of a flue gas with only 25 volume-ppm sulphur has been presented in figure 5.3 for flue gas number A5.

**Table 5.3:** Flue gas compositions of the investigated cases for soda-lime glass furnaces.

case	A1 (base)	A2	A3	A4	A5
sulphur (vol-ppm)	250	250	500	250	25
sodium (vol-ppm)	125	62.5	125	125	125
chlorine (vol-ppm)	62.5	62.5	62.5	0	62.5

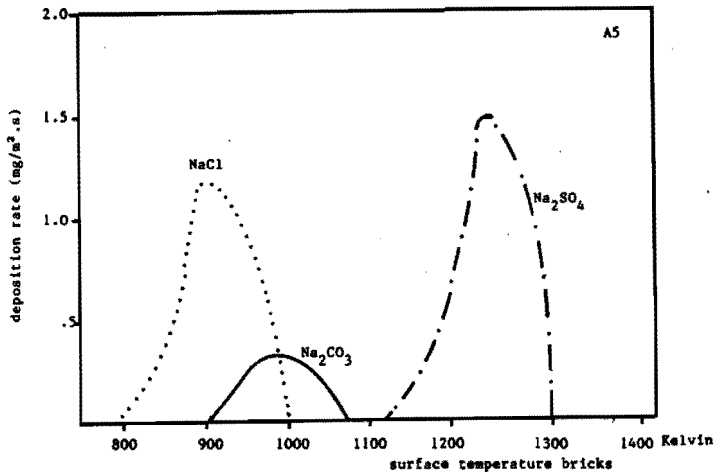


**Figure 5.3:** Deposition behaviour of sulphur lean flue gas in the regenerator of a soda-lime glass furnace.

Sodium sulphate is the only deposition product on the bricks at temperatures above 1100 K in case A5. Between 900 and 1000 K both sodium carbonate and sodium chloride condense at the brick surfaces. Two sections of the regenerator have been fouled rather seriously by salt components. Sodium sulphate deposition takes place in the middle section of the regenerator for checker temperatures between 1100 K and 1300 K. Sodium chloride deposits will be found in the lower parts (with lower brick temperatures) of the regenerator.

### 5.2.3.2 Effect of operating conditions and construction of regenerator on deposition of sodium sulphate

The temperature distribution in the regenerator, the construction of the checker work and gas velocities may influence the deposition rates of flue gas components. With our simulation model these influences have been studied for a couple of cases. The deposition behaviour is calculated and represented in figure 5.4:

1. The deposition curve for the basic situation (A1).
2. The deposition curve for a gas velocity twice as high as the basic situation, example A6.

3. The deposition curve in case of a 50 K temperature difference between the exhaust gas and the brick surface (example A7) instead of 100 K as was the case for A1.

Higher gas velocities result in higher values for the Sherwood number causing a higher mass transfer towards the deposition surface. As may be seen from figure 5.4, curve A6, an increasing gas velocity indeed results in higher deposition rates on the vertical surfaces of regenerator bricks between 1100 K and 1350 K.

This increase amounts to 25% for the maximum deposition rate at 1280 K relative to the maximum deposition rate for A1. In case of a lower temperature difference, namely 50 K instead of 100 K, between the local flue gas temperature and the brick surface, deposition rates decrease considerably as can be seen by comparing curve A7 and A1 in figure 5.4. Moreover, the dew point temperature is slightly decreased for case A7.

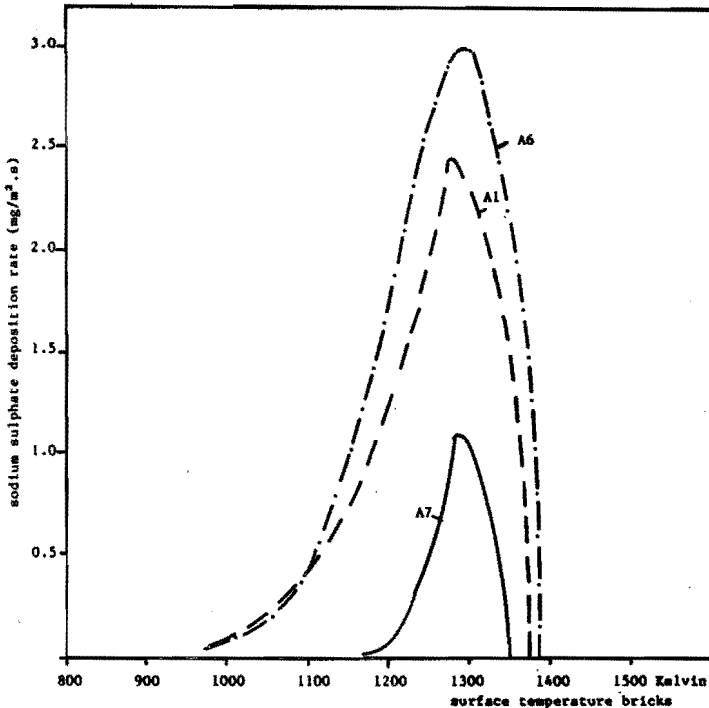


Figure 5.4: Deposition rates for sodium sulphate in regenerators for varying conditions.

Therefore, keeping the temperature difference between flue gas and regenerator bricks low, the fouling rates can be diminished considerably. However, this may result in a less efficient performance of the regenerator system although use of new materials may result in lower temperature differences between flue gas and brick without affecting the efficiency of the regenerator.

#### **5.2.4 Deposition of salt components in regenerators of borosilicate glass furnaces**

Most borosilicate glasses contain sodium oxide and/or potassium oxide. Although the concentrations of alkali oxide compounds in some borosilicate glasses (E-glass for example) may be lower than 1.0 weight-%, these components volatilize rather fast in combination with boron oxide. The main volatilization products from most borosilicate glass melts are sodium and/or potassium compounds, boron compounds and sulphur compounds.

In this section special attention will be paid to the deposition and condensation processes of flue gases from sodium-borosilicate glass melting furnaces. The flue gas composition for such a furnace, fired with natural gas and with addition of sulphates as refining agents is given in table 5.4.

First sodium sulphate condenses below 1370 K at the vertical surfaces of the regenerator bricks. Below 1310 K deposition of sodium metaborate sets on, as shown in figure 5.5. At surface temperatures between 1100 K and 1310 K sodium sulphate and sodium metaborate deposit simultaneously. The maximum deposition rate for liquid sodium metaborate at 1200 K is  $8.5 \text{ mg/m}^2 \cdot \text{s}$  or 13.5 grams per square centimetre per year. In the middle sections of the regenerators with temperatures between 1150 and 1300 K the deposition of these liquid deposits causes high corrosion rates for the refractories of the checker.

Corrosion is especially severe in sections of the regenerator with temperatures ranging around the melting point temperature of sodium metaborate (1174 K) and sodium sulphate (1157 K). The changing specific volume of the deposits in the pores of the refractory material by changing from liquid to solid phases and vice versa generally results in mechanical stresses in this material.

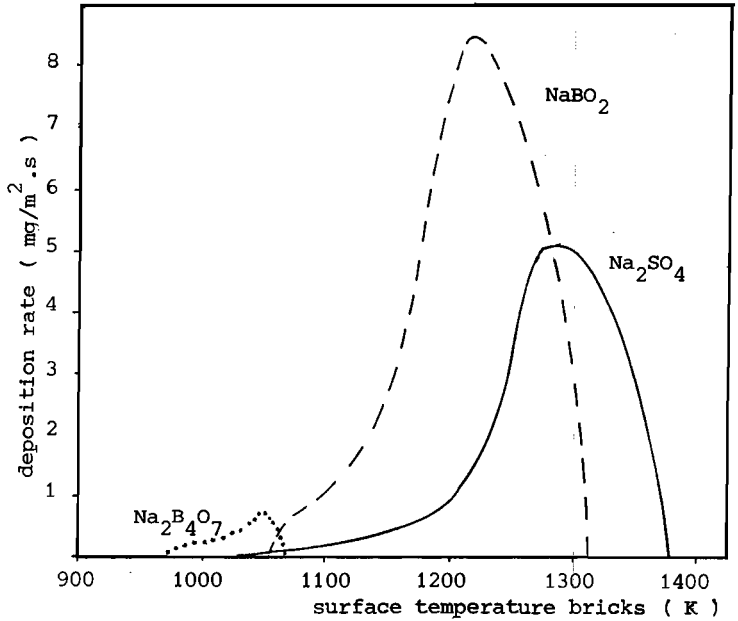


Figure 5.5: Deposition on bricks of regenerator of a sodium-borosilicate furnace.

Table 5.4: Process parameters and composition of exhaust gases in regenerators of a sodium-borosilicate furnace.

type of checker work	pigeon hole
channel dimensions	0.16 * 0.16 m
brick height	0.12 m
temperature difference brick surface-flue gas	100 K
flue gas velocity	0.6 m <sub>n</sub> /s
temperature flue gas at top	1700 K
temperature flue gas at bottom	800 K
oxygen concentration	4.4 volume-%
water vapor concentration	15.0 volume-%
carbon dioxide concentration	10.0 volume-%
boron concentration	6 10 <sup>-2</sup> volume-%
sodium concentration	6 10 <sup>-2</sup> volume-%
sulphur concentration	1 10 <sup>-2</sup> volume-%

Sodium tetraborate deposition takes place below 1070 K according to our calculations for this situation. According to the equilibrium calculations the dust formed in the regenerator during cooling consists of 480 mg sodium sulphate and 1650 mg sodium tetraborate per cubic metre flue gas (under normalised conditions 298 K, 1013 mbar). No gaseous sodium or sulphur components remain in this exhaust gas. According to our calculations and literature data [3] the most important boron component in the stack is  $H_3BO_3$ . Analysis of dust precipitated from flue gases of natural gas fired sodium borosilicate glass furnaces shows that indeed sodium sulphate and sodium tetraborate are the main constituents in these condensates.

Secondly the deposition of salt components of an oil-fired sodium borosilicate furnace has been studied by means of the computer simulation model.

The flue gas composition under study here is presented in table 5.5.

Table 5.5: Flue gas composition of an oil-fired sodium borosilicate glass furnace.

major components volume-ppm		minor constituting elements volume-ppm	
O <sub>2</sub>	4.4	Na	400
CO <sub>2</sub>	10	B	400
N <sub>2</sub>	70.6	S	500
H <sub>2</sub> O	15		

The deposits consist only of sodium sulphate, condensing between 1100 and 1400 K at the regenerator bricks, shown by figure 5.6.

In this case nearly all the boron in the exhaust gases is converted into gaseous boric acid ( $H_3BO_3$ ) during the passage through the regenerator.

The dust, only consisting of sodium sulphate amounts to  $670 \text{ mg/m}_n^3$  exhaust gas.

In oil fired sodium-borosilicate glass furnaces the maximum deposition rate at approximately 1300 K increases with the sodium concentration in the exhaust gas.

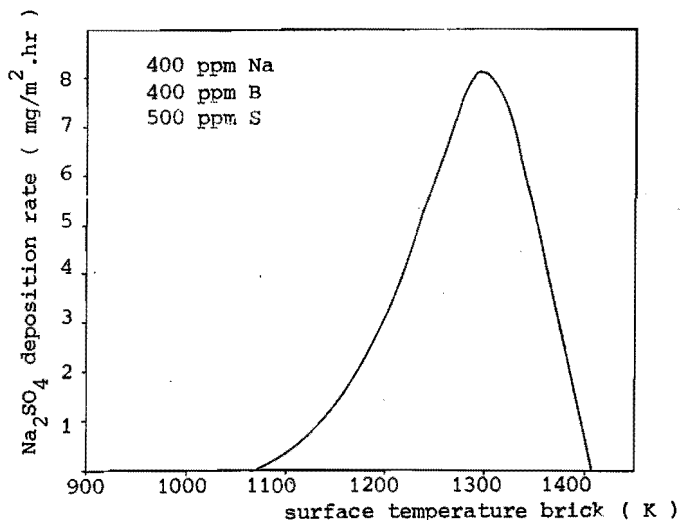


Figure 5.6: Deposition of sodium sulphate at regenerator bricks of a sodium borosilicate glass furnace.

Flue gases from furnaces melting borosilicate glasses with potassium oxide instead of sodium oxide contain gaseous potassium metaborates, meta boric acid and potassium hydroxide as the most important components above 1400 K. The deposition behaviour of potassium compounds from an exhaust gas given in table 5.6 is shown in figure 5.7.

The main deposition product from flue gases with a composition as in table 5.6 is potassium sulphate condensing below 1370 K. This deposition product is solid below 1342 K. In this case corrosion by liquid deposits is of smaller importance than for sodium sulphate deposition in regenerators of sodium-borosilicate or soda-lime glass furnaces. The rates of deposition of liquid potassium sulphate are generally low (lower than 2 mg/m<sup>2</sup>.s) and deposition in this phase only takes place in a very small part of the regenerator.

**Table 5.6:** Typical composition of a flue gas from a gas-fired sodium borosilicate glass furnace.

major components volume-%		minor constituents volume-ppm	
O <sub>2</sub>	4.4	K	300
CO <sub>2</sub>	10.0	B	300
N <sub>2</sub>	70.6	S	125
H <sub>2</sub> O	15.0		

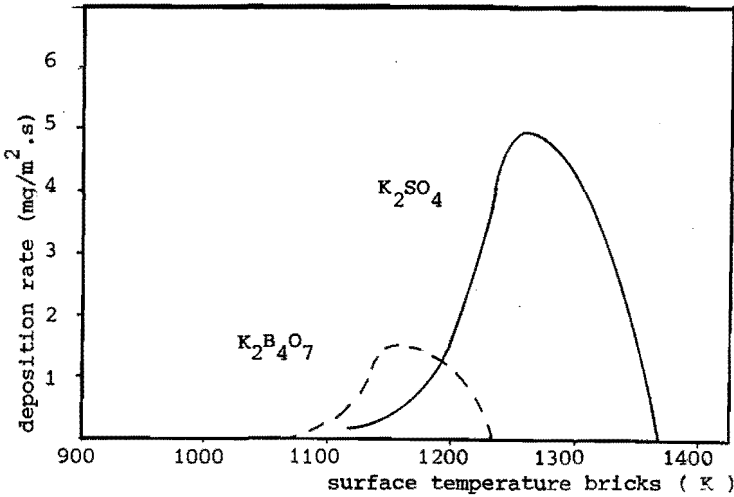


**Figure 5.7:** Deposition in the regenerator of a gas-fired potassium borosilicate furnace.

According to the calculations with the model no potassium metaborates are expected to deposit in regenerators of these potassium borosilicate glass furnaces. Below 1230 K deposition of potassium tetraborate sets on and continues till 1070 K. For higher potassium or lower sulphur concentrations, potassium tetraborate deposition is of increasing importance in these regenerators.

For this case the dust formed in the regenerator consists of 720 mg potassium sulphate and 210 mg potassium tetraborate per cubic metre exhaust gas volume (under normalized conditions 298 K and 1013 mbar).

### 5.2.5 Deposition of salt components in regenerators of lead glass furnaces

From lead glass melts, produced in industrial furnaces, lead vaporizes as  $PbO$  or  $Pb(OH)_2$ . The concentrations of all lead compounds in the exhaust of the furnace vary for most practical cases between 75 volume-ppm and 300 volume-ppm. Kaiser [4] gave retention factors of approximately 95% for the lead remaining in the glass melt of a furnace producing a glass with 24 weight-%  $PbO$ . Approximately 5% of the added lead vaporizes. This value gives a concentration of approximately 100 volume-ppm of lead components in the exhaust gases.

However, for some glass furnaces producing lead glass, the retention factor may be as low as 90%. The deposition behaviour of a flue gas from a natural gas-fired furnace producing lead glass with high volatilization rates is presented in figure 5.8.

The total concentration of lead compounds in the exhaust of this furnace is 280 volume-ppm, the sulphur concentration amounts to 50 volume-ppm. Lead oxide deposits between 980 and 1150 K in the regenerator of this furnace; the maximum deposition rate is  $12.5 \text{ g/cm}^2$  per year.

Lead oxide and lead sulphate condense simultaneously at the refractories between 980 and 1070 K, compounds like  $2PbO.PbSO_4$  may be formed.

Below 900 K no deposition takes place according to our model. The dust contains  $PbSO_4$ ,  $PbO$  and combinations of these components. For a flue gas containing only 140 volume-ppm lead compounds and no sulphur components, lead oxide deposition sets on below 1110 K. The maximum deposition rate for this case has been calculated to amount to  $6 \text{ g/cm}^2$  per year. The deposition behaviour of the sulphur free flue gas is represented by figure 5.9.

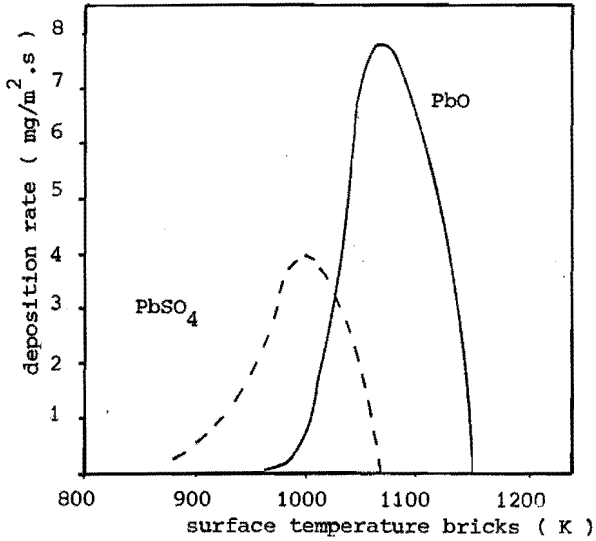


Figure 5.8: Deposition rates of PbO and PbSO<sub>4</sub> in the regenerator of a gas-fired lead glass furnace composition.

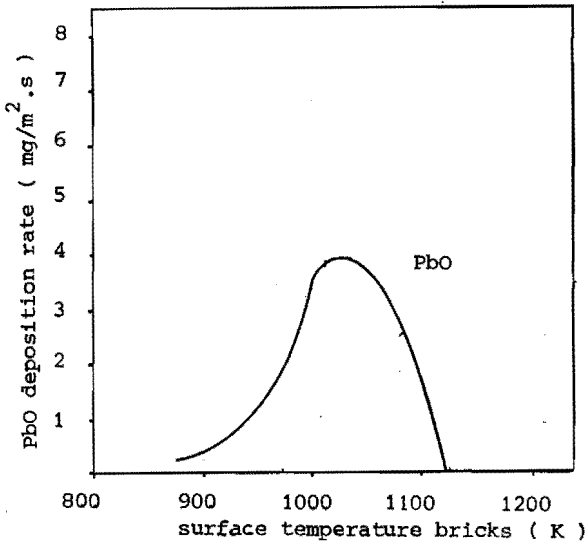


Figure 5.9: Deposition rates of PbO in regenerators of gas-fired lead glass furnaces, with sulphur free flue gas.

Little or no lead oxide condenses in the regenerators of heavy oil-fired glass furnaces. This is in accordance with the analysis of dust precipitated from stack gases of oil-fired lead glass furnaces. Figure 5.10 shows the deposition behaviour of a flue gas with 140 volume-ppm lead and 500 volume-ppm sulphur. Deposition of lead sulphate takes place between 970 and 1125 K. The deposition rate for lead sulphate in this case is especially high between 1020 K and 1100 K and amounts to  $7 \text{ mg/m}^2 \cdot \text{s}$ . The exhaust gases from these regenerators contain 1500 mg  $\text{PbSO}_4$  dust per cubic metre exhaust gas volume (under normalized conditions 298 K and 1013 mbar).

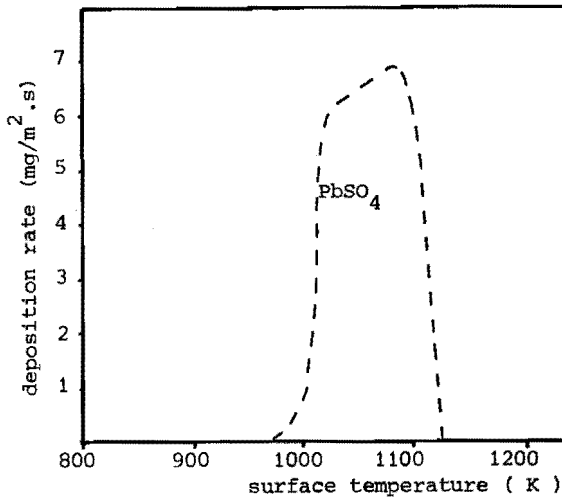


Figure 5.10: Deposition rates of  $\text{PbSO}_4$  in regenerator of an oil-fired lead glass furnace.

### 5.3 Deposition processes in recuperators of glass furnaces

#### 5.3.1 Flow conditions in radiative recuperators

Various recuperator constructions have been applied in the glass industry. The most commonly used recuperator type is the so-called radiation recuperator (section 1.1.4.2) where flue gases flow in a inner circular tube, heating the combustion air flowing between the inner and outer walls of the recuperator.

The flue gases cool down from 1550 - 1400 K to 1250 à 1050 K. The air preheat temperature may reach values of 1050 K in case of counter flow models. The flow conditions of the exhaust gases in these recuperators are turbulent, Reynolds numbers vary from  $2 \cdot 10^4$  to  $10^5$ . Normally the air velocities in the space between the inner and outer tube are so high that the heat transfer is mainly determined by the transport from the flue gas to the inner wall of the recuperator.

The occurrence of salt deposits or batch carry-over deposits at the flue gas side of these heat exchangers leads to a decrease in heat transfer towards the inner wall. The Reynolds number for flue gas conditions is given by relation 5.6.

$$Re = \rho \cdot v \cdot d / \mu \quad (5.6)$$

where:  $d$  = the diameter of the inner tube of the recuperator (m).  
From Bird, Stewart and Lightfoot [5] the following relations for the Nusselt number and Sherwood number have been derived for turbulent flows in a circular tube:

$$Nu = 5.0 + 0.025 (Re \cdot Pr)^{0.8} \quad (5.7)$$

$$Sh = 5.0 + 0.025 \cdot (Re \cdot Sc)^{0.8} \quad (5.8)$$

Equation 5.8 is used to calculate the mass transfer coefficients for recuperators as a function of exhaust gas velocity, temperature and recuperator diameter.

The values for the Sherwood number for practical situations are in the order of  $10^2$ . Relation (5.8) is valid for positions in the recuperators in axial direction after a length of one channel diameter from the flue gas entrance.

### 5.3.2 Temperature distribution in the recuperator

Two types of recuperators are distinguished: parallel flow recuperators and counter flow recuperators.

In parallel flow recuperators the combustion air flows parallel to the flue gases preventing overheating of the recuperator materials in sections where the flue gas temperatures are extremely high. Recuperators may also be constructed in the counter flow device to achieve high air preheat temperatures. In recuperators the inner wall temperature reaches values generally differing only slightly from the local air temperature. Initially the wall temperature is equal to the deposition temperature as the inner surface of the recuperator tube has not yet been fouled by deposits. The temperature of the deposition surface increases with time due to the layer of material that sticks to the inner wall resulting in decreasing heat transfer rates from the flue gases to the combustion air. The temperature of the deposition surface is always higher than the temperature of the metallic wall or the air. The temperature distribution for the flue gas, the deposition surface, the inner wall and the combustion air for a counter flow recuperator is given in figure 5.11. In the next section the deposition behaviour for flue gas condensates is presented for counter flow as well as parallel flow conditions.

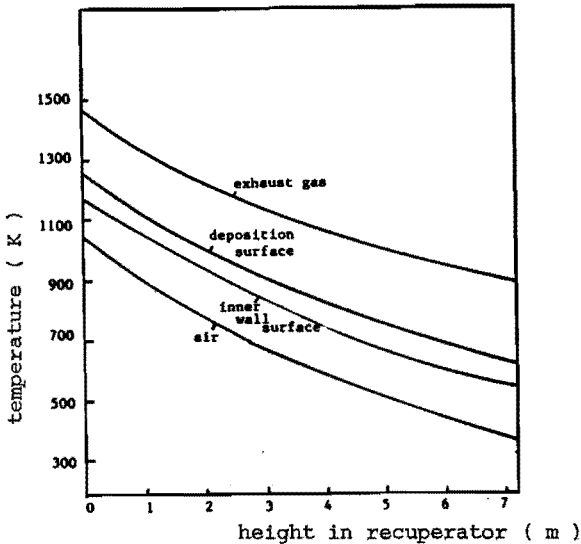


Figure 5.11: Typical temperature distribution in recuperator with combustion air in counter flow direction.

### 5.3.3 Deposition of salt components in recuperators of soda-lime glass furnaces

In section 5.2.3 was shown that the most important deposition and condensation products in exhaust gases of soda-lime glass furnaces are generally liquid or solid sodium sulphate.

The sodium sulphate deposits from the flue gases are formed at surface temperatures below 1300 - 1400 K. The surface temperatures in recuperators never exceed these temperatures, sodium sulphate deposition sets on at the inner surface of the recuperator directly at the flue gas entrance.

This deposition of sodium sulphate together with batch carry-over, for example silica or alumina, may lead to formation of glassy layers at the surface near the flue gas entrance. The simulation model does not account for carry-over deposition and only the condensation of salt components at the surfaces of the recuperator has been studied. The flue gas composition for the basic situation is given in table 5.7 together with two other situations. The basic situation may be realistic for a furnace fired with a light oil using synthetic soda as the sodium oxide supplier.

Table 5.7: Flue gas compositions of recuperative soda-lime glass furnaces.

	basic situation 1	situation 2	situation 3
fuel	light oil	natural gas	light oil
synthetic/natural soda	synthetic soda	synthetic soda	natural soda
chlorine concentration vol.-ppm	62.5	62.5	-
sodium concentration vol.-ppm	125	125	125
sulphur concentration vol.-ppm	250	125	250
oxygen concentration vol.-ppm	4.4	4.4	4.4
water concentration vol.-ppm	15	15	15
carbon dioxide concentration vol.-%	15	10	10

Sodium sulphate deposits as a result of condensation at the inner surface in the lower parts (with higher flue gas temperatures and wall temperatures) of the counter flow recuperator above temperatures of 900 K. The maximum deposition rate amounts to  $2.6 \text{ mg/m}^2 \cdot \text{s}$  at approximately 1100 K as may be seen from figure 5.12 for the basic situation.

Changing from light oil-firing to natural gas-firing leads to a slightly altered deposition behaviour as is shown by curve 2.

Curve 3 represents the deposition rates of sodium sulphate from chlorine free gases. Deposition of gaseous components condensing at the surface takes place only at high surface temperatures in this case, with maximum rates 5% higher than for the previous cases.

Deposition of particulates (below 1000 K) formed in the flue gases by homogeneous or heterogeneous condensation processes is described briefly in section 5.4.

Our model predicts that deposition rates in recuperators increase by about 80% by doubling the flue gas velocities in the same recuperator. Only 2 to 4 percent of the formed sodium sulphate deposits at the surface of the inner wall of these recuperators. More than 96% is emitted by the flue gases as sodium sulphate dust as shown in section 5.5. Figure 5.13 represents the temperature profile of a radiation recuperator with the combustion air flowing parallel to the exhaust gases. These recuperators are preferably applied for exhaust gas flows with inlet temperatures above 1500 K.

The deposition of sodium sulphate in a parallel flow recuperator for the flue gas composition of the base case is shown in figure 5.14. The exhaust gas temperature decreases from 1600 to 1150 K, in the direction towards the top of the recuperator.

Since the air temperature at the bottom is approximately 400 K, the wall and deposition temperatures are rather low in this section. The deposition temperature increases for this particular case from 650 to 1050 K. Figure 5.14 presents the deposition rates of sodium sulphate in this recuperator for the basic case composition and the chlorine free flue gas, curve 3. Deposition is nearly constant for both cases in the lower half of the recuperator tube. For the chlorine free case deposition decreases faster than in the basic case. The only deposition product in the counter flow recuperator, is sodium sulphate.

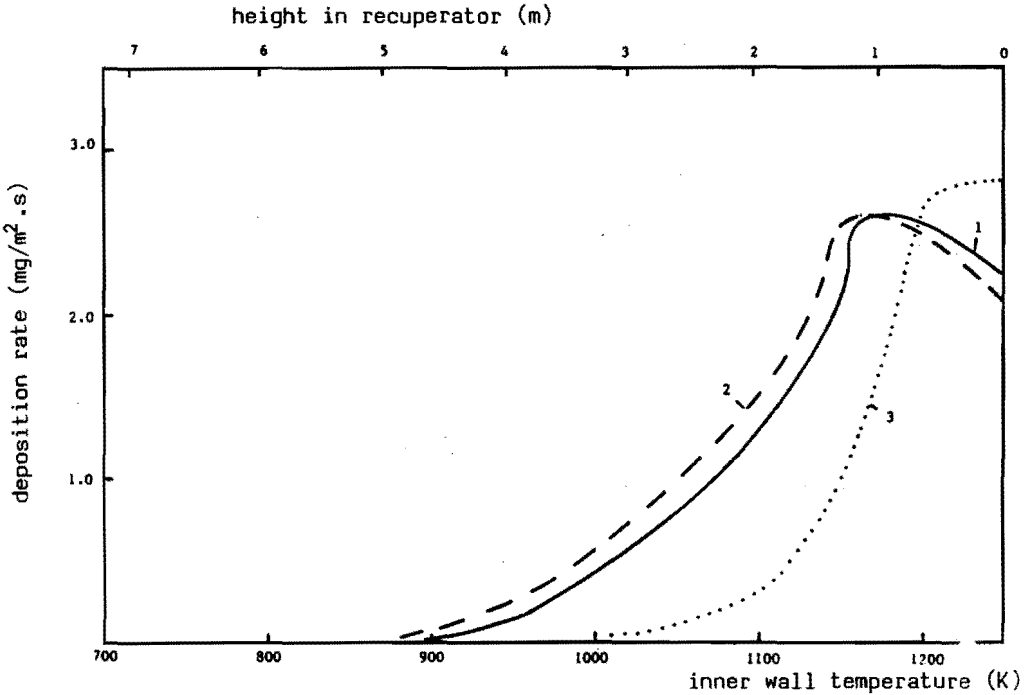


Figure 5.12: Calculated deposition rates for  $\text{Na}_2\text{SO}_4$  in the recuperator (counter flow) of a soda-lime glass furnace.

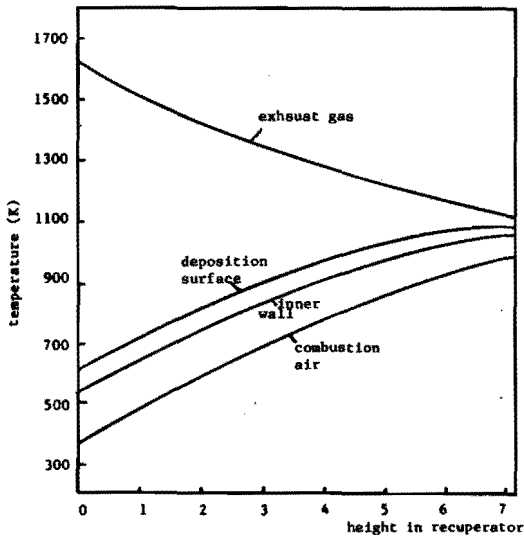


Figure 5.13: Typical temperature distribution in the recuperator with combustion air in parallel flow direction.

From calculations for counter flow as well as parallel flow recuperators it is concluded that deposition mainly takes place at the lower parts of the recuperator tubes. For both cases the deposition rates reach values upto  $2.9 \text{ mg/m}^2 \cdot \text{s}$  or a growth of the deposition layer of 6.0 cm per year. In these parts of the recuperator the flue gas temperatures exceed 1200 K; condensation in the main flow at lower temperatures leads to a decrease in deposition in the higher parts of the recuperator, with lower flue gas temperatures.

### 5.3.4 Deposition of salt components in recuperators of sodium-borosilicate glass furnaces

Furnaces producing sodium-borosilicate glasses are predominantly of the recuperative type producing 50 to 150 tons/day. The exhaust gas compositions considered here to study the deposition behaviour in counter flow recuperators are given in table 5.8.

Table 5.8: Typical compositions of exhaust gases from recuperative sodium-borosilicate glass furnaces.

	basic case 1	case 2	case 3	case 4
fuel	natural gas	natural gas	natural gas	oil
sodium concentration vol.-ppm	400	600	300	400
sulphur concentration vol.-ppm	100	100	100	500
boron concentration vol.-ppm	400	400	300	400
oxygen concentration vol.-%	2.2	2.2	2.2	2.2
carbon dioxide concentration vol.-%	10	10	10	10
water vapor concentration vol.-%	15	15	15	15
nitrogen concentration vol.-%	72.8	72.8	72.8	72.8

The sulphur present in the flue gases originates from the dissociation of sodium sulphate as a refining agent in the melt. In case number 4 additional sulphur comes from the combustion of the sulphur rich fuel. The deposition of sodium sulphate and sodium borates for flue gas composition number 1 and 2 at the inner wall of the recuperator is presented in figure 5.14. Sodium sulphate deposits in the lower part of the recuperator in both cases. The concentration of sodium is in excess relative to that of sulphur regarding sodium sulphate conversion. The deposition of  $\text{Na}_2\text{SO}_4$  is for these cases mainly determined by the sulphur concentration in the flue gases.

However, in case 2, sodium metaborate deposition rates in the bottom parts of the recuperator are much higher than in the basic case. This enhancement in  $\text{NaBO}_2$  deposition for higher sodium concentrations leads to lower  $\text{Na}_2\text{SO}_4$  deposition rates at deposition temperatures between 1000 and 1150 K.

At deposition temperatures of approximately 1050 K sodium metaborate is converted into sodium tetraborate by absorbing one  $\text{B}_2\text{O}_3$ -molecule per two  $\text{NaBO}_2$  monomers. This leads to a sudden increase in the deposition rate at this point as may be seen from the dotted line in figure 5.14.

In the basic case the sodium/boron ratio is unity, but in the second case this ratio increased to 1.5. For this composition (case 2) the sodium/boron ratio is too high for the conversion of sodium metaborate into sodium tetraborate.

For the four cases mentioned in table 5.8, the regions in the recuperator for the different deposition products are given in table 5.9.

Table 5.9: Deposition products in the different sections of the recuperator (distances given in metres from the bottom or flue gas inlet).

	case 1	case 2	case 3	case 4
$\text{NaBO}_2$	0 - 2.5 m	0 - 4 m	0 - 2.5 m	-
$\text{Na}_2\text{B}_4\text{O}_7$	2.5 - 5 m	-	2.5 - 5 m	-
$\text{Na}_2\text{SO}_4$	0 - 3 m	0 - 2 m	0 - 3 m	0 - 4 m

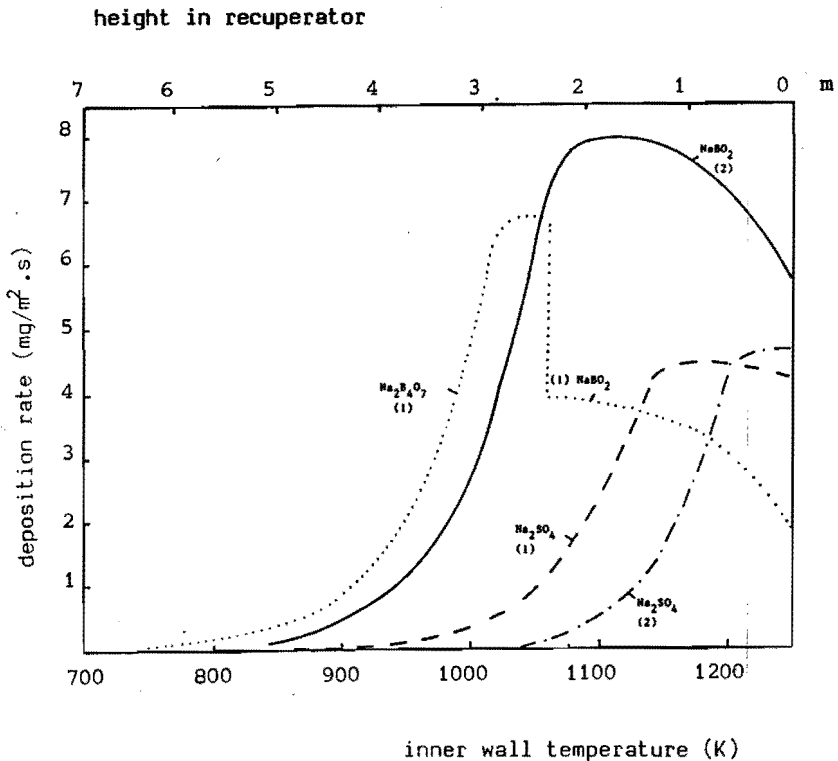


Figure 5.14: Calculated deposition behaviour of the exhaust gas from a sodium-borosilicate glass furnace in counter flow recuperator.

The maximum deposition rate for flue gas number 2 is  $8 \text{ mg/m}^2 \cdot \text{s}$  sodium metaborate, this value is among the highest rates calculated for these flue gases. The deposition of sodium sulphate hardly exceeds values of  $5 \text{ mg/m}^2 \cdot \text{s}$  in natural gas-fired furnaces, but reaches values of  $8 \text{ mg/m}^2 \cdot \text{s}$  ( $16 \text{ cm}$  per year) for oil-fired tanks.

For flue gas number 1, 96% of the sodium present in the exhaust is emitted as sodium tetraborate or sodium sulphate from the recuperator. Only 3% of the sodium is deposited as a borate or sulphate. Only 4% of the boron present in flue gas 1 deposits in the recuperator as a sodium borate and approximately 3.5% of the total sulphur contents remains at the inner wall of the recuperator. Generally not more than 5% of the impurities deposits as a result of condensation at the recuperator surfaces. The remainder is transported partly as condensed and partly as gaseous material with the flue gas flow to the stack.

## **5.4 Deposition of particulates in secondary heat exchangers and in the colder parts of regenerators**

In this section the deposition of condensed matter like dust or particulates in the colder parts of heat exchanger devices is discussed. Deposition of components transported as gaseous species through the boundary layers of the immersed obstacles and condensing at the surface of the bricks, tubes or cylindrical objects is mostly negligible in these exchangers.

In the next discussion the complexity of the processes involved in the deposition of particulates is shown and the different kinds of deposition processes are presented in brief.

### **5.4.1 Mechanisms for particulate deposition from dust laden flue gases**

The deposition of particulate matter in the submicron range originates from five different mechanisms (neglecting electrostatic forces) (Fuchs [6]):

1. gravitational settling (for example sedimentation);
2. deposition by inertia of the particulates;
3. interceptional deposition;
4. deposition by Brownian diffusion;
5. deposition by thermophoretic forces.

These processes may take place simultaneously or separately. For the practical situation of mainly submicron sized dust particles in exhaust gas flows with velocities of 2 to 10 m/s and local temperature differences of 100 to 300 K, only inertial deposition mechanisms, deposition by Brownian diffusion and deposition caused by thermophoretic forces have to be considered.

### **5.4.2 Deposition by inertia effects**

The particle trajectories deviate from the flow patterns of the gas phase of flue gases flowing along a flat plate or around cylindrical or spherical surfaces, illustrated by figure 5.15.

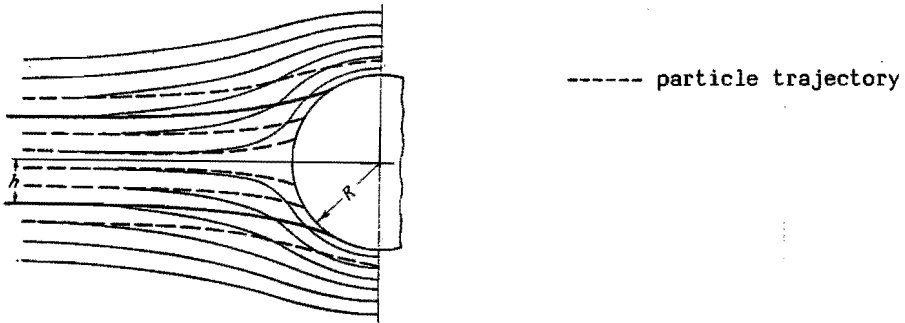


Figure 5.15: Particle and gas trajectories of a potential flow field around a cylinder.

Considering a two-dimensional field, for example the flow in upstream direction of an obstacle, the particle velocities  $U_x$  en  $U_y$  in both directions generally differ from the gas velocities  $V_x$  en  $V_y$ . These inertia forces result in increasing particle concentrations near the obstacle. However, only for Stokes numbers larger than 0.125 this leads to non-zero deposition rates for stagnation point flow at a cylindrical surface.

In the case of flue gases from glass furnaces Stokes is of the order of  $10^{-3} - 10^{-4}$ . Inertia effects only cause an increase in particulate concentration near the deposition surface but do not directly lead to deposition of dust.

Fernandez de la Mora and Rosner [7] showed that deposition takes place by thermophoretic or Brownian diffusion, but that the increase of the concentration of particulates near the deposition surface enhances these diffusion rates.

The coupled effects of inertia forces, thermophoretic forces and Brownian diffusion depend on the geometry of the deposition surface, the particle sizes of the dust, the local temperature gradients and the flue gas velocity. The real situation for exhaust gases of glass furnaces is much too complex for a detailed description of the deposition process of dust particles in the lower parts of the regenerator or in secondary heat exchanging devices. The description of these processes is beyond the scope of this thesis.

Zimon [8] used a more practical approach and distinguished three types of deposition processes.

The first type is the formation of free-running deposits. The contamination by this process for example in case of a flow around a heat exchanging tube depends strongly on the flue gas velocity.

At first deposition increases with increasing velocity but after reaching a certain value deposition rates decrease again. Free running deposits are primarily formed at the surface of the circular tubes in the stagnation point of the flow (front side) and the back side of the tube see figure 5.16.

Secondly, tacky deposits may be formed: these deposits contain 'tacky' particulates, which are especially important in exhaust gases of glass furnaces since alkali sulphates and pyrosulphates ( $K_2S_2O_7$  or  $Na_2S_2O_7$ ) are usually rather tacky.

Thus especially in exhaust gases of glass furnaces fired with heavy oil, deposition of alkali sulphates and reactions of sulphates with  $SO_3$  to form alkali pyrosulphates may lead to tacky deposits.

The third form are the dense deposits like the reaction products of sodium sulphate or potassium sulphate dust with iron oxide  $Fe_2O_3$  (corroded in the heat-exchanger). Dense deposits are also formed by reaction of already deposited alkali sulphate with  $SO_3$  leading to dense  $Na_2S_2O_7$  deposits and the corrosive  $NaHSO_4$  or  $KHSO_4$  deposits.

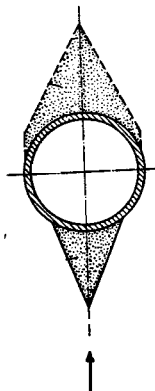


**Figure 5.16:** Form of deposits on a heat-exchanger pipe.

## **5.5 Emission of particulates and gaseous components from glass furnaces according to equilibrium calculations**

The composition of furnace stack gases strongly depends on the glass composition and the fuel. Thermodynamic equilibrium calculations have been carried out, as described in chapter 3, to determine the stack gas composition at 550 K. This temperature is realistic for the exhaust gases in the stack of the glass furnaces.

The equilibrium calculations have been carried out first to investigate the nature of the thermodynamic stable compounds in the flue gases. The main purposes of these calculations are the determination of the gaseous composition of the stack gases and the possible reactions of the dust constituents with gaseous species. The chemical equilibrium composition of sulphur oxide or other sulphur compounds may differ considerably from the real composition below 700 K, due to the limited reaction rates for the conversion of  $\text{SO}_2$  to  $\text{SO}_3$ . However, in spite of the discrepancies between the equilibrium composition and real composition, the thermodynamic approach gives a rather good estimation of the behaviour of the flue gases at low temperatures (below 700 K).

### **5.5.1 Composition of dust and gaseous pollutants from soda-lime glass furnaces**

To estimate the emission from soda-lime glass furnaces we calculated the equilibrium composition of the gas phase and the dust particles for 4 representative flue gases. These flue gases are presented in table 5.9 together with the main constituents at a stack temperature of 550 K. According to Gebhardt et al [9], further cooling of the stack gases in oil fired furnaces may result in formation of sodium bisulphate ( $\text{NaHSO}_4$ ) dust. Addition of magnesium oxide or calcium oxide lowers the concentrations of the gaseous sulphur oxide compounds. The formation of corrosive compounds as sulphuric acid, sodium pyrosulphate ( $\text{Na}_2\text{S}_2\text{O}_7$ ) or sodium bisulphate ( $\text{NaHSO}_4$ ) may be inhibited by addition of  $\text{MgO}$  or  $\text{CaO}$  to the flue gases of oil-fired furnaces, according our equilibrium calculations and observations of Webb et al [10].

**Table 5.9:** Composition of dust and gaseous pollutants from stack gases of different regenerative soda-lime glass furnaces (on a basis of 8 volume-% oxygen in exhaust gas).

case	1	2	3	4
fuel	heavy oil	light oil	natural gas	natural gas
sodium vol.-ppm	150	125	125	125
chlorine vol.-ppm	62.5	62.5	62.5	62.5
sulphur vol.-ppm	1000	250	125	25
equilibrium composition at 550 K:				
gaseous sulphur oxides (presented as SO <sub>2</sub> ) mg/m <sup>3</sup> <sub>n</sub>	1740	51.6	126	-
HCl mg/m <sup>3</sup> <sub>n</sub>	72.0	72.0	72.0	-
Na <sub>2</sub> SO <sub>4</sub> dust mg/m <sup>3</sup> <sub>n</sub>	-	-	245	97
NaHSO <sub>4</sub> dust mg/m <sup>3</sup> <sub>n</sub>	-	-	-	-
Na <sub>2</sub> S <sub>2</sub> O <sub>7</sub> dust mg/m <sup>3</sup> <sub>n</sub>	456	380	-	-
Na <sub>2</sub> CO <sub>3</sub> dust mg/m <sup>3</sup> <sub>n</sub>	-	-	-	34
NaCl dust mg/m <sup>3</sup> <sub>n</sub>	-	-	-	103
* with only minor sulphate additions to the batch				

For heavy oil fired furnaces addition of 1.5 grams of MgO or 2.0 grams of CaO per m<sup>3</sup><sub>n</sub> flue gas limits the emission of gaseous sulphur oxide compounds to nearly zero.

### 5.5.2 Composition of dust and gaseous pollutants from sodium-borosilicate glass furnaces

According to our calculation, the dust from gas-fired furnaces producing sodium borosilicate glass the dust consists mainly of sodium sulphate and sodium metaborate.

At temperatures as low as 550 K sodium borates (NaBO<sub>2</sub>) may react with the water vapor or the residual gaseous boric acid to complex forms of borates. According to our chemical equilibrium calculations the main gaseous constituent of flue gases of these furnaces is boric acid (H<sub>3</sub>BO<sub>3</sub>) but for heavy oil-fired furnaces emission of gaseous sulphur oxides may take place.

### 5.5.3 Composition of dust and gaseous pollutants from lead glass furnaces

Natural gas-fired lead glass furnaces normally emit only chloric acid as a gaseous compound to the atmosphere. The dust from these furnaces consists mainly of lead oxide, some alkali sulphates ( $\text{Na}_2\text{SO}_4$  or  $\text{K}_2\text{SO}_4$ ) and minor amounts of lead sulphate. According to our equilibrium calculations also combinations of lead oxide and lead sulphate may be formed for example  $4\text{PbO} \cdot \text{PbSO}_4$ .

In the exhaust gases of oil-fired furnaces all the alkali compounds and lead compounds will be converted into sulphate dust ( $\text{Na}_2\text{SO}_4$ ,  $\text{K}_2\text{SO}_4$  and  $\text{PbSO}_4$ ). This is in agreement with the observations made by Kaiser [4] for natural gas-fired and oil-fired lead glass furnaces.

The remainder of sulphur containing species may react with the alkali sulphates to pyrosulphates ( $\text{Na}_2\text{S}_2\text{O}_7$ ,  $\text{K}_2\text{S}_2\text{O}_7$ ) or will be emitted as gaseous sulphur oxide.

## 5.6 Summary and conclusions

The physical - chemical model to determine deposition rates in flue gas systems has been successfully applied for regenerative and recuperative glass furnaces. Calculations have been carried out to estimate the deposition as a result of condensation of salt or metal oxide compounds at regenerator bricks or recuperator walls. Besides, this model provides information about the amount and composition of the dust, formed in the flue gas and transported to the stack.

Thermodynamic calculations have been carried out to determine the stable flue gas components and the possible reactions of the dust with gaseous components down to 550 K. In spite of the discrepancies between the equilibrium composition and the real composition of the stack gases at temperatures below 1000 K, this method gives a fairly good description of the chemical nature of these gases.

With the aid of some practical examples the applicability of the deposition model has been demonstrated for different situations. It has been shown that the influence of glass composition, fuel composition and heat exchanger type on the nature of deposition products and deposition rates can be calculated with this deposition model.

### **Deposition in regenerators and recuperators of soda-lime glass furnaces**

Sodium sulphate is the most important condensate deposited at regenerator bricks between temperatures of 1000 K and 1350 K. The deposition rate is proportional to the sodium content of the flue gases.

At high chloride concentrations deposition of sodium sulphate sets on at temperatures lower than in case of chlorine-free flue gases. The deposition rate for  $\text{Na}_2\text{SO}_4$  reaches values of 5 g/cm<sup>2</sup> year in the middle-section of the regenerators at temperatures between 1250 K and 1300 K resulting in a thickness of the deposition layer of 2.5 cm - 3.0 cm per year.

In recuperators of soda-lime glass furnaces the maximum  $\text{Na}_2\text{SO}_4$  deposition rates amount to 10 g/cm<sup>2</sup> year, in the lower sections, with flue gas temperatures above 1300 K. According to our calculations the maximum deposition rate depends only very slightly on the fuel used.

The deposition of liquid sodium sulphate in regenerators of oil-fired furnaces takes place at surface temperatures a little (20 K - 30 K) higher than in case of natural gas-firing, due to the higher sulphur amounts in the former case.

Sodium carbonate is formed at deposition temperatures between 900 and 1050 K and sodium chloride between 800 and 1000 K in sulphur lean flue gases of soda-lime glass furnaces.

Changes in oxygen, water vapor and carbon dioxide concentrations hardly influence the deposition behaviour in regenerators or recuperators of glass furnaces.

The deposition rates increase for higher flue gas velocities especially in recuperators. Condensation of sodium sulphate in parallel flow as well as in counter flow recuperators takes place in the part where the main flue gas temperature exceeds 1200 K.

#### **Deposition in regenerators and recuperators of borosilicate glass furnaces**

In regenerators or recuperators of oil fired sodium-borosilicate glass furnaces, the only deposition product to be expected according to our calculations is sodium sulphate. Deposition of  $\text{Na}_2\text{SO}_4$  in regenerators of these furnaces predominantly takes place below 1400 K, deposition rates may reach values of  $10 \text{ g/cm}^2 \cdot \text{year}$ . In regenerators of natural gas-fired sodium borosilicate glass furnaces the deposition products are: sodium sulphate at brick temperatures below 1370 K, sodium metaborate between 1060 K and 1320 K and sodium tetraborate between 970 and 1060 K. Potassium tetraborate and potassium sulphate are the main deposition products in regenerators or recuperators of potassium-borosilicate glass furnaces.

#### **Deposition in regenerators of lead glass furnaces**

For alkali free flue gases lead sulphate and lead oxide are the main deposition products in regenerators for lead glass furnaces. In oil-fired furnaces the main deposition product is lead sulphate at brick surface temperatures between 980 and 1120 K, reaching deposition rates of  $8 \text{ mg/m}^2 \cdot \text{s}$  ( $6 \text{ g/cm}^2 \cdot \text{year}$ ). Lead oxide deposition takes place in these flue gases with lower rates between 900 K and 1120 K.

In regenerators of natural gas-fired furnaces lead oxide predominantly condenses at the surfaces of the bricks between 1000 and 1150 K, lead sulphate deposition is expected below 1070 K. In alkali lead glass furnaces deposition of sodium sulphate or potassium sulphate will take place before deposition of lead compounds sets on.

## Literature references chapter 5

- [ 1] Schmalenbach B.;  
'Einfluss von Gasgeschwindigkeit und Strömungsverhalten auf den Thermischen Wirkungsgrad von Regenerativkammern'.  
XXVIII International Colloquium on Refractories Aachen (1985)  
248-262.
- [ 2] Trier W.;  
'Glasschmelzöfen'  
Springer Verlag Berlin-Heidelberg-New York-Tokyo (1984).
- [ 3] Barklage-Hilgefort H.;  
'Wärmetechnische Messungen an Kammergitterungen'  
Glastechn. Ber. 58 (1965) 65-79.
- [ 4] Kaiser M.;  
'Erfahrungen mit einem filternden Abscheider hinter einer Bleiglaswanne'.  
Glastechn. Ber. 51 (1978) 189-195.
- [ 5] Bird R.B., Stewart W.E., Lightfoot E.N.;  
'Transport Phenomena'.  
John Wiley, New York (1960).
- [ 6] Fuchs N.A.;  
'The Mechanics of Aerosols'  
Pergamon Press, New York (1964).
- [ 7] Fernandez de la Mora J., Rosner D.E.;  
'Inertial Deposition of Particles Revisited and Extended: Eulerian Approach to a Traditionally Lagrangian Problem'.  
Physico Chemical Hydrodynamics vol. 2 (1981) 1-21.
- [ 8] Zimon A.D.;  
'Adhesion of dust and powder'.  
Plenum Press - New York - London (1969).
- [ 9] Gebhardt F., Schumacher K.;  
'Verschlackungsvorgänge in den Regenerativkammern von Glasschmelz zur Herstellung von Soda-Kalk-Kieselglas'.  
XXIII International Colloquium on Refractories Aachen (1985) 1-27.
- [ 10] Webb R.L., Marchiori D., Durbin R.E., Wang Y.J., Kulkarni A.;  
'Heat Exchangers for Secondary Heat Recovery from Glass Plants'.  
Heat Recovery Systems 4 (1984) 77-85.

## NOMENCLATURE CHAPTER 5

A	semi-empirical derived parameter in equation 5.5
A'	constant in Nu-relation (5.2)
B	semi-empirical derived parameter in equation 5.5
B'	constant in Nu-relation (5.2)
D	diffusion coefficient ( $m^2/s$ )
d	characteristic diameter (m)
$m_n^3$	cubic metre under normalized condition (1013 mbar, 295 K)
Nu	Nusselt number (equation 5.2)
Pr	Prandtl number (5.4)
p.p.m.	volume parts per million
Re	Reynolds number
R	radius of cylinder
Sc	Schmidt number (5.3)
Sh	Sherwood number (5.1)
v	gas velocity (m/s)

### Greek symbols

$\rho$	gas density ( $kg/m^3$ )
$\mu$	dynamic gas viscosity (kg/m.s)

**APPENDIX A: Diffusion coefficients for inorganic gaseous molecules in combustion gases\* (given in  $\text{cm}^2/\text{s}$ ).**

Temperature Component	1600 K	1200 K	800 K
Na	2.88	1.74	0.83
NaOH	2.26	1.35	0.64
NaCl	1.90	1.14	0.54
Na <sub>2</sub> SO <sub>4</sub>	1.38	0.83	0.4
NaBO <sub>2</sub>	2.16	1.29	0.61
Na <sub>2</sub> B <sub>4</sub> O <sub>7</sub>	1.70	1.02	0.48
(NaBO <sub>2</sub> ) <sub>2</sub>	1.69	1.01	0.48
HCl	3.15	1.94	0.97
KCl	1.61	0.96	0.45
KOH	1.86	1.11	0.53
K <sub>2</sub> SO <sub>4</sub>	1.26	0.75	0.35
KBO <sub>2</sub>	1.79	1.07	0.50
Pb	1.20	0.73	0.35
PbO	1.13	0.68	0.32
Pb <sub>2</sub> O <sub>2</sub>	1.00	0.60	0.28
Pb <sub>3</sub> O <sub>3</sub>	0.93	0.54	0.25
Pb <sub>4</sub> O <sub>4</sub>	0.83	0.49	0.23
Pb <sub>5</sub> O <sub>5</sub>	0.76	0.45	0.21
Pb <sub>6</sub> O <sub>6</sub>	0.70	0.42	0.20
SO <sub>2</sub>	2.31	1.42	0.71
SO <sub>3</sub>	2.13	1.31	0.65
HBO <sub>2</sub>	2.88	1.75	0.85
H <sub>3</sub> BO <sub>3</sub>	2.03	1.24	0.60

\* Combustion gas mainly consists of: 13 volume% H<sub>2</sub>O  
 4.4 volume% O<sub>2</sub>  
 9.0 volume% CO<sub>2</sub>  
 0.8 volume% Ar  
 72.8 volume% N<sub>2</sub>

APPENDIX B : Thermal diffusion factor parameters for inorganic vapors in combustion gases\*.

Molecules	$\sigma_{i,g}$ Å	$\alpha_{\infty}$	$(-\alpha_1/\alpha_{\infty})$ K
Na	3.576	-0.0607	551.2
NaOH	3.804	0.1592	429.52
NaCl	4.186	0.3462	420
Na <sub>2</sub> SO <sub>4</sub>	5.000	0.7828	476
NaBO <sub>2</sub>	3.649	0.3886	447
Na <sub>2</sub> B <sub>4</sub> O <sub>7</sub>	4.041	0.820	594
(NaBO <sub>2</sub> ) <sub>2</sub>	4.265	0.62	447.01
HCl	3.339	0.0687	92
KCl	4.715	0.427	456
KOH	4.352	0.311	419
K <sub>2</sub> SO <sub>4</sub>	5.34	0.858	494
KBO <sub>2</sub>	4.149	0.4774	489
Pb	5.80	0.800	550
PbO	5.80	0.810	596
Pb <sub>2</sub> O <sub>2</sub>	6.25	1.10	596
Pb <sub>3</sub> O <sub>3</sub>	6.70	1.25	596
Pb <sub>4</sub> O <sub>4</sub>	7.15	1.35	596
Pb <sub>5</sub> O <sub>5</sub>	7.60	1.40	596
Pb <sub>6</sub> O <sub>6</sub>	8.05	1.45	596
SO <sub>2</sub>	4.112	0.3131	198
SO <sub>3</sub>	4.207	0.3977	184
HBO <sub>2</sub>	3.177	0.1808	315.4
H <sub>3</sub> BO <sub>3</sub>	4.279	0.3649	294.6

\* Combustion gas mainly consists of: 13 volume% H<sub>2</sub>O  
4.4 volume% O<sub>2</sub>  
9.0 volume% CO<sub>2</sub>  
0.8 volume% Ar  
72.8 volume% N<sub>2</sub>

## APPENDIX C

### Calculation procedure for deposition in flue gas channels

The deposition of salt components at surfaces in flue gas channels or regenerators has been described with a computer simulation model. This model assumes a certain temperature profile for both the flue gas flow and the deposition surfaces. Starting point is the flue gas entrance, the calculation process follows the direction of the flue gas flow.

The initial concentrations of the flue gas elements is dependent on the volatilization process in the glass melting furnace.

The average temperature of the flue gas and deposition surface is determined for a small section in the flue gas channel. The diffusion parameters, the Sherwood numbers and reaction equilibrium constants are determined for this section for the relevant temperature.

As an example, here the calculation procedure is presented for sodium sulphate deposition in a flue gas with sodium, sulphur and chloride compounds. The deposition of other compounds like sodium borates, lead oxide, lead sulphate etc. or deposition of several components together is calculated in a similar way.

The procedure for the example of sodium sulphate deposition exists of the following steps.

1. The equilibrium composition of the host flue gas phase is calculated in a small section of the exhaust gas channel for the prevailing temperature and dopant concentration. So the concentrations of the most important components, NaOH, Na, (NaOH)<sub>2</sub>, NaCl, HCl, Na<sub>2</sub>SO<sub>4</sub>, SO<sub>2</sub> and SO<sub>3</sub> are calculated by means of the equilibrium calculations introduced in chapter 3. In case of condensation in the host gas, the condensed product is assumed not to take part in the transport process through the boundary layers.
2. Two cases have to be considered:
  - a. no condensation at the surface
  - b. condensation of Na<sub>2</sub>SO<sub>4</sub> at the surface leading to Na<sub>2</sub>SO<sub>4</sub> deposition.

First, no condensation at the surface is assumed (case a), the concentration of NaOH, SO<sub>2</sub> and HCl at the deposition surface are roughly estimated and the concentrations of the other compounds are calculated by means of the thermodynamic equilibrium model.

3. The flux of every component through the boundary layer towards or from the surface is calculated by formula (4.5), neglecting chemical reactions in the boundary layer.

For case a (no deposition) the total flux of all chloride species has to be zero and the total flux of all sodium and all sulphur has to be zero. If these fluxes deviate from zero, the concentrations of NaOH, SO<sub>2</sub> and HCl at surface locations have to be adjusted by an iterative calculation procedure until the condition of a zero net-flux for sodium, sulphur and chlorine is met.

4. The flue gas composition at the surface is calculated for a net deposition rate equal to zero. In case the sodium sulphate vapor pressure exceeds the saturation value, deposition of sodium sulphate takes place. For this second situation (case b) the concentrations or vapor pressures of NaOH and SO<sub>2</sub> are related to the following equation:

$$\frac{p^{1/2} \text{O}_2 \cdot p \text{SO}_2 \cdot p^2 \text{NaOH}}{p \text{H}_2\text{O}} = p^* \text{Na}_2\text{SO}_4 \cdot K \quad C(1)$$

where:

$p^* \text{Na}_2\text{SO}_4$  = the saturation value for the sodium sulphate partial pressure

K = equilibrium constant at temperature for the reaction:  
 $\text{Na}_2\text{SO}_4 (\text{g}) + \text{H}_2\text{O} \rightarrow 1/2 \text{O}_2 + \text{SO}_2 + 2\text{NaOH}(\text{g})$ .

The concentrations of NaOH and HCl are estimated for the flue gas at the surface, with relation C(1) the SO<sub>2</sub> concentration or vapor pressure is calculated.

5. For case b (sodium sulphate deposition) the total flux of chloride containing species has to be zero, but the total flux of sodium has to be twice the sulphur flux for  $\text{Na}_2\text{SO}_4$  deposition. The NaOH and HCl concentrations are iteratively adjusted until these conditions are met.

The deposition rate of sodium sulphate is calculated by means of equation (4.9) per unity of deposition area.

6. From the known values of the specific surface of the flue gas channel, the deposition of sodium sulphate is calculated. The composition of the flue gas flowing from the section under consideration to the next section is corrected for the deposition of sodium and sulphur as  $\text{Na}_2\text{SO}_4$ .

7. This method was successively applied out for all the sections in the flue gas channel resulting in:

- a. calculation of the deposition rates for  $\text{Na}_2\text{SO}_4$  at every location in the flue gas channel.
- b. calculation of the nature of the condensed product in the flue gas and the amount of condensed material.
- c. the calculation of the composition of the gaseous components at every position in the flue gas channel.

## SUMMARY

The formation of flue gas deposits leads to a decreasing thermal efficiency in the heat exchanging systems of industrial glass furnaces. Eventually it may even result in blockages of flue gas channels. Condensation particles in the exhaust gas cause the emission of dust from the furnace chimney.

This thesis describes the origin of deposits and condensation phenomena in exhaust gases of glass furnaces.

A simulation model was developed to describe the condensation and deposition processes in exhaust gas channels. The Chemically Frozen Boundary Layer (CFBL) theory -originally developed for other combustion systems- has been modified to calculate the deposition rates and the exhaust gas composition in regenerators and recuperators. The model consists of a combination of the thermodynamic theory and mass transport equations for the diffusion of gaseous components towards the deposition surface. The composition of the condensation products and the deposition rates were studied experimentally and compared with the results from the model.

Experiments were carried out on a laboratory scale using simulated flue gases. In most cases, the nature of the condensation products in the simulated flue gases agreed satisfactorily with the results from the model.

Deposition rates of salts or metal oxides from the flue gases or flames on cooled cylindrical surfaces and in exhaust gas channels were measured and compared with theoretical estimates.

In most cases the CFBL theory provides rather accurate results for the deposition rates on the cooled cylindrical surfaces, but the dew point temperatures for alkali sulphate deposition tend to be overestimated by the theory. This discrepancy could be due to reaction kinetic limitations.

The deposition model, which makes use of the CFBL-theory, was successfully used to describe the deposition rates of flue gas components condensing on the surfaces of the exhaust gas channel. The deposition of dust, formed in the main flue gas flow is neglected in the model and this results in differences between the experimental deposition rates and theoretical deposition rates, at low temperatures.

According to the experimental results and the theory, condensates in the flue gases are mainly:

1. sodium sulphate in oil-fired and gas-fired soda-lime glass furnaces and oil-fired sodium-borosilicate glass furnaces.
2. alkali sulphates ( $K_2SO_4$  and/or  $Na_2SO_4$ ) and alkali borates in gas-fired borosilicate glass furnaces.
3. lead oxide in gas-fired lead glass furnaces and lead sulphate in oil-fired lead glass furnaces.

Condensation occurs mainly in a temperature range of: 150-200 K. Alkali sulphate condensation and deposition begins below 1300-1400 K; whereas condensation or deposition of alkali borates and lead compounds takes place below 1150 K.

According to the simulation model, deposition of salts causes fouling of the middle sections of the regenerator. In a recuperator, deposition occurs mainly in the lower section, at higher flue gas temperatures. Deposition behaviour in recuperators and regenerators depends strongly on the concentration of volatiles originating from the molten glass and on the flue gas velocity. Higher deposition rates in regenerators are more likely with larger temperature differences between the regenerator packing material and the main gas flow.

The concentrations of oxygen, water vapor and carbon dioxide are of minor importance regarding condensation and deposition behaviour.

Chloride volatilization from the molten glass results in a reduction of the maximum sodium sulphate deposition rate.

The model gives a clear insight into the chemical reactions that occur in exhaust gases and the formation of dust particles in the regenerator, recuperator and chimney. Reactions between sulphur oxides and alkali sulphates at temperatures below 600 K lead to the formation of corrosive alkali bisulphates and/or pyrosulphates in oil-fired furnaces.

The model provides the glass industry with a method for investigating the fouling of regenerators and recuperators, as well as the reactions that can lead to the formation of dust particles and gaseous pollutants.

So far calculations have agreed satisfactorily with practical situations in the glass industry, therefore, the model appears to be a valuable tool in design studies for new types of heat exchangers.

## SAMENVATTING

Depositie van rookgascomponenten leidt tot een vermindering van het warmtetechnische rendement in warmtewisselaars van industriële glasovens. Eventueel kunnen verstoppingen in rookgaskanalen het gevolg zijn. Condensatie in het rookgas resulteert in de emissie van fijne stofdeeltjes uit de glasovenschoorsteen. Dit proefschrift beschrijft de processen die leiden tot depositie en condensatie in afgassen van industriële glasovens.

Een simulatiemodel is ontwikkeld om deze processen in rookgaskanalen te bestuderen. De 'Chemically Frozen Boundary Layer' (CFBL) theorie -oorspronkelijk opgesteld voor andere verbrandingssystemen- is aangepast om depositiesnelheden en rookgassamenstellingen in regeneratoren en recuperatoren te berekenen. Het model bestaat uit een combinatie van thermodynamische theorieën en stoftransportvergelijkingen voor diffusie van gassen naar oppervlakken waaraan depositie plaatsvindt.

De samenstelling van het gecondenseerd materiaal en de mate waarin depositie optreedt werd experimenteel onderzocht en vergeleken met de resultaten van het model.

De experimenten werden uitgevoerd op laboratoriumschaal met gebruikmaking van gesimuleerde glasovenrookgassen. In de meeste gevallen kon de chemische samenstelling van de gevonden condensatieproducten met het theoretisch model verklaard worden. Depositiesnelheden van zouten of metaaloxiden van hete rookgassen of vlammen op gekoelde cilindrische oppervlakken en in rookgaskanalen werden gemeten en vergeleken met theoretische afschattingen.

Voor de meeste gevallen blijkt het model gebaseerd op de CFBL-theorie vrij nauwkeurige resultaten te leveren, om de depositiesnelheden op het gekoelde cilindrische oppervlak te bepalen. Maar de berekende dauwpunten voor zoutcondensatie zijn in het algemeen hoger dan de waargenomen dauwpunttemperaturen. Deze afwijkingen worden voornamelijk veroorzaakt door reactiekinetische limiteringen.

Het depositiemodel is met succes toegepast om depositiesnelheden van rookgascomponenten, die condenseren aan wanden van rookgaskanalen, te beschrijven. De afzetting van stofvormig materiaal, dat in de hoofdstroming door afkoeling gevormd is, wordt in het model verwaarloosd.

Deze verwaarlozing leidt tot verschillen tussen de experimenteel bepaalde depositiesnelheden en modelberekeningen bij lage rookgastemperaturen.

Volgens de experimentele en theoretische resultaten zijn de meest voorkomende condensatieproducten:

1. natriumsulfaat in oliegestookte en aardgasgestookte natronkalkglasovens en in oliegestookte natronborosilicaatglasovens.
2. alkalisulfaten ( $\text{Na}_2\text{SO}_4$  en  $\text{K}_2\text{SO}_4$ ) en alkaliboraten in gasgestookte borosilicaatglasovens.
3. loodoxide in gasgestookte en loodsulfaat in oliegestookte loodglasovens.

Condensatie vindt meestal plaats in een beperkt temperatuurgebied tot 150 à 200 K onder de dauwpuntstemperatuur. Alkalisulfaatcondensatie en -depositie begint beneden 1300-1400 K; terwijl condensatie en depositie van alkaliboraten en loodcomponenten beneden 1150 K plaatsvindt.

Volgens het simulatiemodel leidt zoutdepositie vooral in de middensecties van regeneratoren tot vervuiling en eventueel verstoppingen. In recuperatoren vindt depositie vooral in de benedensectie, bij hoge rookgastemperaturen plaats. Het depositiegedrag in recuperatoren en regeneratoren is sterk afhankelijk van de gehalten aan verdampingsproducten van de glassmelt en de rookgassnelheid. Grote temperatuurverschillen tussen het rookgas en de regeneratorstenen leiden tot hoge depositiesnelheden.

De depositie van zouten in de rookgaskanalen wordt slechts beperkt beïnvloed door de zuurstof-, waterdamp- en kooldioxideconcentraties in de gassen. Verdamping van chloriden uit de glassmelt resulteert in een vermindering van de maximumwaarde voor de  $\text{Na}_2\text{SO}_4$ -depositiesnelheid.

Het simulatiemodel geeft een inzicht in de chemische reacties die plaatsvinden in glasovenrookgassen en in de vorming van stofvormig materiaal in de regenerator, recuperator en schoorsteen.

Beneden 600 K reageren zwaveloxiden met de stofvormige alkalisulfaten in oliegestookte glasovens waarbij de corrosieve alkalipyrosulfaten en/of alkalibisulfaten gevormd worden.

Het model voorziet de glasindustrie met een methode om vervuiling van regeneratoren en recuperatoren te bestuderen en identificeert de reacties die leiden tot de vorming van stofdeeltjes en gasvormige verontreinigingen.

De berekeningen die zijn uitgevoerd stemmen in het algemeen vrij goed overeen met praktische situaties in de glasindustrie en daarom blijkt het model een belangrijk middel voor het ontwerp van nieuwe warmtewisselaarsorten voor deze industrietak.

### Curriculum Vitae

Ruud Beerkens werd in Venlo geboren op 31 mei 1957. Vanaf 1969 tot 1975 volgde hij de Atheneum-opleiding aan het Thomascollege te Venlo. Na een korte periode 1975/1976 Civiele Techniek gevolgd te hebben aan de TH-Delft is hij van studierichting veranderd. Vanaf 1976 studeerde hij Scheikundige Technologie aan de Technische Hogeschool te Eindhoven. In 1982 slaagde hij cum laude voor het ingenieurs-examen bij de vakgroep voor fysische technologie bij Prof.ir. M. Tels.

Vanaf maart 1982 is hij werkzaam als wetenschappelijk medewerker bij de sectie Glastechnologie van de Technisch Fysische Dienst van TNO. Onder leiding van Prof.dr.ir. H. de Waal heeft hij zijn promotie-onderzoek uitgevoerd.

## Dankwoord

Het promotieonderzoek is verricht aan de Technische Universiteit Eindhoven in de vakgroep voor Fysische Technologie. Alle medewerkers van deze vakgroep wil ik graag bedanken voor hun bijdragen die mijn onderzoek hebben mogelijk gemaakt.

Het onderzoek werd mogelijk gemaakt door de Technisch Fysische Dienst van TNO waaronder ik als werknemer vanaf maart 1982 in dienst ben. Veel dank ben ik verschuldigd aan Frank Simonis die het onderzoek vanaf het begin op stimulerende wijze heeft begeleid.

Prof. De Waal en Prof. Brassier dank ik voor de begeleiding van het onderzoek.

Dank gaat uit naar Ir. Tromp van Silenka, Ir. Vonk van Philips en Ir. Enneking van de Vereenigde Glasfabrieken voor hun ondersteuning tijdens het onderzoek.

Het tot stand komen van dit proefschrift is mede mogelijk gemaakt door TU- en HTS-studenten met name: Hans Voezenek, Eric Deliège, Jan Denissen, Leo Heinen, Jan Hoogenboom, Robert Veltman, Rob Borsjé en John Kremers. Het verwerken en drukklaar maken van dit werk is verricht door Anja Bos van de Technisch Fysische Dienst, mijn waardering gaat uit naar haar vakkundige en werkzame inzet.

Bovendien wil ik Lies Janssen van de Technisch Fysische Dienst bedanken voor haar medewerking aan het proefschrift.

Dank gaat ook uit naar Tom van der Heijden die op de juiste momenten altijd bereid was te assisteren.

Mijn ouders, zus, vrienden en vriendinnen ben ik erkentelijk voor hun steun 'langs de lijn'.

## STELLINGEN

behorend bij het proefschrift van R.G.C. Beerkens

1. De beweringen van Williams dat het gasvormige  $BO_2$  en  $B_2O_3$  de belangrijkste boriumhoudende componenten in rookgassen van borosilicaatglasovens zijn is op grond van thermodynamische overwegingen onjuist.

*Williams R.O., Pasto A.E.;*

*Journal of the American Ceramic Society* 65 (1982) 602-606

2. De aanname van Brown, dat alleen transport van gasvormig natriumsulfaat door grenslagen aan aangestroomde koude wanden de depositiesnelheid van natriumsulfaat in rookgassen bepaalt blijkt volgens uitgebreidere modelleringen niet te kloppen.

*Brown T.D.;*

*J. Inst. Fuel* 39 (1966) 378-385

3. Lage waarden voor de stofoverdracht tussen vaste stofdeeltjes en de gasfase in gepakte bedden bij lage Reynolds-getallen zijn in principe niet alleen te wijten aan de lage waarden voor de stofoverdrachtscoëfficiënt maar worden bovendien bepaald door de lage waarden voor de drijvende kracht.

*Nelson P.A., Galloway T.R.;*

*Chem. Eng. Sci.*, 30 (1975) 1-6

4. De aanname van Matousek dat verdamping van loodoxide uit een glas-smelt gelimiteerd is door diffusie van loodoxide door de oppervlaktelaag van de smelt is niet voldoende onderbouwd.

*Matousek J., Hlavac J.;*

*Glass Technology* 12 (1971) 103-106

5. Veranderingen in de temperatuur van de gemengdeken van de grondstoffen in een glassmeltoven zijn van groot belang met betrekking tot afwijkingen van de glaskwaliteit.

*Leyens G., Moreau R.;*

*Glastechn. Ber. 51 (1978) 43-47*

6. De emissie van stikstofoxiden van industriële glassmeltovens is gezien de te verwachten ontwikkelingen in branderontwerp en -geometrie met minstens 50% te beperken.

*Abbassi H.A., Khinkis H.J., Fleming D.K., Kurzynske F.R.;*

*Wärme Gas International 34 (1985) 325-329*

7. De verwisseling van het begrip 'welvaart' met het begrip 'welzijn' is kenmerkend voor de moderne welvaartstaat.
8. De activiteiten van uitzendbureaus dragen bij tot de toename van de werkeloosheidscijfers in Nederland.
9. De teruggang in de economische toestand, volgens politici veroorzaakt door de sterk stijgende prijzen van de energiedragers in 1973, blijkt in 1986 een niet-omkeerbaar proces.
10. Recente gebeurtenissen bij het gebruik en misbruik van kernenergie geven de term 'verrijking' van uranium een twijfelachtige betekenis.